ALMA MATER STUDIORUM A.D. 1088

UNIVERSITÀ DI BOLOGNA

DIPARTIMENTO DI SCIENZE BIOLOGICHE,
GEOLOGICHE E AMBIENTALI

Corso di Laurea Magistrale in Geologia e Territorio
Curriculum *Raw Materials Exploration and Sustainability*

Tesi di Laurea Magistrale

Assessing Mineralisation, Penalties and Acid Rock Drainage: Characterization of a Ni-Cu Sulfide Prospect Using Drill Core Laser-Induced Breakdown Spectroscopy, Geochemical Analysis and SEM Mineral Liberation Analyser Data

Candidato:
Vinícius Alves de Andrade

Relatore:
Prof. Paolo Garofalo

Correlatore:
Dott.ssa Debora Araujo

Sessione Luglio 2023
Anno Accademico 2022-2023

To my mother Rita, my father José Geraldo and my sister Niquelle for their unconditional love and support.

À minha mãe, Rita, ao meu pai, José Geraldo, e à minha irmã, Niquelle, pelo amor e apoio incondicionais.

To my whole family and friends, thank you for always making challenging times easier.

ACKNOWLEDGEMENTS

Special acknowledgement to Rio Tinto Exploration for providing resources for the project and to their technical team for their unvaluable contribution. The Master project, internship and this thesis are a result of extensive collaborative work. I would like to thank my academic supervisor Prof. Paolo Garofalo for his important guidance and help. My profound gratitude to my internship supervisor Dr. Debora Araujo for her support, time, commitment and genuine interest in the development of this master project. Acknowledgements to Rio Tinto Exploration, Geometallurgy and Mineral Processing teams in the Bundoora Technical Development Centre (BTDC) in Australia, and the teams in the UK, Finland and USA, especially to: Paul Agnew, Fernando Fontana, Ryan Bartlett, Melissa Gregory, Rebecca Sproule, Karen Elkin, William Powell, Jessika Gluchowska, Jennie Politis, Marina Veter, Kate Cocker, Raymond Bryant, Alice Merry, Rosalind Green, Robin Chant, Amy Lamb, Daniel Kittelty, Pieter Bhota, Christopher Smith, Susanna Metso and Tom Hunt. I also thank Datarock team in Australia, Prof. Kurt Aasly, Aurélie Chopard and Abdellatif Elghali for their discussions and contributions.

ABSTRACT

The mineral industry plays a crucial role in addressing climate change by supplying essential materials for clean energy technologies. Base metals like Ni and Cu are becoming increasingly critical and strategic for global economies.

Ore body knowledge (OBK) is vital for efficient recovery of these metals, and ore characterization is a key step in optimizing the project production and economic value. In this thesis, drill core Laser-Induced Breakdown Spectroscopy (LIBS), Mineral Liberation Analyser (MLA), and geochemical data were used to analyse a Ni-Cu sulfide prospect in Finland. The aim of this work was to enhance OBK through exploratory data analysis and development of workflows. Enrichment of sulfide and penalty elements in the concentrate and zoning of high-grade areas were determined. Early assessments on Acid Rock Drainage (ARD) potential were conducted using mineralogical and geochemical data to inform environmental studies.

The proposed workflows demonstrated homogeneity in sulfide distribution in the high-grade zone, while clustering algorithms were more sensitive to talc, chlorite, and As distributions, which are commonly associated with valuable sulfides. The results effectively increased OBK and identified priority areas for metallurgical testing. Regarding ARD analysis, intrusive rocks showed higher acidification potential than host rocks. Mineralogical static tests provided more optimistic results compared to geochemical static tests, with silicates identified as potential neutralizing phases and sulfide speciation indicating reduced acidification potential due to the dominance of pyrrhotite.

The detailed and continuous data obtained from LIBS allowed mapping sulfide variability and the identification of mineralogy/elements that may impact mineral processing. LIBS also proved effective in preliminary ARD assessments, enhancing the robustness of estimations. The integration of LIBS with other techniques holds significant potential for optimizing OBK.

LIST OF FIGURES

LIST OF TABLES

LIST OF ABBREVIATIONS

AMD – Acid Mine Drainage
AP – Acidification Potential
ARD – Acid Rock Drainage
Assoc. – Association
avg – average
CMC – Carboxy Methyl Cellulose
conc. – concentrate
DH – Drill hole
dmt – dry metric tone
EDA – Exploratory Data Analysis
EDS – Energy Dispersive X-ray Spectrometer
EF – Enrichment Factor
EIT – European Institute of Innovation and Technology
Geomet. – Geometallurgical
GTK – Geological Survey of Finland
ICP-AES – Inductively Coupled Plasma Atomic Emission Spectroscopy
ICP-MS – Inductively Coupled Plasma Mass Spectrometry
IP – Induced Polarization
KIC – Knowledge and Innovation Community
KPI – Key Performance Indicator
LIBS – Laser-Induced Breakdown Spectroscopy
LME – London Metal Exchange
Min. – Mineral
Minerals abbreviations – IMA Commission on New Minerals, Nomenclature and Classification (CNMNC)
ML – Machine Learning
MLA – Mineral Liberation Analyser
MVP – Minimum Viable Product
NNP – Net Neutralisation Potential
NP – Neutralisation Potential
NPV – Net Present Value
QA/QC – Quality assurance/quality control
REE – Rare Earth Element
OBK – Ore Body Knowledge
PV – Photovoltaic
rep. – representative
ROM – Run of Mine
SEM – Scanning Electron Microscope
Spec – specification
sulf – sulfide

LIST OF CONTENTS

1 INTRODUCTION

Mineral industry is constantly changing, and it is necessary to meet market demands while following legal regulations, societal needs and environmental expectations. More than ever, being optimal, reliable and innovative is crucial for having a successful project and prosper a business. According to Lokuwaduge & Heenetigala, 2017, stakeholders are important assets for enhancing the compliance of the companies with the Environmental, Social and Governance (ESG) reporting.

Together with the awareness of being engaged with the ESG and the 17 Sustainable Development Goals (SDGs) proposed by the United Nations in 2015 (Assembly, 21 October 2015), discovering and exploring mineral prospects every time less obvious is another great challenge the mineral industry needs to face. Nonetheless, this is especially urgent for some critical materials of utmost importance to facilitate energy transition.

Considering all these aspects, the mineral exploration industry has been massively investing in tools, techniques and methodologies that help meeting supply demands while following the required guidelines. The present work investigates innovative tools and approaches on mineral exploration to optimize its pipeline and subsequent stages of the value chain. For that, Laser-Induced Breakdown Spectroscopy (LIBS) (see section 3.1.1) and additional analytical data are used to develop early workflows for the domaining of sulfide and penalty elements occurrences and to analyse acid drainage potential in a Ni-Cu sulfide prospect in Finland.

1.1 Ni overview

Nickel (Ni) is a transition element with ionic radii similar to Fe and Mg, resulting in inter-substitution in the crystalline structure of some minerals. It is, thus, common that Ni-bearing minerals are found associated to Fe- and Mg-rich mafic and ultramafic rocks. Ni is a siderophile and specially chalcophile element, and in magmatic deposits, it forms sulfides like pentlandite (Cornwall, 1966; Contessotto, 2017). Another important type of occurrence of the metal is in the form of hydroxides, e.g., limonite, and hydrous silicates, e.g., garnierite, in lateritic prospects.

Nickel is mainly used in stainless steel industry, superalloys and rechargeable batteries (Burton, 2022). Figure 1 shows the variation for Ni price over

the last 10 years. As of the beginning of March 2023, Ni price was at US$22,000/ton and at a decreasing trend after many short-term fluctuations in the last year, when it reached over US$48,000/ton in March 2022. In Q1 2016 it reached its lowest, below US$6,000/ton, and the price had been ramping up since then, boosted by the expectations of future supply shortage and the consideration of the metal as a critical material for energy transition. The European Commission considers Ni a critical and strategic material due to its importance in the battery manufacturing industry (European Commission, 2023). The Australian Government, 2022, stresses its need for batteries used in the increasing electrical vehicle (EV) demand and advertises the Modern Manufacturing Initiative (MMI), which includes an incentive to allocate a total of $1.3 billion for mid-stage critical minerals projects, including Ni, even though the metal is not included among the 26 critical minerals list. The U.S. Geological Survey includes this metal in the list of critical minerals of 2022 (U.S. Geological Survey, 2022). The recent inversion in the price trend is a result of surplus in Ni supply since early 2022 due to the reopening and start of new operations in different locations, such as China and Indonesia.

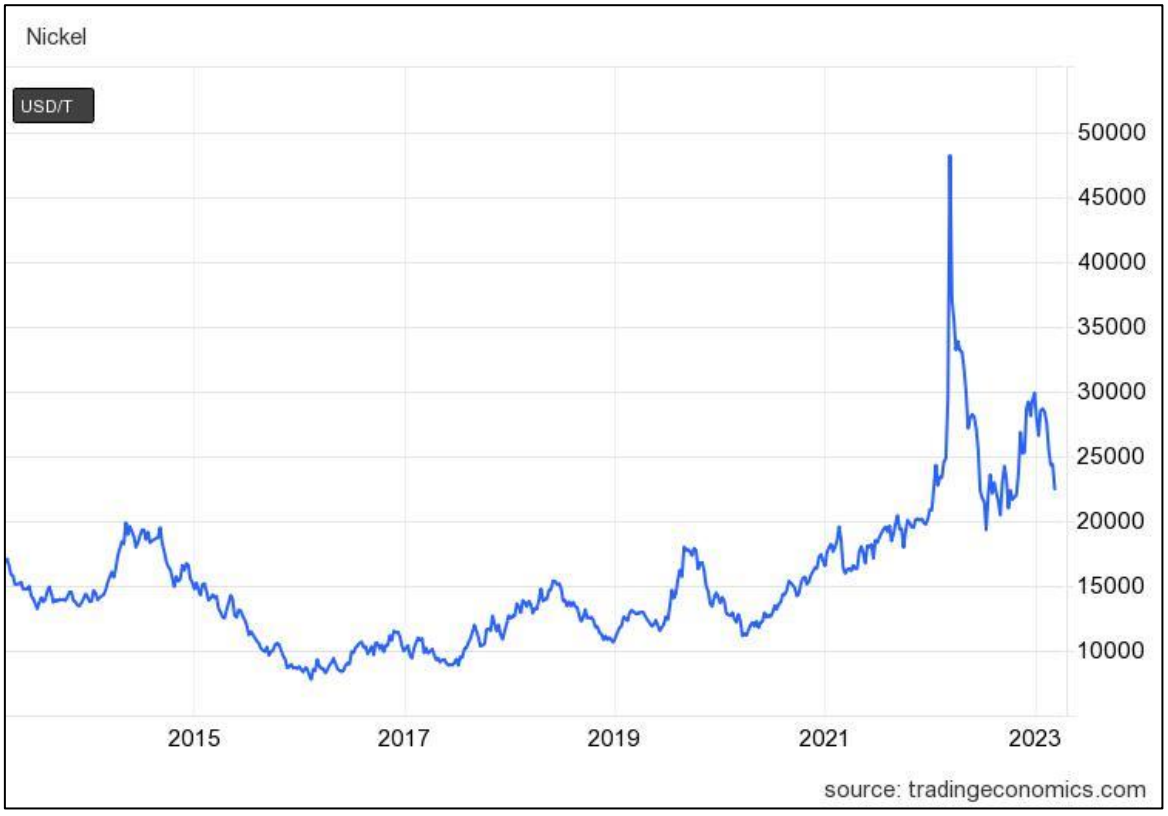

Figure 1 - Ni price fluctuation for the last 10 years (Trading Economics, 2023).

1.2 Energy transition and critical raw materials

There is an ongoing increase in the demand for critical minerals in different sectors, such as solar PV, wind farms, electric vehicles and battery store, as indicated by the International Agency's World Energy Outlook (IEA - International Energy Agency, 2022). This pushes global economies to define strategies to meeting internal and external demands for facilitating energy transition.

On its report on Critical Materials Strategy (Australian Government, 2022), Australia defines as its vision to become a global critical minerals powerhouse by 2030. The development of the critical raw materials market faces challenges such as ill-defined, concentrated and weak supply chains, which generates price volatility. This holds back investors and partnerships. Because of that, Australia presents some actions to support the mineral sector. Its most recent critical minerals list includes 26 minerals, from which two are new, i.e., high-purity alumina and silicon, and their use is linked to lithium-ion batteries and semiconductors.

On its report (EU Commission, 2020), the European Union defines that their priority is to achieve more strategic autonomy in order to make the transition to climate neutrality feasible. Reducing and reusing materials, increasing efficiency and circularity are indicated as strategies for dealing with increasing global demand for resources, in addition to the reduction on external dependency. The list of Critical Raw Materials screened 83 materials, based on economic importance and supply risk. The list was defined by analysing previous data and checking the behaviour trends. Based on this list, the Commission is able to prioritize and guide research projects under the so-called EU's Horizon, Horizon Europe and other scopes, such as in the private sector.

A total of 34 materials are listed in the newest version of the report (Table 1) from 2023 (European Commission, 2023). Nickel is listed as both a critical and strategic material for the first time. It also lists China as the global major supplier of the metal, with 33% share, and Finland as an internal source, with 38% of EU supply.

Table 1 – List of Critical Raw Materials in the (European Commission, 2023). New compared to 2020's report in italic and strategic marked with *.

2020 Critical Raw Materials – European Commission		
Aluminium/bauxite	Gallium*	Platinum group metals*
Antimony	Germanium*	Phosphate rock
Arsenic	Hafnium	Phosphorus
Baryte	*Helium*	Scandium
Beryllium	Heavy Rare Earth Elements*	Silicon metal*
Bismuth*	Lithium*	Strontium
Boron/Borate*	Light Rare Earth Elements*	Tantalum
Cobalt*	Magnesium*	Titanium*
Coking Coal	*Manganese**	Tungsten*
*Copper**	Natural Graphite*	Vanadium
Feldspar	*Nickel**	
Fluorspar	Niobium	

The need of EU to improve its autonomy relies on the fact that 98% of all Rare Earth Elements (REEs) supply to the economic bloc comes from China. The same number also applies for borate supplies from Turkey and above 71% of PGEs from South Africa. Brazil supplies 85% of Niobium and, even inside the EU, there is great concentration within specific companies or countries: 100% Strontium comes from one single company in Spain. This study allows the EU to investigate what the challenges for achieving net zero emissions by 2050 are. It is reported the need of 18 times more Li and 5 times more Co in 2030 for EVs and batteries demands. In a scenario of 2°C increase in temperature by 2050, the demand for metals such as Ni, Al, Co, Fe, Pb, Li and Mn would increase in more than 1000%.

1.3 Ore body knowledge assessments for geometallurgy

Geometallurgy deals with understanding, quantifying and modelling the variability of parameters of a deposit that influence in mining, processing and recovery of the ore in a tridimensional space (Contessotto, 2017; Lamberg, 2011). It is the integration of interdisciplinary knowledge in geology, mining and geotechnical engineering, metallurgy, mineral economics and environmental sciences, with the objective of maximizing the economic value, such as Net Present Value (NPV), reducing risks and improving or optimizing the exploration of natural resources (Dominy et al., 2018). Variables such as mineralogy, grade, grain size, deleterious elements, mineral association, hardness and structures are considered primary or intrinsic to the studied prospect, and secondary or response variables are those measured as a response to mining operations and ore processing, such

as material recovery, grindability, liberation and intact rock mass strength. These parameters result in the improvement of the OBK and are then used within the geometallurgical model as proxies to predict the so-called Key Performance Indicators (KPIs), which can be, for instance, the concentrate grade and quality, and energy and reagent consumption (Lang et al., 2018; Dominy et al., 2018).

The potential of informing valuable data and guidance throughout a mining project makes the introduction of early geometallurgical concepts and assessments a powerful tool for increasing the OBK at an exploration stage. The identification of opportunities and flagging of potential flaws related to ore minerals and undesired passives can lead to optimized and targeted studies in mine planning, exploitation, recovery and closure. The following sections (1.3.1 and 1.3.2) introduce some of the aspects that can be assessed by early ore body characterization, and which are the focus of this thesis.

1.3.1 Ore body domaining, penalties and credits

Mine planning requires the understanding of the spatial distribution of valuable minerals and intrinsic characteristics of the mineral prospect, and for that it is useful to group zones of homogeneous properties (Fouedjio et al., 2018) for grade and reserves estimations, as well as for pit optimization, sequencing and metallurgical studies. This simplifies the complexity of the ore body into geostatistical stationary zones, which does not mean that the variables that define a certain domain are constant within it (Rossi & Deutsch, 2014). A common practice in the industry is to generate grade shells for subsequent generation of a block model. This model can, nevertheless, include a series of additional information on texture, modal mineralogy, and interpretation of secondary variables, such as metallurgical properties, for forecasting ore recovery performance (Emery & Julián, 2005). Geometallurgical models are usually based on representative samples that are submitted to metallurgical testing, and this selection must be carefully planned as at this stage tests are limited (Rajabinasab & Asghari, 2019). Considering that traditional core logging is time-consuming and can lead to biased results both due to human visual interpretation limitation and the simplification of metallurgical response by petrographic classification, automated core logging is a new frontier on the acquisition of systematic quantitative data. Reliable ore characterization and

careful metallurgical tests are required for a trustworthy geometallurgical model. Moreover, given the high number of variables that can be considered (see below), the use of geostatistical and machine learning tools are introduced to deal with the complexity of the data. For instance, using cluster algorithms to domain zones within the ore body based on similarities in the considered parameters, and then characterizing the domains using statistical analysis (Adeli & Emery, 2017; Oliver & Willingham, 2016).

In addition to the characterization of valuable ore minerals, e.g., sulfides, and consequently base metals enrichment, the characterization of deleterious elements/minerals present in the deposit is of extreme importance for defining the quality of the concentrate. For Ni, a minimum grade of the metal, maximum levels of deleterious elements such as Mg, As, Pb, Se, Te and Cl, as well as the levels of credit elements such as Cu and Co present in the concentrate, define its quality and consequent price. Differently from Cu, there is a lack of "benchmark pricing" and standard penalties in nickel concentrate terms due to the wider range of Ni concentrate specifications (Selby & White, 2011). The H_2O limit of 0.3 wt% and P_{80} of 75 µm (i.e., 80 wt% passing materials at a certain fraction) are also described as possible specifications for Ni concentrates (Selby & White, 2011).

Table 2 displays a summary of specifications for penalties and credits for both Ni and Cu concentrates found in the literature. For MgO, 5 wt% is also reported as typical no charging limit (Correia, et al., 2020). Given the characteristics of the mineralisation in the prospect studied in this thesis, presented in the next chapters, some of these elements are described in further detail in sections 1.3.1.1 and 1.3.1.2.

Table 2 – Summary of penalty and credit elements for Ni (Selby & White, 2011) and Cu (Lane et al., 2016; Wood Mackenzie, 2022).

	Theoretical sulfide nickel concentrate (Selby & White, 2011)		Japanese Cu smelter penalty elements (Lane et al., 2016)			Penalty per DMT over Free Limit (Wood Mackenzie, 2022)	
Element	**Value**	**Selling limit**	**No charge max. (NCM)**	**Selling limit**	**Charge (US$/dmt)**	**No charge max. (NCM)**	**Charge range (US$/t)**
Al_2O_3	-	-	-	-	-	3.0 wt.%	$1-$2/1 wt.% above NCM
As	300 ppm	max. 400 ppm	0.2 wt.%	0.5 wt.%	$2.50/0.1% above NCM	0.2 wt.%	$2-$12/0.1 wt.% above NCM
Bi	-	-	0.05 wt.%	-	$0.30/0.01% above NCM	0.02 wt.%	$1.5-$3/0.01 wt.% above NCM
Cd	-	-	-	0.005 wt.%	-	0.03 wt.%	$1-$5/0.01 wt.% above NCM
Cl	100 ppm	max. 0.5%	0.05 wt.%	-	$0.50/0.01% above NCM	300 ppm	$1-$3/100 ppm above NCM
Co	0.5 wt.%	-	-	-	-	-	-
Cu	0.4 wt.%	-	-	-	-	-	-
F	-	-	330 ppm	0.1 wt.%	$0.10/10 ppm above NCM	300 ppm	$1-$2/100 ppm above NCM
Fe	33 wt.%	-	-	-	-	-	-
Hg	-	-	10 ppm	0.01 wt.%	$0.20/1 ppm above NCM	5 ppm	$0.1-$5/1 ppm above NCM
MgO	6.5 wt.%	max. 7 wt.%	-	-	-	-	-
Ni	10 wt.%	min. 9 wt.%	-	-	-	-	-
Ni + Co	-	-	0.5 wt.%	-	$0.30/0.1% above NCM	0.5 wt.%	$1/0.1 wt.% above NCM
Pb	5 ppm	max. 50 ppm	1 wt.%	6.0 wt.%	$1.50/1.0% above NCM	1.0 wt.%	$1-$2/1 wt.% above NCM
S	33 wt.%	-	-	-	-	-	-
Sb	-	-	0.1 wt.%	-	$0.50/0.01% above NCM	0.05 wt.%	$1-$2/0.01 wt.% above NCM
Se	10 ppm	max. 50 ppm	-	-	-	300 ppm	$1.5/t/100 ppm above NCM
SiO_2	-	-	-	-	-	10.0 wt.%	$1/1 wt.%
Zn	-	-	3.0 wt.%	-	$1.50/1.0% above NCM	3.0 wt.%	$1-$5/ 1 wt.% above NMC

1.3.1.1 Mg-silicate-bearing sulfide ore

Magnesium silicate minerals in Ni concentrates can produce viscous slags, generating problem during smelting (Pietrobon et al., 1997) due to a hardness of Mg silicates that is lower than that of sulfides. This may lead to a high proportion of fines. The so-called slime coatings may decrease the collector adsorption into the surface of sulfides, e.g., pentlandite, and decrease its hydrophobicity; or attach to their surface, decreasing the effectiveness in the flotation rate and hence, the recovery. The presence of these Mg silicates may still generate penalties from the smelters as they dilute the Ni concentrate grade.

On their research, Fornasiero & Ralston, 2005, simulated the behaviour of chlorite in Ni and Cu ores recovered using the xanthate collector. They observed that the presence of Cu activates chlorite, as the positively charged Cu is adsorbed into the surface of the negatively charged MgO silicate, promoting its flotation. Copper(II) can be in solution to speed up pentlandite flotation or also naturally occurring as a Cu sulfide. In the second case, chlorite activation is weaker. A pH value between 7 and 10 of the solution also contributes to increase chlorite partition into the concentrate. Ni may also trigger such phenomenon, but in a much lower extent. This is an important consideration as it is another case on which chlorite,

which is a hydrophilic mineral, may refer to the concentrate, in addition to when very fine particles are produced or when the silicate is locked within sulfides. Talc, on the other hand, is a hydrophobic phase that can dilute Cu and Ni concentrates in levels usually above 1-2 wt% (Connelly, 2019).

According to Pietrobon et al., 1997, and Eltham, 1973, soda ash could be used to increase dispersion in the pulp and increase Ni recovery and selectivity against Mg silicates. It is also suggested that the use of Carboxy Methyl Cellulose (CMC) group as an additional dispersant lead to the stabilization of Mg minerals after interacting with their surfaces and creating hydrogen bonding. Zhao, et al., 2015, however, stresses that CMC may not be very effective when dealing with low grade, fine or texturally complex Ni-Cu sulfide ores. Talc pre-floatation using frother but no collector, or talc deslime on cyclones after flotation, like it is used in Mt Keith in Western Australia, are other options for dealing with this Mg mineral (Connelly, 2019).

In addition to the effect of flotation efficiency, Mg minerals that report to the concentrate increase its Mg grade, requiring high smelting temperatures (Selby & White, 2011), around 1,600°C. Because of that, smelters usually apply limits for MgO content (Table 2) and MgO:metal and Fe:MgO ratios (Warner, et al., 2007).

1.3.1.2 Arsenic

High arsenic levels can decrease the concentrate value down to 50% of its London Metal Exchange (LME) value and for each 10 ppm As over 200 ppm, a penalty of 1 A$/dmt is levied (Selby & White, 2011). Since 2004, Cu concentrates with As levels above 5,000 ppm are not allowed in China (Wood Mackenzie, 2022). Among other elements such as Cd, Hg, Pb and Sb, As tends to be highly volatile during smelting. This increases the risk of emissions to the atmosphere and harm to the environment and human health (Fountain, 2013; Lane et al., 2016; Alloway, 2013). The conductivity of the valuable metal, such as Cu, can also be compromised by elevated As levels (Wood Mackenzie, 2022).

Differential flotation (Wood Mackenzie, 2022), the use of depressants and re-flotation of the concentrate (Connelly, 2019) can decrease As levels in the final concentrate. Selective pre-roast to volatize and oxidize As phases and then condense it for the generation of high-grade As concentrate (Connelly, 2019) is

another option for As removal from the Cu and Ni concentrate. The Toowong Process™ (Core Resources, 2023) removes As and Sb phases, including gersdorffite, by alkaline leaching, resulting in 90 wt% removal of these penalty elements from Ni and Cu concentrates.

1.3.2 Environmental impact by sulfidic mine wastes

As stated by Lottermoser, 2010, only a few percents of metals, such as Ni and Cu, are extracted out of the initial volume of ore that is exploited and then processed. Moreover, the continuous decreasing in average global discoveries leads to a change in the economic feasibility paradigms in the mining industry. Low-grade orebodies, which were considered uneconomic in the past, may be considered reserves today, increasing the proportion of what is considered mineral waste (Dold, 2020).

Among a series of variables that can be included in a geometallurgical model, some of them previously mentioned, early information on the potential environmental impact directly arising from mining activity can also be assessed. The exposure of sulfidic mine wastes to oxygenated environments, for instance, can lead to the generation of acidic solutions from redox reactions involving sulfides and gangue minerals (Lottermoser, 2010). The presence of organic compounds, such as graphite, can lead to spontaneous combustion hazards (Green & Borden, 2011).

During mineral exploration, mine companies may conduct preliminary assessments of Acid Mine Drainage (AMD) and Acid Rock Drainage (ARD). These assessments focus on the identification of likely AMD sources rather than on management solutions (Green & Borden, 2011). A zone of an ore body and host rock, or their resulting wastes, can be classified as acid-producing, neutral or acid-buffering, depending on mineral dissolution, oxidation and precipitation. These are controlled by chemical and mineralogical compositions and by a series of other variables such as mineral size, porosity, surface area, crystallography, mineral association, temperature, pH and microbiological activity (Lottermoser, 2010). Contaminated Neutral Drainage (CND) occur in the presence of neutralising minerals bearing toxic elements (Chopard et al., 2019). These behaviours are predicted by OBK and by the use of tests for the classification of representative samples as acid-generating or acid-consuming, at an early stage, directly on the ore

and before metallurgical pilot tests. This information can thus be included in a predictive model that will optimise later management and mine closure plans, and produce a more realistic feasibility study.

Sulfide minerals can be exposed in a mine environment, e.g., open-pit and underground mine, as it is developed, but it can also be in contact with the atmosphere as run-of-mine, that is mined as waste, or as tailings, after processing and recovering stages. In either way, these sulfides will most likely be dumped in piles or dams. The weathering of gangue mineralogy is of great importance, as they tend to behave as acid-buffers, consuming the hydrogen ions and decreasing the acidity in sulfidic wastes. That is, hydrolysis reactions occur, and silicate phases, for instance, react with H+ to form aqueous solutions or, most commonly, alter to secondary hydrous mineral phases. Carbonate minerals are dissolved in the presence of hydrogen ions or CO_2 and form HCO_3^- and H_2CO_3, increasing the pH of the system. Their weathering resistance also dictates the buffering potential. Carbonates have a much higher reaction rate, and thus, can rapidly neutralize produced acids (Lottermoser, 2010). Silicates, on the other hand, are considered to have up to intermediate weathering and reactivity, making them not as efficient acid-buffers.

Iron sulfides, such as pyrrhotite and pyrite, tend to be highly reactive in the presence of oxygen, resulting in rapid and efficient acidification of the environment. In addition, the release of Fe^{2+} as a result of the reaction to form H_2SO_4 enhances the acidification potential, as the former can be oxidized to Fe^{3+} and then hydrolysed, liberating more H^+. In this sense, pyrite has higher acidity potential than pyrrhotite as its Fe/S ratio is 0.5, whereas for pyrrhotite it can be as high as 1, thus, more acid can be generated from S reaction in pyrite per mole of mineral (Equation 1 and Equation 2 below). On the other hand, pyrrhotite is more reactive due to crystalline defects. In their work, Chopard et al., 2017, and Chopard et al., 2015, defined an oxidation rate of up to 8.2 mg S/kg/day and relative reactivity rate of 8.43 for pyrrhotite, while for pyrite the highest values were 1 mg S/kg/day and 4.8, respectively. Gersdorffite (NiAsS) had an oxidation rate of 93.6 mg S/kg/day and relative reactivity factor of 19.53, the highest among the analysed sulfides.

Equation 1 – Pyrite complete oxidation reaction:

$FeS_{2(s)} + 15/4\ O_{2(g)} + 7/2\ H_2O_{(l)} \rightarrow Fe(OH)_3(s) + 2\ SO_{4(aq)} + 4\ H^+_{(aq)}$

Equation 2 – Pyrrhotite complete oxidation reaction:

$Fe_{0.9}S_{(s)} + 2.175\ O_{2(g)} + 2.35\ H_2O_{(l)} \rightarrow 0.9\ Fe(OH)_{3(s)} + SO_{4(aq)} + 2\ H^+_{(aq)}$

At an exploration stage, when the access to kinetic and Net Acid Generation (NAG) tests (Miller et al., 1997) are limited, chemical or geochemical static tests and mineralogical static tests can be used for estimating Neutralization Potential Ratio (NPR or NP/AP) and Net Neutralization Potential (NNP), which are calculated using the Acidification Potential (AP) and Neutralisation Potential (NP). For NNP, NP is subtracted from AP. A sample is acid-generating if its NP/AP < 1 or NNP < -20 kg $CaCO_3$/t, within the uncertainty zone if NP/AP is 1-2 or NNP is in between -20 and 20 kg $CaCO_3$/t, or is acid-consuming if NP/AP > 2 or NNP > 20 kg $CaCO_3$/t, as displayed in Table 3 and Figure 2 (Price, 2009; Ferguson & Morin, 1991; Elghali A. et al., 2023).

Table 3 – NNP and NP/AP for acid-generating, uncertain and acid-consuming classification.

	NNP (kg $CaCO_3$/t)	**NP/AP**
Acid-generating	< -20	< 1
Uncertain	-20 to 20	1 to 2
Acid-consuming	> 20	> 2

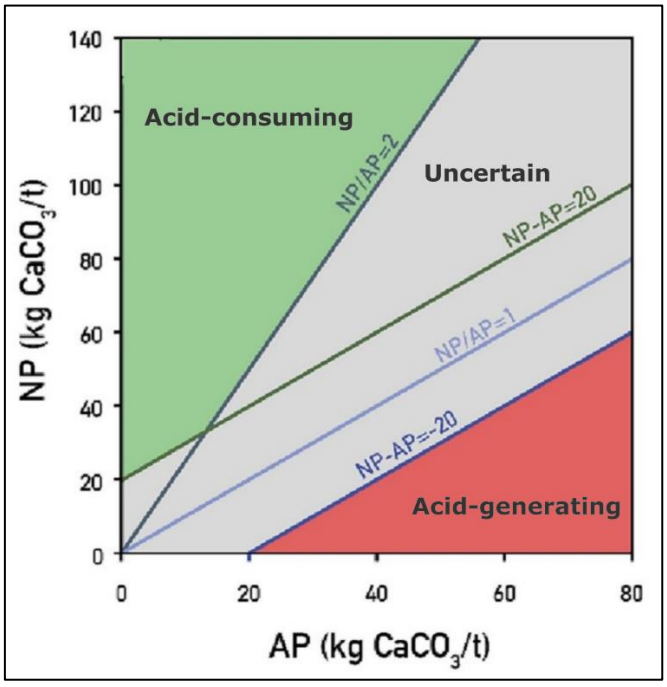

Figure 2 – Combined classification plot for both NNP and NP/AP. Modified after (Elghali, et al., 2023).

Different methodology is proposed in the literature for the calculation of AP and NP (Elghali, et al., 2023). For chemical or geochemical static tests, Sobek test is one of the first proposed, on which the Maximum Potential Acidity (MPA) or AP is calculated according to Equation 3, on which wt% S is the sulphur from sulfide (Sobek et al., 1978). The NP can be calculated using Equation 4, on which wt% C is the total inorganic carbonate content in the sample (Morin & Hutt, 2001). NP equation was later amended to consider Fe carbonates, given that the neutralization potential of siderite is very low (Plante et al., 2012). The liberation degree can also be used as a factor to be accounted in the equation (Elghali A. et al., 2018).

Reliable and representative modal mineralogy allows the AP and NP calculation using mineralogical static tests. The advantage is that the variability in mineralogy is being considered, instead of simplifying the NP as calcite content and the AP as pyrite content. It allows to account for different reactivity factors and acidity potential of mineral phases. This is useful because pyrite generates more acidity than pyrrhotite, even though pyrrhotite tends to be more reactive than pyrite (Karlsson et al., 2018). Moreover, silicates can also be accounted in the neutralization potential, instead of only carbonates. Their neutralization potential is lower, however, non-accounting for them can lead to an underestimation of the NNP. For mineralogical AP, Equation 5 (Paktunc, 1999) can be used. n_M is the number of moles of H_2SO_4 produced by the oxidation of one mol of sulfide phase, X_i is the percentage of sulfide content and ω_a and ω_i are the molecular weight of $CaCO_3$ and of the sulfide, respectively. The relative reactivity factor, which is defined by the oxidation rate of the mineral, is multiplied to the result to obtain a more robust estimation, when it is available (Chopard et al., 2017). In Equation 6, used to calculate NP, M_{CaCO3} and M_{Mi} are, respectively, the molecular weight of $CaCO_3$ and of the neutralising phase. C_{Mi} is the percentage of the neutralising mineral and R_i is the reactivity factor of neutralising minerals (Lawrence & Scheske, 1997).

Table 4 presents relative reactivity for groups of neutralising minerals at different modal compositions. NP calculations from mineralogical tests distinguishing non-oxidizable and oxidizable cations are also proposed in the literature (Paktunc, 1999; Plante, et al., 2012).

Equation 3:

$$MPA\ or\ AP\ =\ wt.\%S\ \times\ 31.25\ (kg\ CaCO_3/t).$$

Equation 4:

$$NP\ =\ wt.\%C\ \times\ 83.3\ (kg\ CaCO_3/t).$$

Equation 5:

$$AP\ =\ \sum_{I=1}^{K} 1000 \times n_M \times X_i \times \frac{\omega_a}{\omega_i}\ \ (kg\ CaCO_3/t).$$

Equation 6:

$$NP\ =\ \sum_{I=1}^{K} 1000 \times \frac{M_{CaCO3}}{M_{Mi}} \times C_{Mi} \times R_i\ \ (kg\ CaCO_3/t).$$

Table 4 - Relative reactivity in terms of the acid neutralisation capacity for selected minerals in soils, at pH 5, modified after (Karlsson et al., 2018).

Mineral class	Typical minerals	Relative reactivity Average mineral class content			
		100%	30%	3%	0.30%
Carbonates	Calcite, dolomite, magnesite, aragonite, brucite	1	1	1	1
Fast-weathering	Anorthite, olivine, garnet, diopside, wollastonite, jadeite, nepheline, leucite, spodumene	0.6	0.67	0.3	0.1
Intermediate-weathering	Enstatite, augite, hornblende, tremolite, actinolite, biotite, chlorite, serpentine, talc, epidote, zoisite, hedenbergite, glaucophane, anthophyllite, phlogopite, anthophyllite	0.4	0.2	0.03	0.01
Slow-weathering	Plagioclase (Ab100-Ab30), kaolinite, vermiculite, montmorillonite, gibbsite	0.02	0.013	0	–
Very slow-weathering	K-feldspar, muscovite	0.01	0.007	0	–
Inert	Quartz, rutile, zircon	0	7E-04	–	–

1.4 Motivation and objectives

Considering a Ni-Cu sulfide prospect in Finland as a case study, the present thesis intends to use multi-source analytical data as the input for the development of workflows to be used at exploration stage with the objective to increase the OBK and inform in advance possible flaws and/or opportunities to subsequent operational teams. The use of drill core Laser-Induced Breakdown Spectroscopy (LIBS) scanning data provides continuous and detailed information on modal mineralogy

and texture, aiming to enhance the sample representativeness and reliability. Data gathered with Mineral Liberation Analyser (MLA) and geochemical assay data complements the input information.

Mineralogical information is important for all the mining departments throughout the whole exploration pipeline: geology, metallurgy, and environment (Chopard et al., 2019). Considering yet the challenge of the mine industry of optimizing its resources while developing sustainable solutions and the available dataset, multiple opportunities can be explored on how to provide insightful, simplified and efficient information in order to inform, guide and optimize the whole mineral value chain.

Core scanning LIBS technology provides the mining industry an unprecedented opportunity for comprehensive OBK. Two main workflows are proposed for early geometallurgical and environmental assessments of the studied prospect, with the objective to investigate the potential of using data from drill core LIBS scanning for high- and low-grade zones characterization in exploration. Existing mineralogical and geochemical dataset is integrated to the analyses. The two scopes are: 1) the domaining of sulfide and penalty elements considering metal recovery via flotation (Kittelty & Smith, 2021) and 2) the early investigation on ARD at exploration stage. These workflows are aligned with current multidisciplinary collaboration, optimization and sustainable development of mining projects.

2 GEOLOGICAL CONTEXT

2.1.1 Nickel prospects in Finland

The European Nordic countries, and specifically Finland, have an important tradition in the exploration of Ni-sulfide magmatic deposits. From mid-20th century until nowadays, at least fifteen Ni mine activities have been recorded in Finland as reported by GTK – Geological Survey of Finland, with a total of almost 6 Mt Ni recovered (Makkonen, et al., 2017). The Talvivaara mine, located in the central part of the country, has alone produced around 1/5 of the total Ni exploited during this time period.

The economic potential of some areas in Finland are yet not completely explored, such as the Fennoscandian Shield, including the Svecofennian mafic-ultramafic intrusions in south Finland, where the case study prospect is located. The

Archean and Paleoproterozoic komatiites, komatiitic basalts and related mafic-ultramafic rocks (Konnunaho et al., 2015), are other fields also known for their Ni enrichment and economic potential. The Kevitsa Ni-Cu-PGE mine, located in north Finland, is one example of these intrusions, which is hosted in ultramafic to gabbroic rocks (Mutanen, 1997). Santaguida, et al., 2015, classified the deposit in “normal ore”, i.e., the ore bodies with similar contents of Ni and Cu, the high Ni grade ore, i.e., the ore bodies with high Ni/Cu ratios, and the “false ore”, with low Ni tenors and high pyrrhotite enrichment.

The Ni-Cu-(PGE) deposits of Finland are found mainly within greenstone belts and in the eastern and northern sectors of Archean terranes, composed of gneissic TTG terrains (Makkonen, et al., 2017). Many prospects record metal-content enrichment due to the occurrence of post-magmatic processes and can be subdivided in PGE-Ni-Cu deposits and Ni-rich, PGE-poor orebodies (Konnunaho et al., 2015). According to Makkonen, et al., 2017, most of the deposits hosted in komatiites present MgO contents lower than 25 wt%, and this may explain the lower grades and tonnages for these compared to those in Western Australia, e.g., Perseverance Ni deposit (Barnes et al., 1995) and Wildara-Leonora Belt (Thébaud et al., 2012).

Located in central-north Finland, the Archean Tornio-Näränkävaara Belt hosts the Portimo Complex, which is composed of layered intrusions from ultramafic gabbroic cumulates. These are PGE-enriched ore bodies associated with Cu-Ni-Fe sulfides, which are disseminated and grading into massive mineralised bodies (Makkonen, et al., 2017). The Koillismaa marginal intrusions and layered series form another complex located within this belt. They are thought to have been generated after the breakage of a single-layered intrusion during compressional period in the Paleoproterozoic, around 2.45 Ga (Karinen, 2010). Among all the mineralisation types recognized within the Koillisma Complex, Ni occurs as Cu-Ni-Fe sulfide disseminations in marginal series.

In central Finland, the low-grade Ni mineralisation Outokumpu Cu prospects occur near the Talvivaara area. These prospects are located within a Paleoproterozoic assemblage of metamorphosed and altered zones around serpentinised ophiolites that are enclosed by metaturbidites of 1.91-1.94 Ga

(Makkonen, et al., 2017). At Outokumpu, the massive sulfides are found in decametric to kilometric lenses having Ni contents up to 1500 ppm, and have their formation related to secondary and tertiary enrichments due to assimilation of sulphur-rich sediments and hydrothermal fluids driving the mixing between the different sulfide end-members (Makkonen, et al., 2017). The disseminated-type ore occurs in veinlets below the massive mineralisation and is enriched in Co and Ni. The Kokka-type Ni mineralisation is hosted mainly in carbonate-skarn rocks lenses with Ni contents of over 3000 ppm, in metric to decametric intervals and 0.79 wt% Ni grade (Kontinen, et al., 2006).

The Talvivaara in eastern Finland is another example of Ni prospect, which is the largest of its kind under exploitation in Western Europe. Here, Zn, Co and Cu are also associated with the Ni and are hosted in medium-grade black shales of the homonymous formation (2.0-1.9 Ga) within the Kainuu schist belt (Kontinen & Hanski, 2015). Rasilainen, et al., 2017, assessed the potential undiscovered Ni prospects in Finland. These authors estimated that 84% of the undiscovered Ni resources are related to contact- and reef-type PGE-rich prospects in central-north Finland, 9.6% are intrusion-related Ni-Cu in the Svecofennian belt, 5.6% are of komatiite type in the eastern area of the country and 0.8% are of the Outokumpu-type and occur in southeast Finland. Makkonen, et al., 2017, concluded that the exploration potential for Ni resources in komatiitic rocks is good due to the yet lack of information regarding these areas, despite the increasing data from geophysical surveys. For the contact-type prospects, the potential is also good given the high percentage of estimated undiscovered prospects. However, the grades are likely uneconomic.

2.1.2 Geological setting

2.1.2.1 Svecofennian Orogen

The prospect being studied is located in Finland, in the Paleoproterozoic Svecofennian Orogenic Belt (Figure 3). The orogen encompasses:

a) The NW-SE-trending primitive arc complex of 1.93-1.91 Ga in contact with an Archean craton basement to the NE of the area;
b) The Central Finland Granitoid Complex, which is the largest Svecofennian plutonic complex (Makkonen et al., 2008);

c) The Häme Belt in the southernmost area of the orogen;
d) The 1.89-1.87 Ga syntectonic arc complex in western and southern Finland (Korsman, et al., 1997; Nironen et al., 2006). Further divided as Pirkanmaa and Tampere belts. The first is composed of polydeformed and high-grade metamorphosed psammites, then turned into tonalitic migmatites, presenting a more mafic composition and intrusions with higher potential for Ni-Cu mineralisation. The Tampere is a medium-grade meta-volcanosedimentary belt.

Peltonen, 2005, described three main groups of mafic-ultramafic intrusions within the 1.89-1.87 Ga Svecofennian orogen. These groups are of higher interest for this thesis as some of them host Cu-Ni mineralisation, especially Group I.

Group I intrusions were emplaced in accretionary wedges and in transtensional shear zones during the collision of the Svecofennian arc and the north-eastern Archean craton. Given their syntectonic nature, deformation and assimilation of country rocks are common features. This type is the most important in terms of Ni-Cu sulfide mineralisation in Finland and are subdivided in the Kotalahti Ni-belt (Group Ia) presenting NW-SE trend in the suture zone between the orogen and the Archean craton, and the Vammala Ni-belt (Group Ib) located in the southwestern area of the orogen. The Kotalahti-type intrusions have elongated shape along the NW-SE fold axis trend, while the Vammala-type have a concentric shape related to the feeder zone of the system (Makkonen, 2015). The fast rise and relative low fractionation within shear zones could be one of the reasons for the Ni-sulfide saturation within Group I, according to Peltonen, 2005. Makkonen H. , 2015 described the belts in between amphibolite and granulite facies. In the Nivala area, located north-western the Kotalahti intrusion, Hitura and Makola are the main recognized prospects (Figure 3) presenting a magma with depleted and residual character: low tenors of incompatible elements and high Cr concentrations. Intense hydrothermal alteration results in obliteration of primary mineralogy, precipitation of chlorite, talc and serpentine and increase in the Al_2O_3/CaO ratio. They are hosted in graphite and sulfide-bearing metavolcano-sedimentary successions and felsic intrusions (Isohanni et al., 1985).

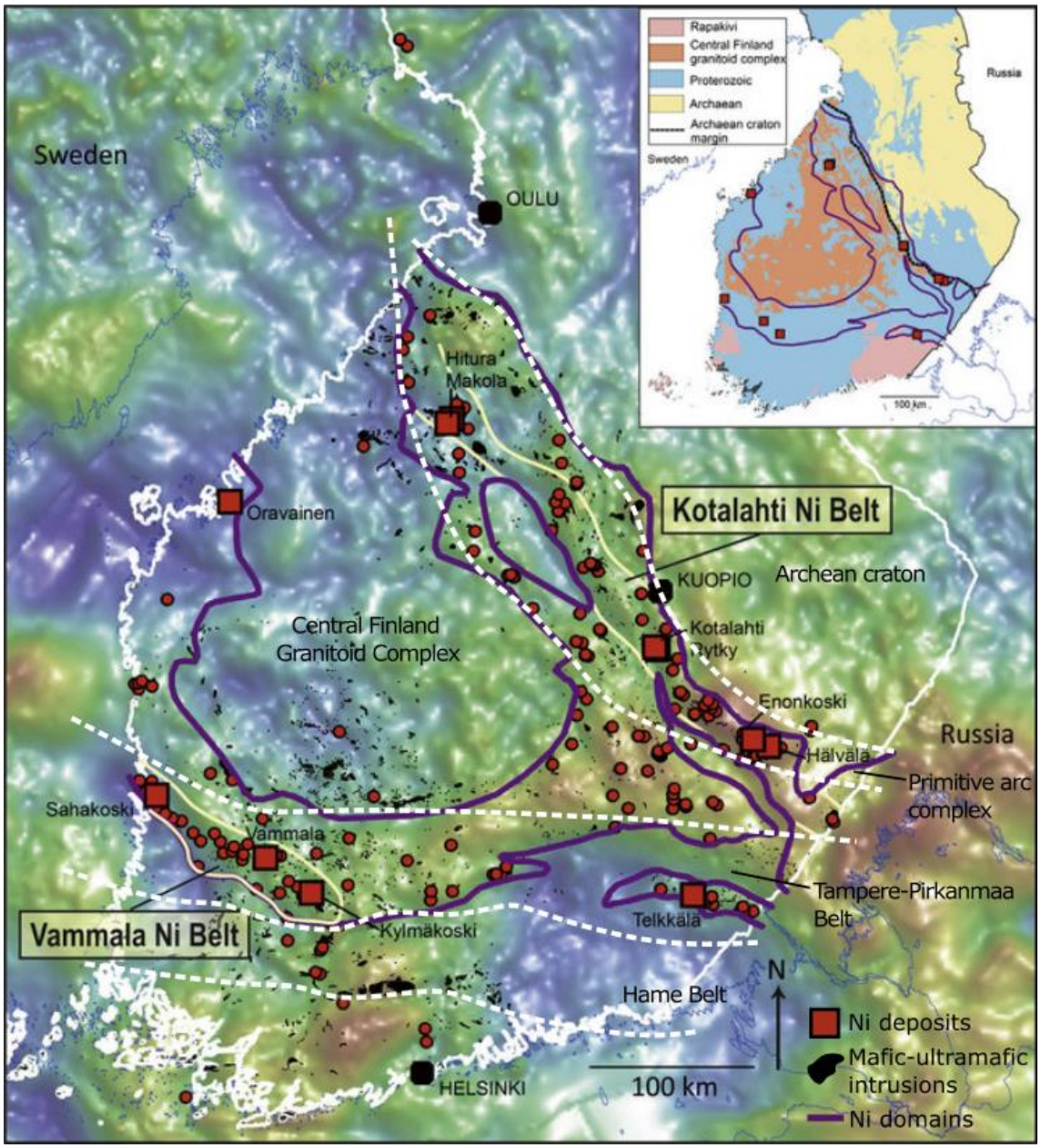

Figure 3 - Svecofennian orogen Bouguer gravity map highlighting the Ni domains in south Finland. Note that the main Ni prospects are located within Vammala and Kotalahti belts, which are part of Group I in the classification by (Peltonen, 2005). Maximum intensity is shown in red and minimum in blue. Modified after Makkonen, 2015.

Group Ia intrusions, which occur in the craton margin, are also found in the NE Archean basement and in its overlying sedimentary units. Some have already been mined for Ni-Cu sulfides, such as Laukunkangas in between 1984-1994 and Kotalahti, 1957-1987. Naistenrako, Niinimäki, Rytky and Törmälä are other examples of mineralised bodies (Makkonen et al., 2008). The host rocks for these intrusions are graphitic- and mica-gneisses, which may be found as xenoliths in the

ore bodies, and banded tonalite-trondhjemite migmatites. The bodies are also found within marine and continental sediments. Crustal assimilation can be as high as 40%. The strongly differentiated intrusions (Makkonen, 2015) are usually composed of cumulates of mafic-ultramafic mineral phases such as olivine, pyroxene, magmatic amphibole and plagioclase in layered and fractionated zones of peridotite, norite, gabbro, anorthosite and locally diorite. Local unfractionated ultramafic rocks are observed. Plagioclase as an intercumulus phase is a result of country rock contamination, leading to Si and Al increase in the magma (Makkonen et al., 2008). Mineralisation is usually hosted in the noritic zone overlying the peridotite, in Ni-Cu-sulfide- and phlogopite-rich intervals. These sulfides may be seen in intercumulus and disseminated textures or as massive veins and breccias in the contact zones. Pyrrhotite (Pyh), pentlandite (Pn) and chalcopyrite (Ccp) are the most common sulfides.

The Tampere and Pirkanmaa belts host the Group Ib intrusions, which present boudin, lenses and pipe shapes and are hosted by medium- to high-grade paragneisses, migmatised metapelites and post-kinematic granitoids. These bodies are formed by cumulates made of olivine, chromite, clinopyroxene and plagioclase, resulting in normal to reverse series of peridotite, pyroxenite and gabbro. According to Makkonen H., 2015, these are less differentiated than type Ia. Clinopyroxene, orthopyroxene, amphibole and phlogopite are observed as intercumulus phases. Neosome veins crosscut the intrusions as a result of the synchronous nature of their formation with the peak of metamorphism and deformation in the orogen. This fact and the absence of cooling haloes in the contact zone suggest a low temperature gradient, as described by Peltonen, 2005. Ni-Cu-Fe sulfides such as Pn, Ccp and Pyh are observed as interstitial phases within the cumulate texture and sometimes as veinlets as a result of later remobilization. Vammala, Porrasniemi and Kaipola are some examples of Group Ib intrusions.

The Mg-content in the primary magma of Group I is around 10-12 wt% MgO and may indicate a relatively evolved ultramafic parental magma. Makkonen H., 2015, inferred that metatholeiites generated in an environment of back-arc were the source for the mafic-ultramafic melts that generated the intrusion. The assimilation of crustal host rocks can also be the reason for the increase in the silica content and

early orthopyroxene precipitation. The R factor varies in between 200 and 1300 (Makkonen, 2015). In fact, it is observed that the intrusions hosted in the Archean crust or in the Primitive arc, composed of terrigenous and chemical metasedimentary successions, show higher orthopyroxene and sulfide contents, probably due to the higher SiO_2 contamination, as well as due to the assimilation of carbonaceous and calcareous sulfidic black schists (Peltonen, 2005). In Group Ib, H_2S- and C-O-H-S-rich fluid circulation may also have played a role in the Zn and S partition into the mafic melts. The Ni-Cu mineralised zones are found as intercumulus bodies at the base of the stratigraphic sequence, however, remobilization due to metamorphism and consequent formation of offset accumulations in veins, shear zones and contacts are also observed. Vammala-type is clinopyroxene-dominated and enriched in CaO, while Kotalahti-type is orthopyroxene-plagioclase-dominated and more enriched in Al_2O_3 (Makkonen, 2015). In Rytky and Niinimäki intrusions, both from Group Ia, the Ni-content in olivine ranges from low to high, indicating probable sulfide melt separation in between these extremes, resulting in Ni partition into the sulfide melt and indicating ore formation (Makkonen et al., 2008).

Ni average grade can vary from less than 1 wt% in disseminated ores, which are the most common, to up to 7 wt% in massive ones. Its content in sulfides is at 2-14 wt% and the ratio Ni/Cu varies in between 1-4 (Makkonen, 2015). Kotalahti-type offset mineralisation presents the highest grades, around 3-6 wt%, as a result of early contamination, segregation of sulfide melts at low levels and later migration of the Ni-rich sulfide melts into low-pressure zones in the wall rock due to deformation and generation of syn-intrusion fracturing and brecciation.

Group II intrusions, hosted in the Häme Belt, present low mineralisation potential and are located in the southern portion of the arc complex, in south Finland. These are synvolcanic, brecciated to layered peridotite, pyroxenite gabbro, gabbronorite and diorite intrusions. Disseminated sulfide and telluride occurrences are described in the contact zones. Ti-Fe-P-rich gabbroic intrusions form, together with granitoid plutons found in central Finland, a post-kinematic bimodal system called Group III, which is hosted in the Central Finland Granitoid Complex. This was

a result of later extensional and transtensional events in the Svecofennian orogen. Ni-bearing metapicrites are also found within this complex (Makkonen, 2015).

2.1.2.2 Prospect case study geology

The prospect area is a mafic-ultramafic, conduit-type, pipe-shaped cluster of intrusions hosting Ni-Cu sulfide mineralisation in central Finland, in the region of the historical mines of Hitura and Makola (Figure 3) (Isohanni et al., 1985). The area was initially surveyed in the 1960's by the GTK. The magnetic and IP anomalies were drilled, resulting in Ni grades of 0.2-0.3 wt% and Cu, 0.11-0.2 wt%, recovered from 6 DHs. The Finnish company Outokumpu also drilled another 9 holes in the area in the 1960's. From 2018 to 2020, the company which currently holds an exploration licence of the prospect carried on re-logging, re-assaying, geophysical surveys and another drilling campaign, with 7 DHs totalling 2400 meters.

According to internal report (Metso, 2022; Evans, 2019) and Isohanni et al., 1985, the country rocks in the Nivala area are composed of gneissic-granitoid rocks to migmatite biotite gneisses with graphite and sulfide-bearing biotitic schistose parts. Disseminated pyrite and pyrrhotite are observed. Gneiss and schist present high Th and moderate Zn, C, V and U concentration. The prospect is composed of medium-grained unmineralized primitive mantle gabbro and coarse-grained sulfide-saturated gabbro (Figure 4). Ultramafic rocks are restricted to pyroxenite veins in country rocks and autoliths in gabbro, peridotite and hornblende-gabbro, all presenting minor sulfide content. Quartz-, plagioclase- and biotite-rich felsic veins with tonalite, granodiorite and quartz-monzodiorite composition are observed, sometimes cross-cutting the gabbro. They can contain sulfides with Ni grades > 1 wt%. At surface, the intrusion has a north-south-trending outline, extending for more than 500 meters in this trend and up to 50 m east-west.

Main mineralisation is observed in variably textured, or simply vari-textured gabbro, with high anisotropy and rapid short-range variations in grain size and mineralogy (Figure 5; Figure 6). Also called taxitic, this texture is commonly associated to net-textured sulfide breccias (Barnes et al., 2017). Cu/Zr ratios are over 10 in mineralised zones, commonly presenting pegmatitic grain size, high plagioclase, and SiO_2 contents typically below 50 wt%. MgO and Cr also tend to be higher in these zones, >7.5 wt% and >200 ppm, respectively, and up to 21 wt%

MgO in pyroxenite. On the other hand, high Th/Nb, Gd/Yb and Lm/Sm in general indicate high crustal contamination and lower grades. Pyrrhotite, pentlandite and chalcopyrite are the main sulfides, occurring in disseminated, blebby and short intersects of semi-massive texture. The tenors are usually relatively high, over 7 wt%. Tenor is defined as the concentration of a metal recalculated to wt% sulfides (Kerr, 2003). A high tenor can make the prospect more valuable, since it means that the metal of interest is in high concentration within the ore, leading to improved recoveries. The Santa Rita Ni sulfide deposit in Bahia, Brazil, has Ni tenors ranging from 15 to 25 wt% (Barnes et al., 2011), while in the nickel sulfide prospects at Voisey's Bay, in Labrador, Canada, the range is around 3-9 wt% (Lightfoot et al., 2011). The Ni grades in the prospect's gabbro with Cu/Zr > 10 tend to be similar to those in peridotite, around 0.3 wt%, however, tenors are higher in the former.

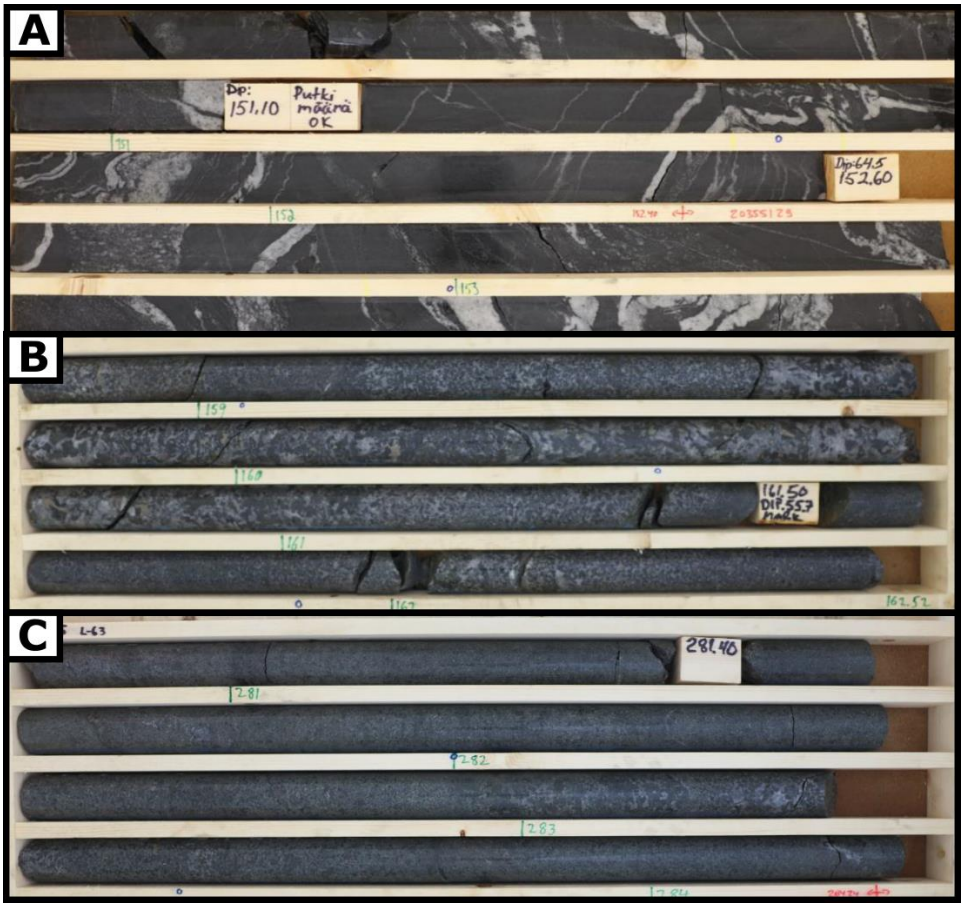

Figure 4 – Core photograph examples of the different lithologies found in the prospect area. A) Country rock migmatite gneiss with biotite-rich melanocratic bands interlayered with plagioclase-quartz-rich leucocratic bands. B) Vari-textured, fine- to coarse-grained mineralised gabbro. C) Mostly fine-grained unmineralized gabbro. Each drill core interval in the boxes is 1-meter long.

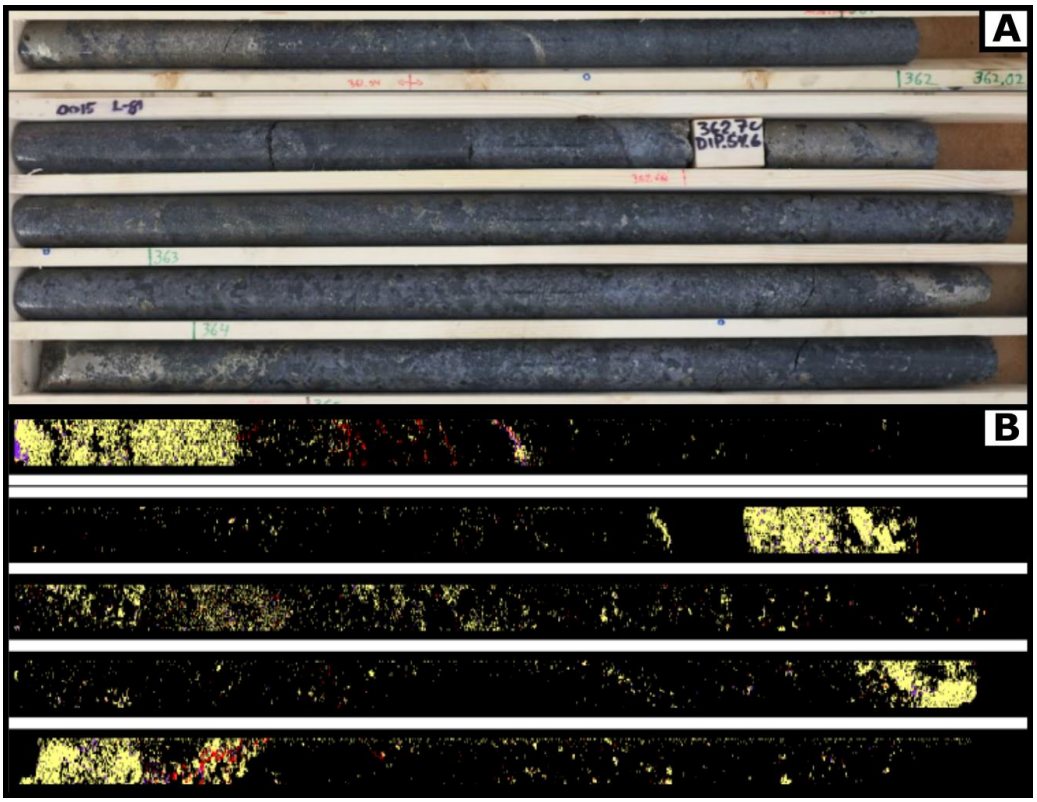

Figure 5 – Semi-massive to disseminated sulfide in vari-textured gabbro from DH0015. A) Core photograph. B) LIBS low resolution core scanning with sulfide mapping image. Yellow: pyrrhotite; purple: pentlandite; red: chalcopyrite.

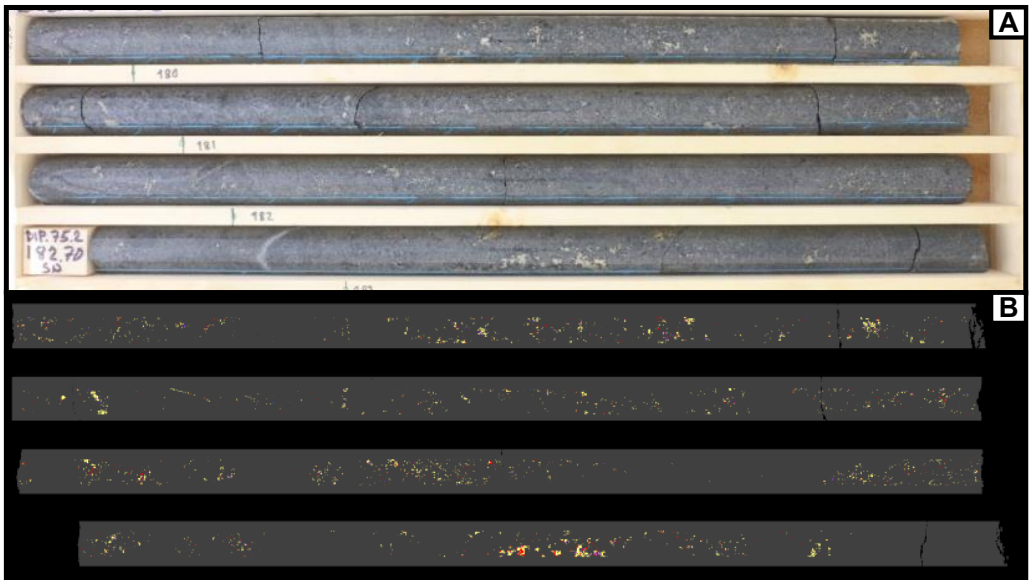

Figure 6 – Disseminated sulfide in vari-textured gabbro from DH0016. A) Core photograph. B) LIBS intermediate resolution core scanning with sulfide mapping image. Yellow: pyrrhotite; purple: pentlandite; red: chalcopyrite.

Gangue mineralogy is mainly composed of biotite, ferrosilite, hornblende and plagioclase, in both the country rocks and the intrusive rocks (Table 5). Biotite and plagioclase averages in country rocks, i.e., gneiss and schist, are higher than in the intrusion, i.e., gabbro and ultramafic, which is amphibolite, pyroxenite and peridotite: for biotite, 23 wt% in the schists to 25 wt% in the gneiss, whereas in the gabbro, biotite content is 7 wt% and ultramafic is 8 wt%. For plagioclase, 48 wt% in the gneiss to 55 wt% in the schist, whereas in the gabbro, plagioclase content is 39 wt% and ultramafic is 10 wt%. For both ferrosilite and hornblende, the contents in the intrusive rocks are in general higher than in the country rocks. Ferrosilite abundances in the gneiss and schist are 8 and 0.5 wt%, respectively, while for gabbro and ultramafic it is 6 and 21 wt%, respectively. Hornblende abundances in the gneiss and schist are 5 and 10 wt%, respectively, while for gabbro and ultramafic it is 35 and 43 wt%, respectively. Quartz abundances are usually higher in the country rocks: in the schist and gneiss, 5 and 9 wt%, respectively, and lower than 1 wt% in the intrusive rocks. Talc is common in pyroxenite intervals, and prehnite, mainly in gabbro. Calcite is mainly observed in veins and K-feldspar is mainly associated to the gneiss. Chlorite is observed as a minor phase throughout all intervals and accessory minerals are apatite, chromite, ilmenite, titanite and tourmaline. Garnet is also reported within gabbro intersects.

Table 5 – LIBS modal mineralogy average abundances (wt%) for different lithologies in the prospect area.

Mineral	Gneiss	Schist	Gabbro	Ultramafic
Apatite	0.04	0.09	0.02	0.01
Biotite	25.29	22.92	6.88	7.97
Calcite	0.02	0.08	0.03	0.02
Chalcopyrite	0.01	0.01	0.12	0.10
Chlorite	1.00	0.84	1.06	1.73
Chromite	0.07	0.00	0.01	0.04
Ferrosilite	8.34	0.48	6.43	20.57
Hornblende	5.07	10.42	34.80	43.34
Ilmenite	0.02	0.04	0.05	0.02
K-Feldspar	1.59	0.80	0.29	0.20
Pentlandite	0.00	0.00	0.14	0.13
Plagioclase	48.03	55.22	39.35	10.53
Prehnite	0.52	3.51	7.67	1.22
Pyrrhotite	0.08	0.16	0.53	0.50
Quartz	8.79	5.32	0.68	0.74
Talc	0.14	0.01	1.10	12.14
Titanite	0.01	0.10	0.26	0.09
Tourmaline	0.98	0.00	0.57	0.64

3 MATERIAL AND METHODS

This chapter introduces the input analytical methods, applications, tools and datasets employed in the development and interpretation of workflows and assessments on the high-grade zone for mineralisation and penalty elements characterization, and on the low-grade and barren zones for acid rock drainage assessments. Because of that, the detailed description of the adopted procedures and workflows for each one are presented in their respective subsequent chapters (see chapters 4 and 5).

3.1 Analytical instrumentation

3.1.1 LIBS

LIBS is the acronym for Laser-Induced Breakdown Spectroscopy. The ablation of the surface of a sample with a pulsed laser generates a high-temperature plasma that is collected in the form of photons emitted after the plasma cools down

(Harmon et al., 2019). These are separated in characteristic wavelengths in spectra and detected to determine the presence of elements, calculate modal mineralogy, estimate geochemistry and provide elemental and mineralogical map (Figure 7). The plasma is formed in small area of tens to hundred microns, allowing the analyses of single grains, inclusions and zonation, which is useful for mineral exploration. One of the greatest advantages of LIBS compared to other analytical techniques is the detection of light elements such as Li, C, F, Na and Mg, and detection limits are in the ppm range. High energy potential elements such as Fl and Cl have weaker emissions and higher detection limits. Matrix effects are critical for quantitative data acquisition from LIBS, thus, calibrations against reference materials are necessary (Harmon et al., 2019). It is a fast-acquisition, relatively inexpensive technique with easy deployment to even harsh and remote localities (Rifai et al., 2022; Fontana et al., 2023). The flexibility of LIBS makes it a fit-for-purpose tool: resolution, for instance, can be adjusted as a function of acquisition time, volume of data and level of detailed needed at a certain stage of the project. LIBS is capable of scanning drill cores and acquiring thousands of measurements per second (Rifai, et al., 2022). Drill core LIBS scanning for mineralogy and chemistry acquisition in exploration projects provides a series of opportunities, such as reduced delivery time, increased time focused on interpretation rather than manual logging, real-time decision and improved data density and reliability for different variables.

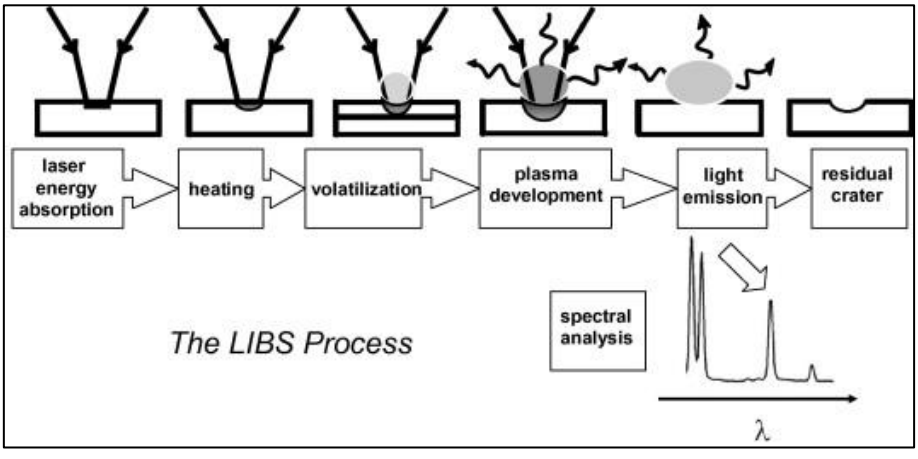

Figure 7 – LIBS acquisition workstream. From Harmon et al., 2009.

LIBS analysis for this work were conducted by LUMO Analytics Ltd, Finland (https://www.lumoanalytics.com/) using a 1064 nm Q-switched diode-pumped solid

state laser source with a 32.5 µm laser beam size, and pulse energy ~500 mJ (millijoule) at repetition rates of up to 1kHz and two spectrometers, which together cover a spectral range from 200 to 950 nm, at resolution of ~0.4 mm (Table 6). Sample preparation involves a laser cleaning step before LIBS analysis. Mineralogical classification is conducted via Spectral Angle Matching (Figure 8). The data acquisition workflow consists on the generation of spectral responses on each spatially-referenced laser spot to generate elemental occurrence and, through spectral matching, the calculated associated mineralogy using a pre-defined library. Scanning resolution is determined by the spacing between each spot analysis.

For purposes of simplifying terminology, exclusively in this thesis, low resolution is referred as the scanning with pixel sizes of 4760 µm and 1587 µm perpendicular to the core length (x axis), and 1000 µm parallel to the core length for both (y axis). For moderate resolution, with a pixel size of 238 µm in x axis; and high resolution, with a pixel size of 119 µm in x axis. For y axis, pixel size is 500 µm for both moderate and high resolutions (Figure 9). The laser crater size is around 30 µm, whereas the step distance, or distance between craters, is of 60 µm in the highest resolutions. That is, the step size is normally slightly larger than the spot size, in order to consider the ejected blanket formed after the crater formation and material deposition around it. The step distances in x and y define the pixel size. The mineral abundance is calculated according to the percentage of pixels of a certain mineral within a defined sample composite length. The sample composites that were used followed the geochemical sampling intervals, ranging from 0.3 to 2.5 m.

Table 6 – LIBS technical specifications.

Laser wavelength	1064 nm
Pulse energy	~500 mJ
Repetition rate	1kHz
Spectral range	200 to 950 nm

The LIBS mineralogy QA/QC was based on collection of reference material and mineralogy validation of project specific samples with SEM-MLA. In this project, all samples from DH0005 analysed by SEM-MLA (see section 3.1.2) were also analysed by LIBS. Mineralogy and EDS major element mineral chemistry of main forming minerals from SEM-MLA were used for the mineralogy QA/QC.

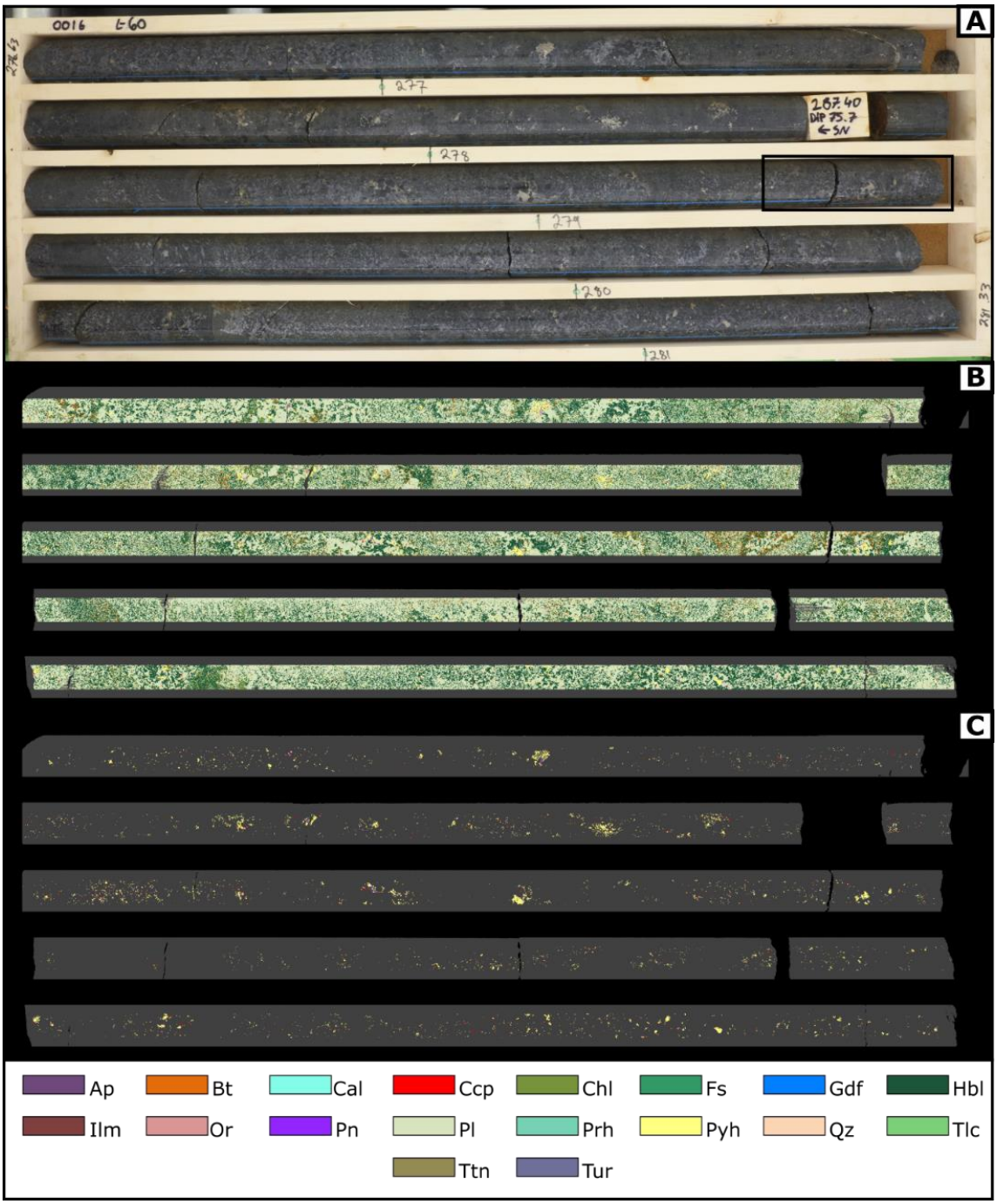

Figure 8 – High-grade zone in KUS0016. A) Core photo with area of detail showed in Figure 9; B) LIBS mineral map; C) LIBS sulfide map.

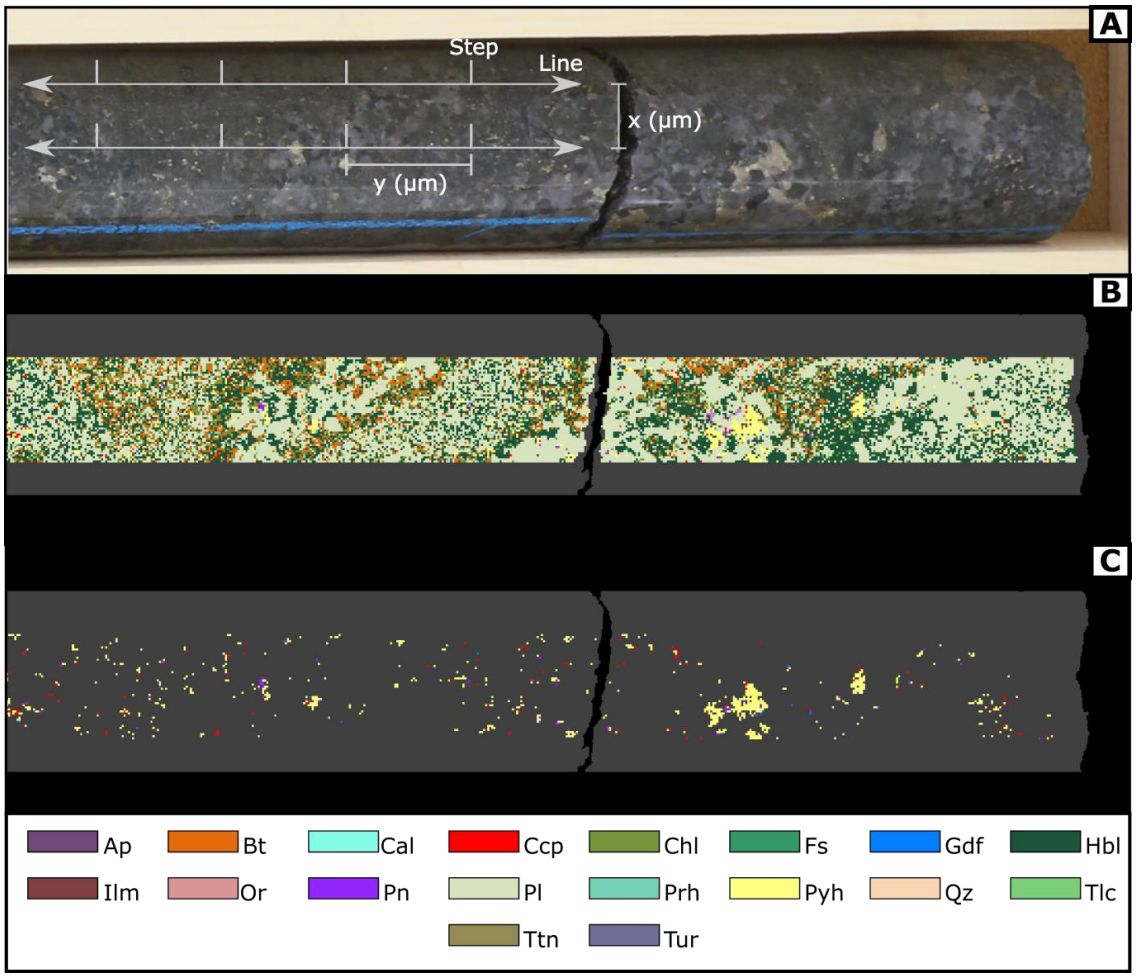

Figure 9 – Detail of high-grade zone in DH0016. A) Core photo with schematic drill core LIBS scanning method; B) LIBS mineral map; C) LIBS sulfide map.

3.1.2 MLA

Modal mineralogy, major element mineral chemistry and texture of 41 drill core samples were carried out. Samples were prepared as thin discs (4 mm) cut along half-core of DH0005 in the interval 237-326 m. The samples were carbon-coated and analysed using a FEI MLA Quanta 600 Scanning Electron Microscope (SEM) coupled with a field emission gun and EDS – Energy Dispersive X-ray Spectrometer (EDAX/BRUKER). Analyses were done using the GXMAP measurement mode on the Mineral Liberation Analyser (MLA), with systematic EDS analysis for major silicates, oxides and sulfides. Analytical settings were carried at 125 times magnification, analytical working distance of 10 mm and voltage 15 kV. QA/QC for mineralogy and element quantification were carried out using Certified Reference Materials and matrix-matching in-house reference minerals.

3.1.3 Geochemical Analysis

Geochemical analyses were made by ALS Global Laboratory (https://www.alsglobal.com/) using 3 different methods (Table 7): 1) major and trace element geochemistry from four-acid digestion via ICP-MS (Inductively Coupled Plasma Mass Spectrometry), including the add-on for REEs. 2) ore grade analysis via four-acid digestion and ICP-AES (Inductively Coupled Plasma Atomic Emission Spectroscopy). 3) total S and C by induction furnace and infrared (IR) spectroscopy.

Table 7 – Methods for geochemical assay analysis.

Method	Description
1	Multi-Element Suite with Au, Pt, and Pd from the ICP-MS analysis. Ag, As, Co, Cu, Mo, Ni, Pb, S, Zn over limits, typically > 10,000 ppm, via four acid digestion and ICP finish, all others with ICP via dilution.
2	4AD/ICP-AES ore grade
3	Total Sulphur and Carbon by Induction Furnace and IR Spectroscopy

3.2 Dataset and analytical tools

The software ioGAS™ v. 8.0 (Imdex Ltd) and Imago and Leapfrog Geo v. 2023 0.1 (Seequent) were used for data processing and analysis.

The processed datasets were: a) company internal reports, loggings and interpretations provided by the project team; b) the geochemical assays of 3806 samples from 22 drill holes, totalling around 7325 meters; c) 4878 meters of drill core LIBS scanning data (Table 8), which include mineral map, calculated modal mineralogy, estimated geochemistry and extracted textural features; d) and 41 samples from MLA analysis of DH0005.

Table 8 – Drill core LIBS scanning dataset.

Drillhole	From	To	Interval (m)	Resolution
DH0005	238.4	241.7	3.3	Low
DH0005	241.7	309.6	67.9	High
DH0005	309.6	314.3	4.6	Moderate
DH0005	314.3	327.0	12.7	High
DH0008	4.4	464.6	460.2	Low
DH0009	4.3	9.1	4.8	Low
DH0010	5.7	479.4	473.7	Low
DH0012	7.6	344.4	336.8	Low
DH0013	4.6	188.4	183.8	Low
DH0014	11.5	167.3	155.8	Low
DH0015	2.5	582.1	579.6	Low
DH0016	7.2	293.7	286.5	Moderate
DH0017	1.5	233.7	232.3	Moderate
DH0018	4.6	596.4	591.8	Moderate
DH0019	6.2	196.4	190.2	Moderate
DH0020	5.0	516.0	511.0	Moderate
DH0021	3.5	359.1	355.6	Moderate
DH0022	4.0	431.4	427.4	Moderate
Total			4877.9	

3.3 High-grade zone definition

The Ni and Cu concentrations in the prospect are displayed in Figure 10. Nickel grade shells were modelled for the prospect, and divided into zones in which Ni < 0.1 wt%, Ni 0.1-0.2 wt%, Ni 0.2-0.3 wt%, Ni 0.3-0.4 wt%, Ni 0.4-0.5 wt% and Ni > 0.5 wt%. The cut-off of 0.2 wt% was set to define the high-grade and potential ore zone in this study. Thus, the intervals and samples within the 0.2 wt% boundary were considered high-grade (Figure 11), and those with Ni < 0.2 wt% were considered low-grade or barren, and potentially classified as waste. Starting from 7.5, 2.5-range isosurfaces or shells were also modelled for Cu/Zr ratio. The isosurface for Cu/Zr > 20 is very similar to that of Ni > 0.2 wt%. A total of 792 samples are part of the high-grade zone, which represents around 21% of the total assay samples. The high-grade zone definition does not consider economic aspects or guidelines for reserves reporting and aims only to delimitate a volume that is representative of typical mineralisation of this type of prospect. It can potentially be converted into ore zone once further information is retrieved.

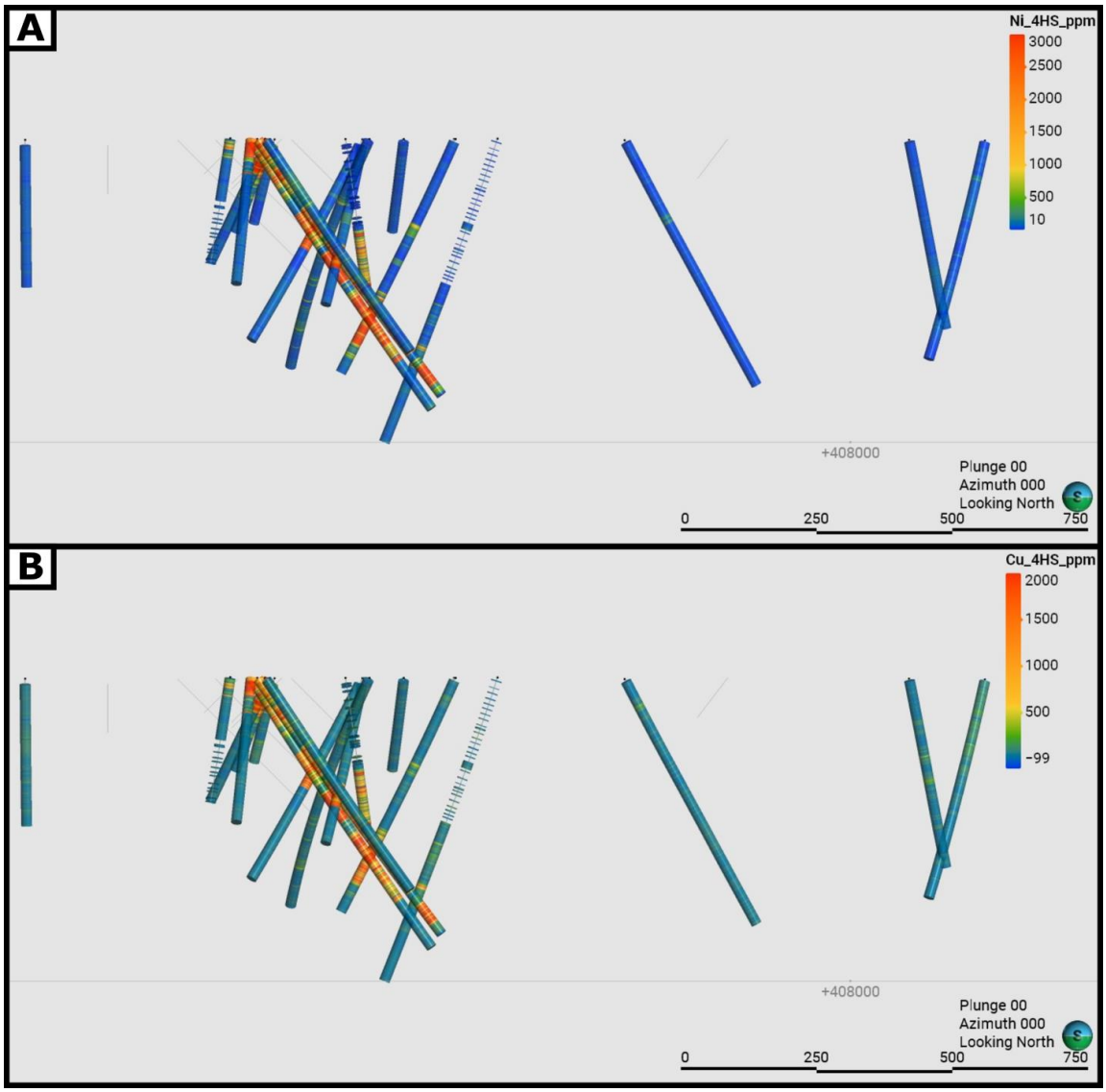

Figure 10 – DH view looking north. A) Ni concentrations; B) Cu concentrations.

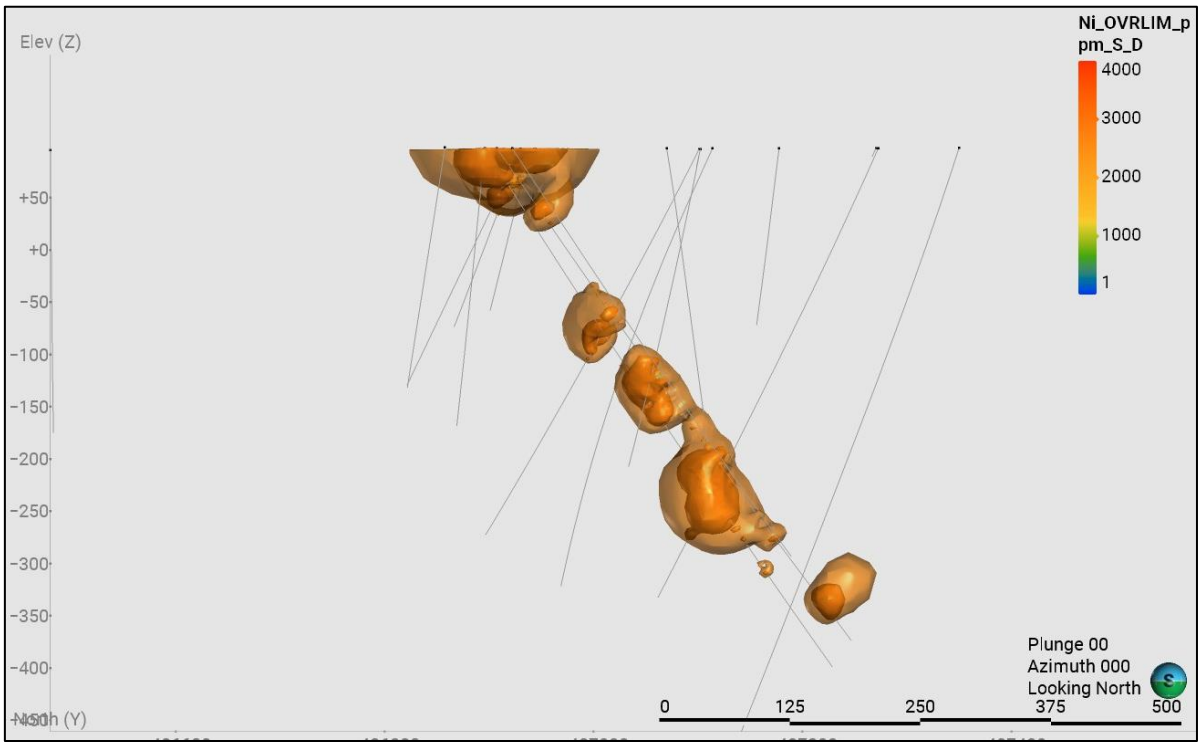

Figure 11 – Ni > 0.2 wt% 3D volumes for the prospect with some of the DHs traces.

Ni and Cu tenors were calculated following two different methodologies, both described in Kerr, 2003. The first considers 36.5 wt% S for pure sulfides, as usually pyrrhotite is the dominant sulfide phase, here referred as average sulfide method. The second accounts for the sulfide minerals individually, based on stoichiometric calculations to estimate the abundances of each sulfide, e.g., pentlandite and chalcopyrite, to then calculate pyrrhotite abundance and tenors (Naldrett et al., 2000; Li et al., 2001). Here referred as stoichiometric method. Only samples with S > 1 wt% were considered. Nickel and Cu tenors for both methods are very well correlated (Figure 12 – Calculated tenors (wt%) using stoichiometry method against average sulfide method for A) Ni and B) Cu.). Average Ni tenors are 7.52 wt% and 8 wt%, using average sulfide and stoichiometry, respectively, whereas for Cu, the averages are 4.04 wt% and 4.17 wt% (Table 9).

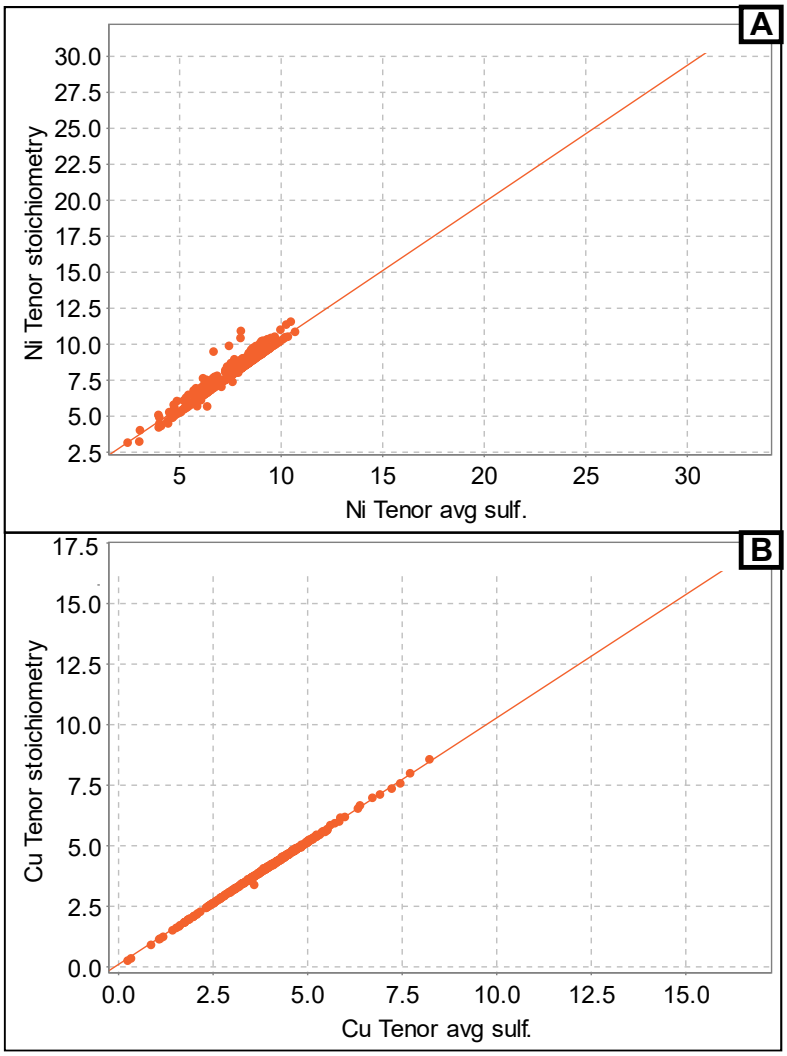

Figure 12 – Calculated tenors (wt%) using stoichiometry method against average sulfide method for A) Ni and B) Cu.

Table 9 – Ni and Cu tenor calculations for the high-grade zone using average sulfide and stoichiometry methods.

Tenors – high-grade zone	Ni Tenor avg sulf.	Ni Tenor stoichiometric	Cu Tenor avg sulf.	Cu Tenor stoichiometric
No. samples	501	460	652	460
Min. (wt%)	2.44	3.17	0.24	0.26
Max. (wt%)	33.23	31.38	16.77	17.03
Mean (wt%)	7.52	8.00	4.04	4.17

4 MINERALISATION AND PENALTIES DOMAINING

4.1 Workflow

The workflow described below provides a general overview of the approach followed in order to use LIBS information, additionally to MLA and geochemical

assay data, to provide insights in terms of chemistry, mineralogy, e.g., sulfide speciation, and textural variations within the high-grade zone. Estimations on the mineral and element concentration of the high-grade zone, mainly regarding penalty element enrichment, are also applied as a tool for defining domains that will inform next stages of the project. Even though this is specific methodology developed for the case study prospect, the general aim of this work is devising an approach that can be used as a guide for ore body characterization at exploration stage in other exploration projects (Figure 13).

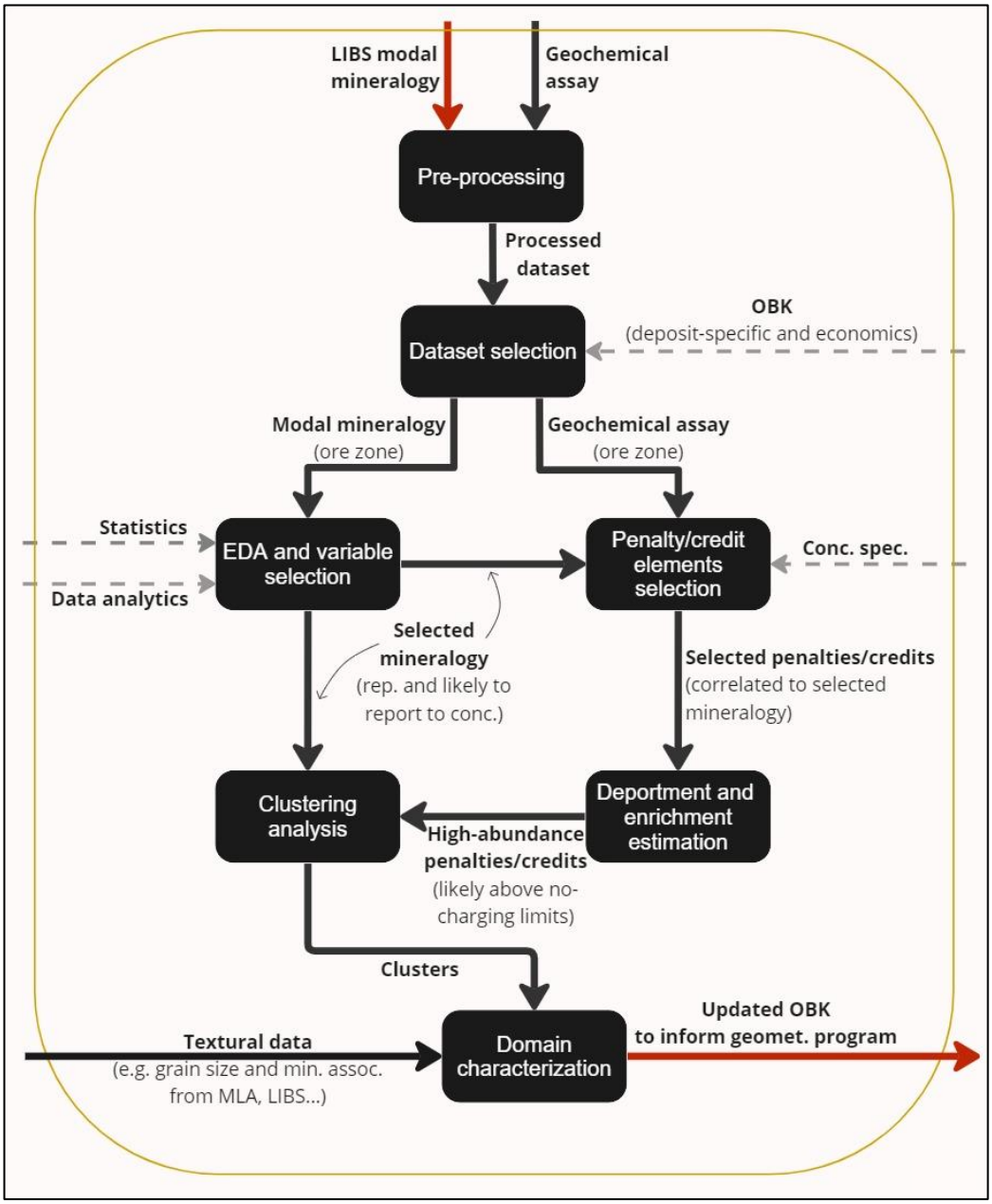

Figure 13 – Workflow for the use of modal mineralogy, additionally to geochemistry and textural data, for OBK enhancement.

4.1.1 Pre-processing

As a pre-processing stage, for modal mineralogy from LIBS, zeros and nulls were replaced by one half of the minimum value present in the data to avoid biases in the estimates. Zeros represent minerals not detected, and nulls, minerals not analysed.

Compositional data, such as geochemical assay and modal mineralogy, is a type of sample space conveniently selected to exploit the information therein contained. It is defined as non-negative that sum up to a constant, e.g., 100 wt% (Buccianti & Grunsky, 2014). This relative character of compositional data given by the sum constrain can lead to spurious correlations, and the use of ratios can eliminate these paradoxes as these are constant (Greenacre, 2021).

Centered log ratio (CLR) was the transformation applied to “open” the dataset previous to performing correlation and clustering analysis. It is an isometric transformation defined by the log ratio to the geometric mean of the variables in each sample (Filzmoser & Karel, 2009). It allows the data to vary from – infinity to + infinity, as the sum of the variables of each sample is zero. Since zeros and nulls were previously replaced, there was no need to apply more robust transformations, such as α-transformation, that includes the α factor, varying from 0 to 1, with the application of Isometric log ratio (ILR) when it tends to 0 and linear transformation when tending to 1 (Clarotto et al., 2022). It is also worth noticing that CLR was applied separately to each dataset with closure, e.g., mineralogy separated from geochemical assay. After transformation, the dataset was selectively scaled when necessary, using the Z-score (robust) option in ioGAS, which is used to adjust the distribution into a defined range and allow comparison, visualization and clustering of the data without generating bias towards variables with higher abundances. That is, domaining could end up being more sensitive to chlorite just because this mineral is more abundant than the sulfides. The observed value is subtracted from the population mean and divided by the standard deviation. The Z-score normalization (Patro & Sahu, 2015) was applied in the cases where the clustering algorithm did not internally perform any scaling.

4.1.2 Data selection and preliminary analysis

Detailed exploratory data analysis (EDA) (Tukey, 1977; Dodge, 2008) had great importance for analysing the characteristics, associations and behaviour of the data, prior to applying any model. EDA can be described as a mode of analysis used for exploring and discovering phenomena in the data (Jebb, et al., 2017). Statistics, such as using probability plots (Figure 14), correlations and geospatial distributions of modal mineralogy, geochemical assay and textural data were analysed for further data selection. It was used, for instance, Principal Component Analysis (PCA) (Jolliffe, 2013) for all mineralogy in the library, for spatial similarity identification together with correlation matrixes for dimensionality reduction. In this sense, the exploration of the dataset included the use of different clustering algorithms to understand the sensitivity of the domains to each variable. That is, the selection prioritized minerals that presented clear distinction in different clusters. Tourmaline, quartz and ilmenite, for instance, have roughly homogeneous distributions along the intervals, thus they are not efficient in domaining.

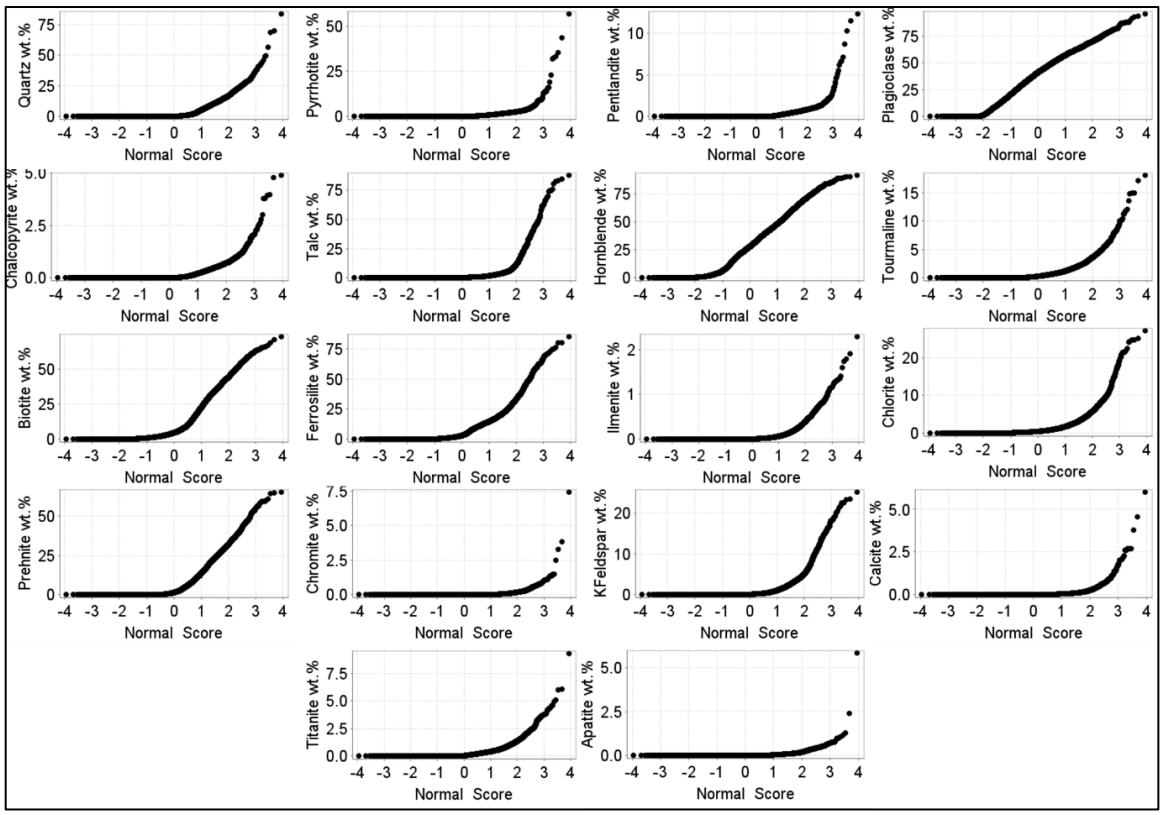

Figure 14 – Probability plot for mineralogy, including whole LIBS dataset. Normal score represents the Z-score from a standard normal distribution, being mean = 0 and a standard deviation = 1.

Two intervals were selected (Table 10) and similar workflows were applied for each one (see section 4.2). They were interpreted separately as they were analysed using different resolutions and configuration (MVP). Only intervals at a minimum of moderate resolution were considered, due to the higher confidence in the modal mineralogy.

Table 10 – Mineralized intervals selected for domaining.

	From	To	Interval (m)	Resolution
DH0005	250.59	309.63	59.0	High
	309.63	314.27	4.6	Moderate
	314.30	326.97	12.7	High
	Total		76.4	-
DH0016	262.00	293.7	31.7	Moderate

With regards to the variables selected, pyrrhotite, pentlandite and chalcopyrite, are of ultimate importance for understanding the mineralisation variability and Ni and Cu grades within the high-grade zone. Additionally, talc and chlorite were also selected; as minerals that can potentially impact mineral processing and recovery (see section 1.3.1.1), they also show compositional and textural changes along the mineralised intervals. Finally, arsenic assay was also selected given the importance of tracking its abundance in the final concentrate (see section 1.3.1.2) and because it did not show clear correlation to any other mineral in the dataset. Figure 15 displays intervals with arsenic above 200 ppm. As described in 1.3.1, arsenic limits for Cu smelters start from 2000 ppm. Considering the probable enrichment during concentration processes, 200 ppm levels can be worrisome. These intervals match well Ni high-grade zones, indicating correlation between these two elements. Because of that, deportment analysis was made on one As-rich interval (10-20 m) in DH0017 (Figure 15). Gersdorffite (NiAsS, 46 wt% As) and nickeline (NiAs, 46 wt% As) were identified in this interval, with calculated As deportment of 152.5 ppm, which does not reconcile with As assay for this interval of 667 ppm (Table 11). The disagreement may be due to undetected As-bearing minerals by LIBS and heterogeneous occurrence of gersdorffite and nickeline in the surface analysed compared to the volume of sample analysed for geochemical assay.

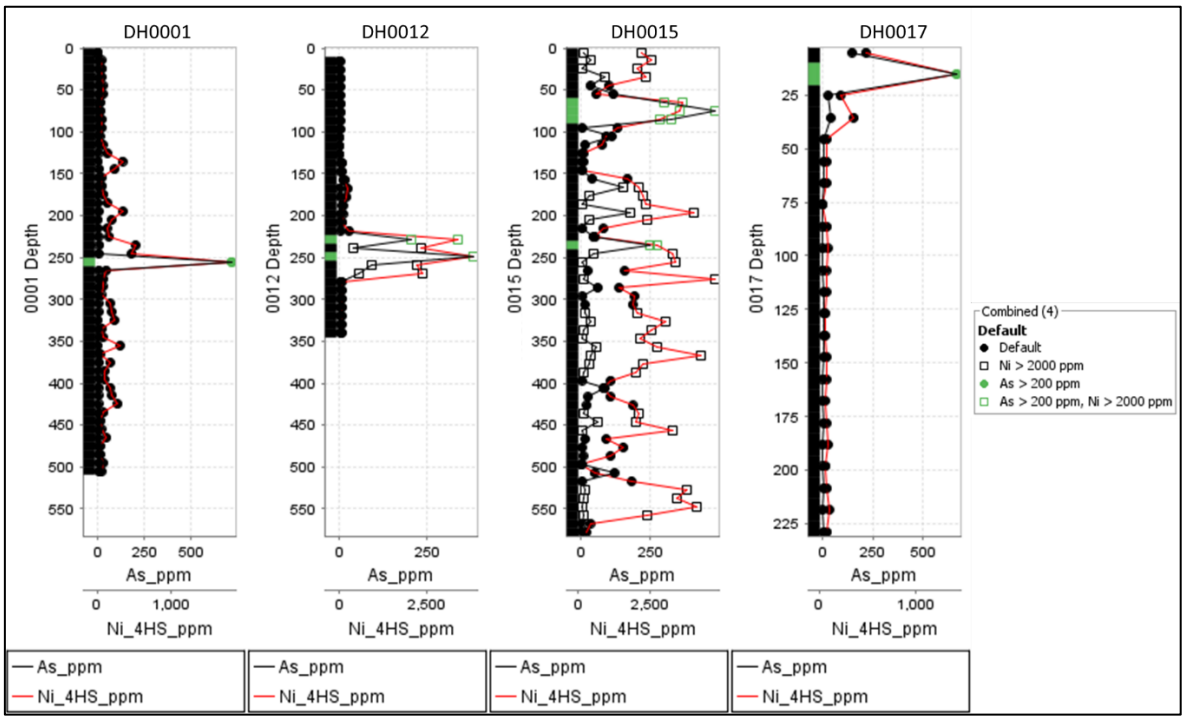

Figure 15 – Downhole As and Ni grades, highlighting intervals for As > 200 ppm.

Table 11 – Arsenic deportment analysis for DH0017, 10-20 m.

As in Gdf (wt%)	45.22
Gdf (wt%) 10-20m	0.013
As from Gdf (ppm) 10-20m	**61.7**
As in Nc (wt%)	56.1
Nc (wt%) 10-20m	0.016
As from Nc (ppm) 10-20m	**90.8**
As from Nc + Gdf (ppm) 10-20m	**152.5**
Assay As (ppm) 10-20m	**667**
As not detected/heterogeneity (ppm)	**514.5**

The minerals and chemical elements that show correlation to variables already selected or that do not have great impact in mineral processing were not considered, for the sake of simplicity and for the focus on red-flagging potential risks and opportunities. The correlation of common penalty elements, i.e., geochemical assay, (see section 1.3.1) with selected mineralogy, i.e., LIBS modal mineralogy, guided the selection of the first for prediction of enrichment in the concentrate by deportment analysis. Arsenic, Bi, Zn, Mg and Se are the only elements that show positive correlation to minerals that may refer to the concentrate, i.e., pyrrhotite, chalcopyrite, pentlandite, talc and chlorite. Others, such as Pb, Sb, Al and Hg, are mainly associated to gangue mineralogy.

Estimations of enrichment in the concentrate of penalty elements correlated with the selected mineralogy were made considering 10-meter-long mining units, aiming to simulate a hypothetical compositional dilution during mining operations. The average concentration of each penalty element in these composites were then used to calculate possible scenarios of their grades in the final concentrate. Aiming to simplify the assessment and given the lack of results on recovery tests at this stage of the project, a recovery of 100 wt% is considered. The enrichment estimations are case specific and are presented with the results (see section 4.2). Enrichment factors (EF) are defined based on two hypothetical Ni grades in the concentrate: 9 wt% and 15 wt%. These are around typical specifications from smelters (Correia et al., 2020; Warner et al., 2007; Santos Junior & Jr, 2016; Contessotto, 2017; Panoramic Resources, 2017).

Mineral Liberation Analyser (MLA) results from DH0005 were used as an additional reference to LIBS data, providing higher resolution modal mineralogy and textural information. Mineral association data was normalized to include only mineral phases, excluding free surfaces and unknown. Since analysis was carried in intact samples, liberation analyses were not possible. Grain sizes from MLA are compared using distribution plots and P_{80}. Figure 16 displays the modal mineralogy for the mineralized interval of DH0005 (see section 4.2.1) from MLA, which corresponds to 27 discs, and LIBS. Although the sample areas analysed by LIBS and MLA are not readily comparable, average mineralogy results show reasonable similarities. Plagioclase, ferrosilite, biotite and tourmaline present higher abundances in LIBS dataset, whereas hornblende, chlorite, pyrrhotite, quartz and pentlandite have higher concentrations in MLA data. Ferrosilite abundances vary from 2.6 wt% to 19.1 wt%, hornblende, 35.4 wt% to 20.8 wt%, and plagioclase from 33.0 wt% to 43.5 wt% when comparing MLA and LIBS, respectively.

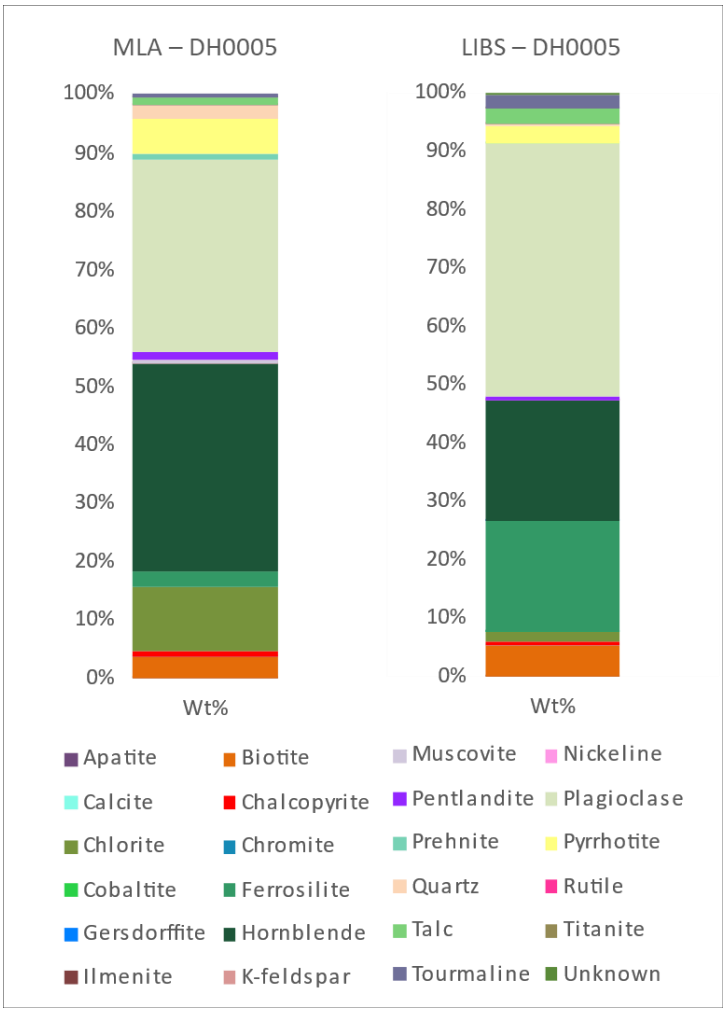

Figure 16 – MLA and LIBS modal mineralogy for the high-grade zone in DH0005.

4.2 Results

4.2.1 DH0005 – Analyses of penalty elements

The high-grade interval 250.59-315.3 m, at moderate (309.63-314.27 m) and high (250.59-309.63 m and 314.30-315.3 m) resolutions (Table 8; Table 10) were used for this assessment. The interval 250.59-262.51 m is logged as pyroxenite, whereas the interval from 262.51 m to 315.3 m, as gabbro.

Chalcopyrite, pentlandite, pyrrhotite, talc and chlorite were initially considered to assess mineralisation variability and penalty element deportment and additional variable selection (see section 4.1.2). The following results assess the correlation between penalty elements described in 1.3.1 and the selected mineralogy.

4.2.1.1 Arsenic

Arsenic has average concentration of 56.6 ppm (0.43 to 454 ppm). The element does not present clear correlation with any of the selected minerals, as discussed in 4.1.2 (Figure 17).

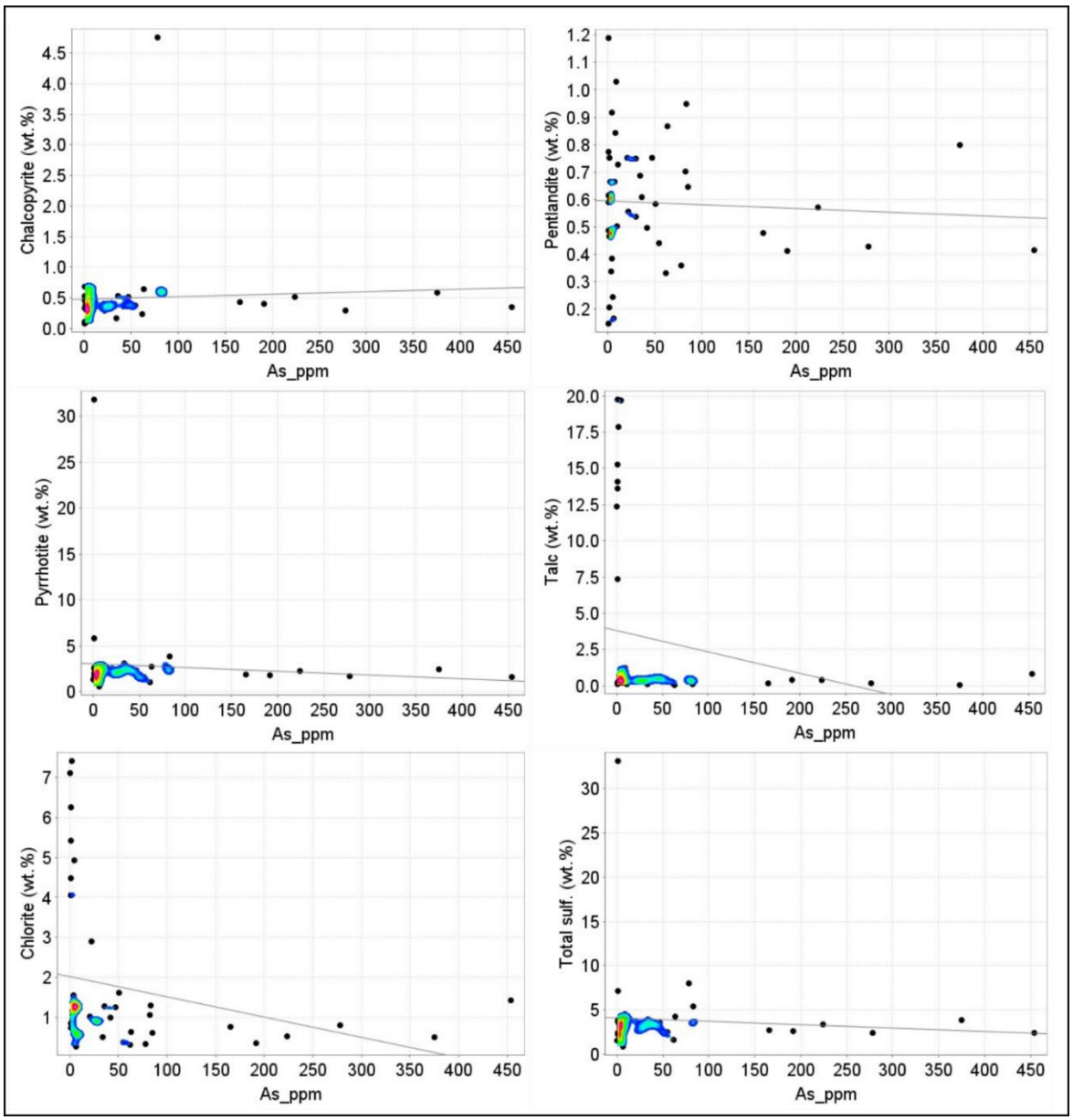

Figure 17 – Arsenic vs. Ccp, Pn, Pyh, Tlc, Chl and total sulfides, displaying point density opacity.

Arsenic concentration is higher in the gabbro compared to the pyroxenite, 70 ppm and 1.5 ppm in average, respectively. Discrete intervals with arsenic reach 454 ppm at 283 m and above 220 ppm between 295 and 310 m for 3 samples (Figure 18).

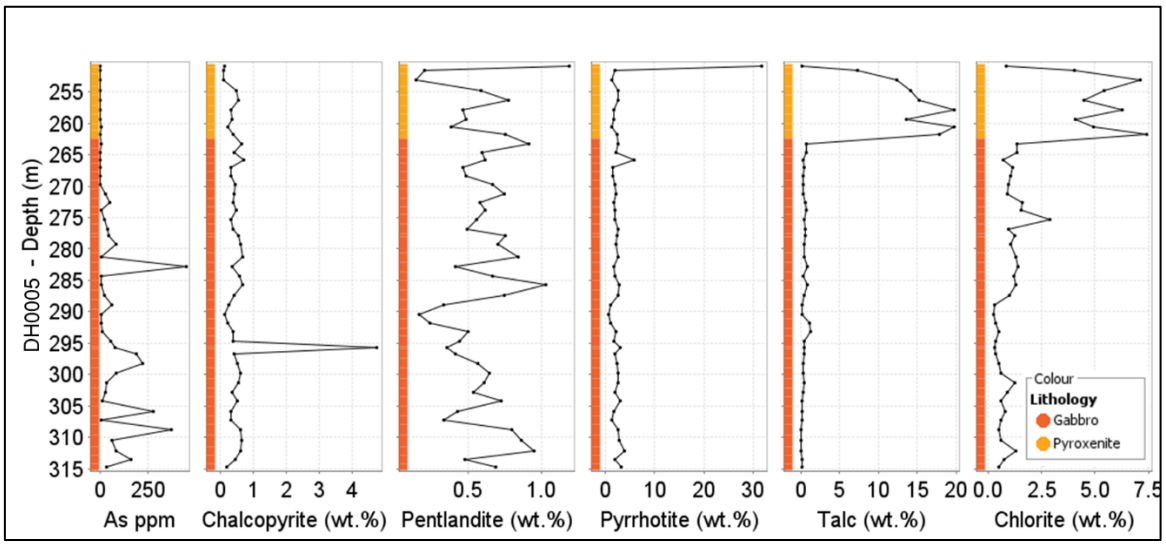

Figure 18 – Downhole As, Pyh, Pn, Ccp, Tlc and Chl abundances in high-grade zone - DH0005.

As-bearing mineral phases, i.e., cobaltite (CoAsS); gersdorffite (NiAsS); nickeline (NiAs), occur intergrown or as rims around other sulfides. Nickeline is 47.7 wt% associated to total sulfides and 12.2 wt% associated to pentlandite or chalcopyrite, therefore it may report to the concentrate. When not associated to sulfides, it usually occurs as finely disseminated grains included in hornblende (Figure 19). Among As-bearing minerals, nickeline is the coarsest (P_{80} = 550 µm). However, it is still finer than valuable sulfides, pentlandite (P_{80} = 1000 µm) and chalcopyrite (P_{80} = 1100 µm). Pyrrhotite has the highest P_{80}, around 2500 µm, and has larger grain size distribution compared to the other sulfides. As-bearing mineral phases, on the other hand, have steeper grain size distribution curves, indicating lower grain size variability (Figure 20). In fact, at fractions below 150 µm, nickeline is in general coarser than chalcopyrite and pentlandite. Gersdorffite is typically finer than 100 µm.

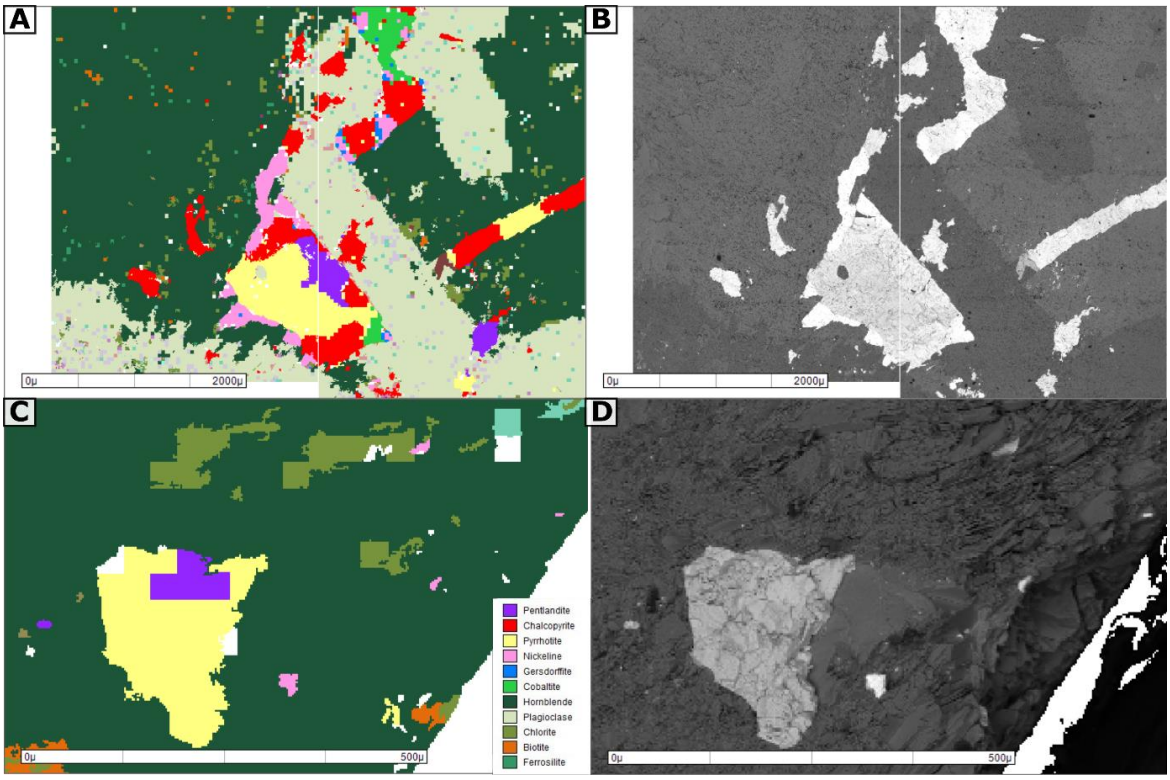

Figure 19 – Sulfide texture in MLA samples in high-grade zone from KUK0005. In A and B, nickeline, gersdorffite and cobaltite are observed intergrown around pyrrhotite, chalcopyrite and pentlandite. Nickeline grain size is coarser than gersdorffite and cobaltite. In C and D, nickeline occurs as fine disseminated grains included in hornblende. A and C: interpreted mineral maps. B and D: BSE images.

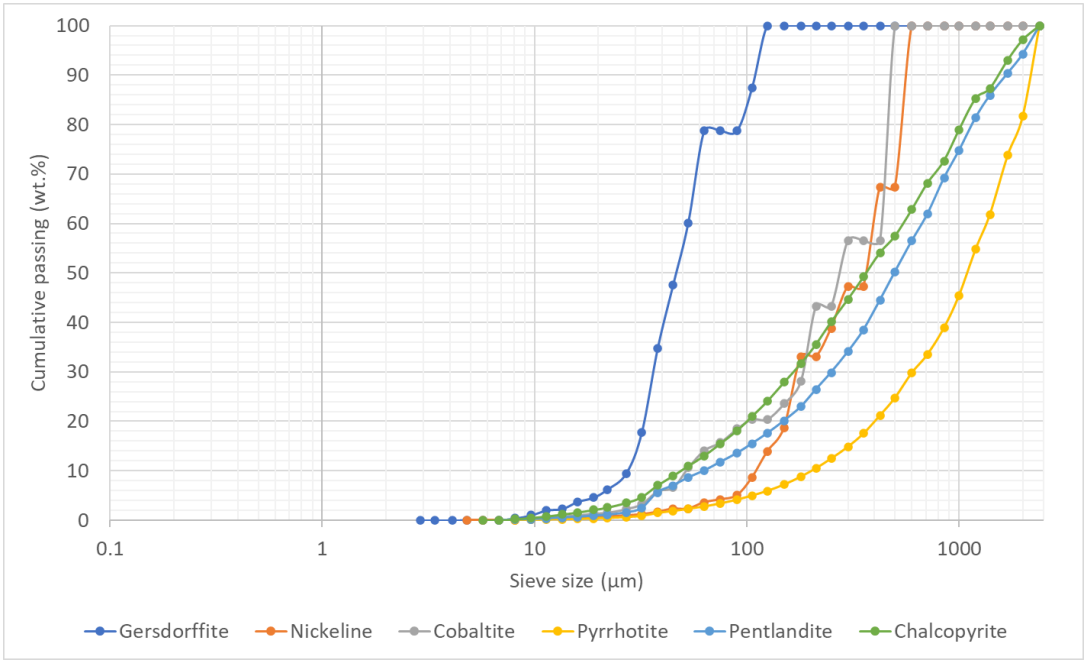

Figure 20 – Mineral grain size distribution for Ccp, Pn, Pyh, Cbt Gdf and Nc. MLA data in high-grade zone from DH0005.

The 65-meter interval was subdivided in 6 approximately 10-meter-long zones (Figure 21), as described in 4.1.2. Five gabbro zones and one pyroxene zone were defined, and their As contents are listed in Table 12. Gabbro 2, 3 and 5 present the highest As concentrations, up to 126.7 ppm in the last zone.

Four scenarios were considered to predict arsenic enrichment in the concentrate and indicate priority areas for further testing. 1) A – EF 26: all As-bearing minerals, and Ni grade in the final concentrate at 9 wt%, resulting in EF = 26; 2) A – EF 46: all As-bearing minerals, and Ni grade in the final concentrate at 15 wt%, resulting in EF = 46; 3) B – EF 26: only As-bearing sulfides, and Ni grade in the final concentrate at 9 wt%, resulting in EF = 26; and 4) B – EF 46: only As-bearing sulfides, and Ni grade in the final concentrate at 15 wt%, resulting in EF = 46. The results are displayed in Table 13. Gabbro 2, 4 and 5 would result in the highest arsenic concentrations, up to 0.57 wt% in the worst-case scenario, A – EF 46 (Table 13), which is above selling limits for Cu concentrates (Table 2). Considering the association of As-bearing mineralogy with valuable sulfides and relatively high As levels in some intervals, this element was selected as a variable for multi-variable high-grade zone domaining.

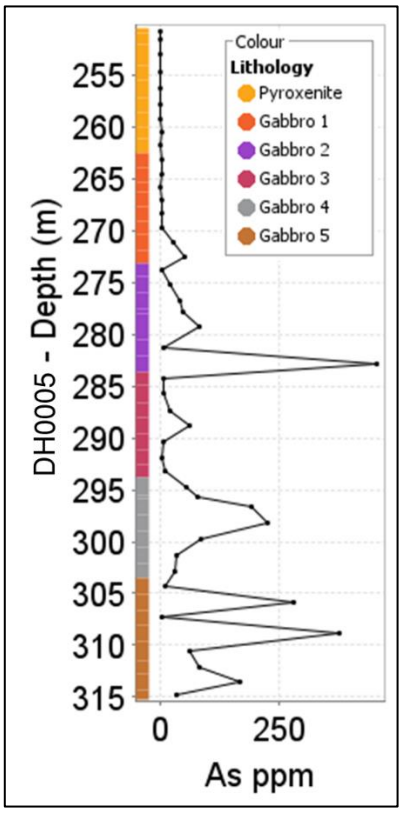

Figure 21 – Downhole 10-meter-intervals used for arsenic enrichment assessment.

Table 12 – Statistics for arsenic 10-meter-intervals.

As ppm	
Total: Count Numeric	46.00
Total: Minimum	0.43
Total: Maximum	454.00
Total: Mean	**56.57**
Pyroxenite: Count Numeric	9.00
Pyroxenite: Minimum	0.43
Pyroxenite: Maximum	4.41
Pyroxenite: Mean	1.50
Gabbro 1: Count Numeric	8.00
Gabbro 1: Minimum	0.99
Gabbro 1: Maximum	50.70
Gabbro 1: Mean	12.04
Gabbro 2: Count Numeric	7.00
Gabbro 2: Minimum	3.78
Gabbro 2: Maximum	454.00
Gabbro 2: Mean	94.22
Gabbro 3: Count Numeric	7.00
Gabbro 3: Minimum	5.06
Gabbro 3: Maximum	62.00
Gabbro 3: Mean	17.12
Gabbro 4: Count Numeric	7.00
Gabbro 4: Minimum	29.80
Gabbro 4: Maximum	224.00
Gabbro 4: Mean	99.89
Gabbro 5: Count Numeric	8.00
Gabbro 5: Minimum	3.76
Gabbro 5: Maximum	375.00
Gabbro 5: Mean	126.73

Table 13 – Estimations of arsenic enrichment in the concentrate. A) considering all As-bearing minerals, i.e., gersdorffite, nickeline and cobaltite; Enrichment factor 26 and 46. B) considering As-bearing sulfides, i.e., gersdorffite and cobaltite; Enrichment factor 26 and 46. Levels close or above no charge limits are highlighted in red.

DH0005	A - EF 26 (ppm)	A - EF 46 (ppm)	B - EF 26 (ppm)	B - EF 46 (ppm)
Pyroxenite	39	69	13	23
Gabbro 1	312	552	103	182
Gabbro 2	2444	4324	807	1427
Gabbro 3	445	782	147	259
Gabbro 4	2597	4594	855	1513
Gabbro 5	3276	5796	1085	1919

4.2.1.2 Bismuth

Bismuth shows moderate correlation with chalcopyrite and pentlandite, however, not with pyrrhotite. It also does not present any correlation to talc nor chlorite (Figure 22). The BSE images from SEM analyses indicate the presence of sulfosalts (tetradymite group minerals) as very fine inclusions in sulfides, such as pyrrhotite and pentlandite (Gregory, 2021). The spectrum is inconclusive in determining whether sulphur is present, thus, the mineral classification (e.g., telluride or sulfide) was not possible (Figure 22).

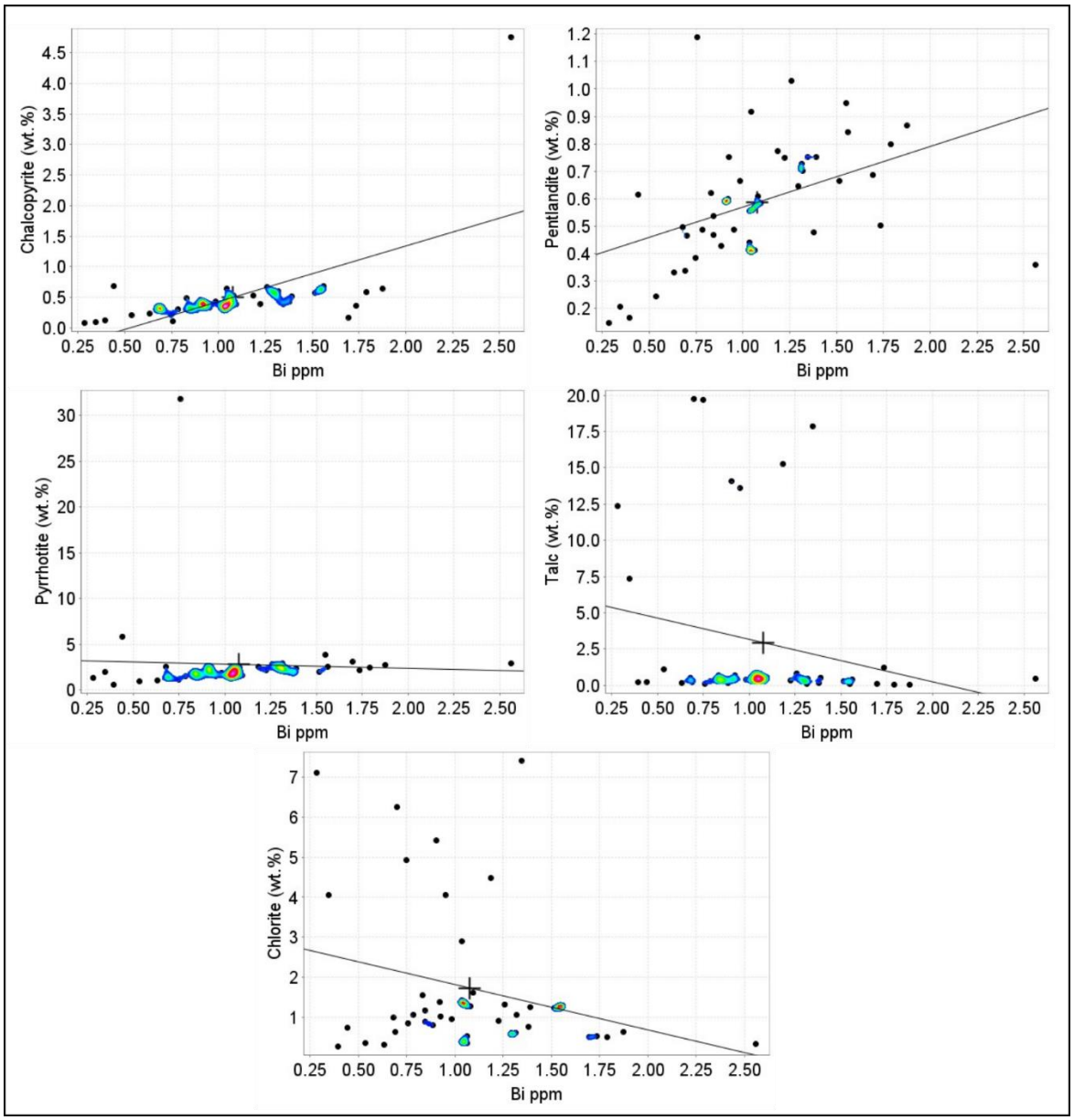

Figure 22 - Bismuth vs. vs. Ccp, Pn, Pyh, Tlc, Chl and total sulfides, displaying point density opacity.

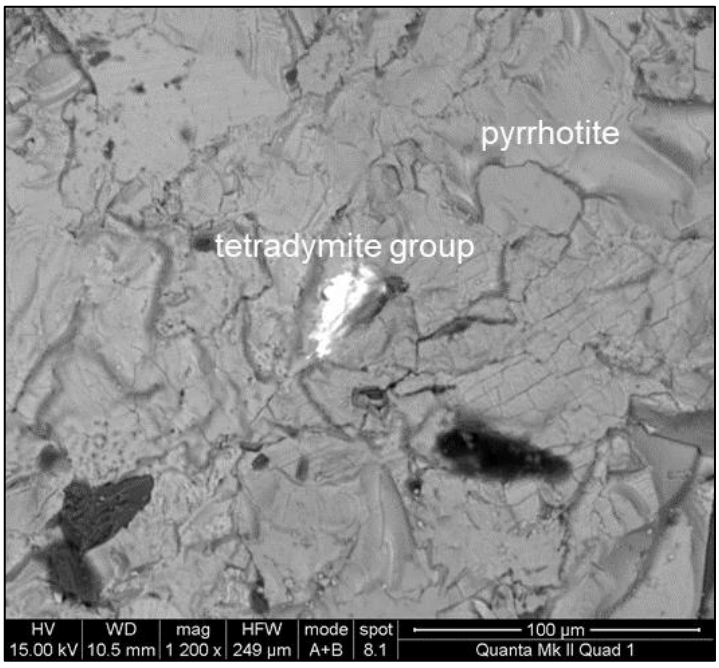

Figure 23 – BSE image displaying tetradymite group mineral inclusion in pyrrhotite grain in a gabbro from DH0005. Modified from internal report.

The average Bi concentration in the high-grade zone from DH0005 is low, 1.1 ppm, from 0.3 ppm up to 2.6 ppm. Considering the worst-case enrichment scenario, where the EF of bismuth is equal to Ni, and for a nickel grade in the concentrate of 15 wt%, i.e., 46, no samples would reach the smelter limit range (Table 2), which is 200 to 500 ppm. Because of that, Bi was not selected as an additional variable for domaining.

4.2.1.3 Zinc

Zinc does not correlate with any of the sulfides considered in the analysis. Chlorite shows a poor correlation, as well as talc (Figure 24). Zn concentration ranges from 42.5 ppm to 129 ppm, averaging 59.8 (Figure 25). The pyroxenite zone has the highest average Zn concentration, equal to 74 ppm. Even considering the worst-case enrichment scenario, as described for Bi, Zn grade in the concentrate would be around 3400 ppm for the pyroxenite zone, which is much lower than the smelter threshold: 30000 ppm (Table 2). Because of that, Zn was also not selected as an additional variable for the domaining.

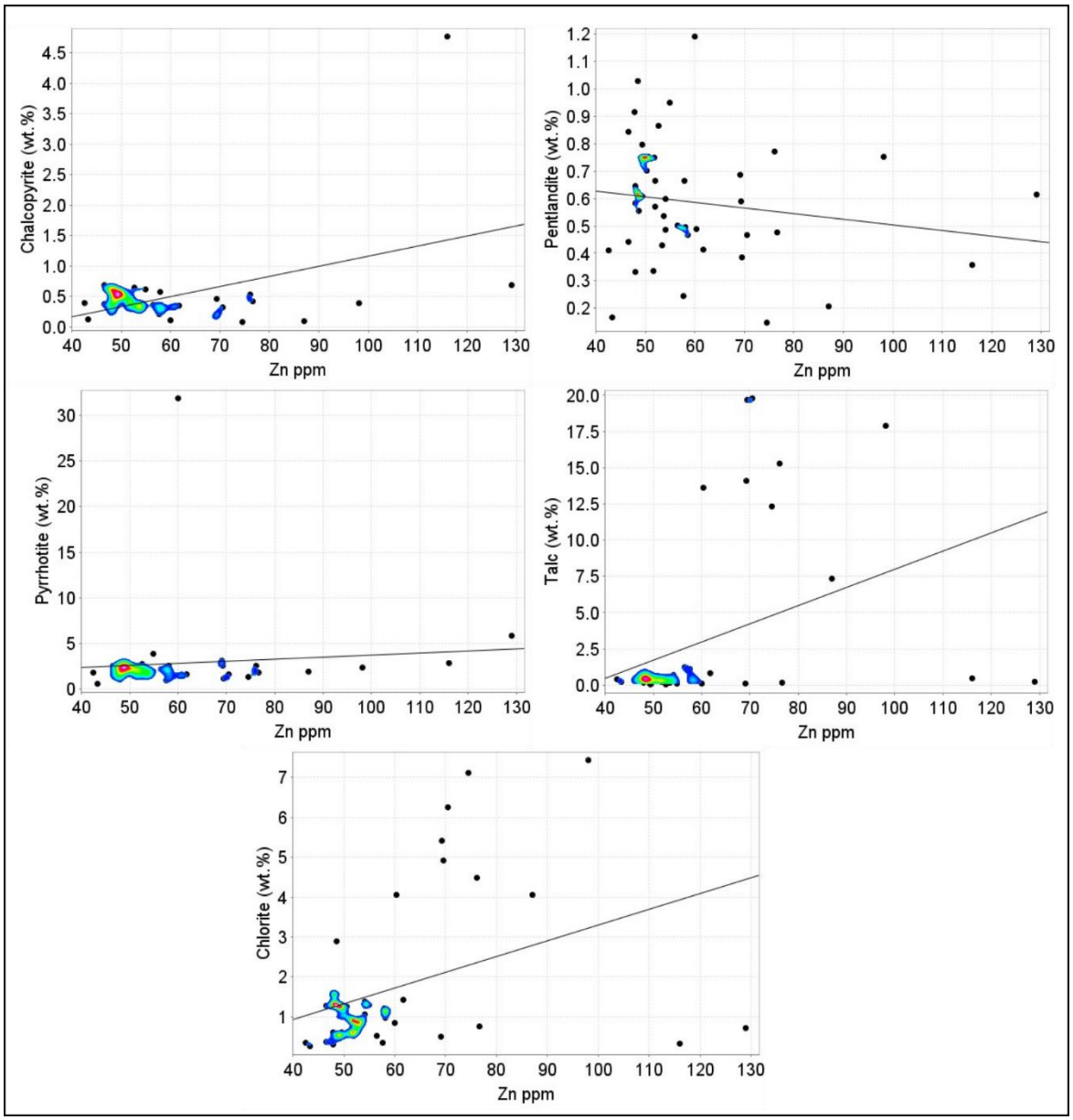

Figure 24 – Zinc vs. Ccp, Pn, Pyh, Tlc, Chl and total sulfides, displaying point density opacity.

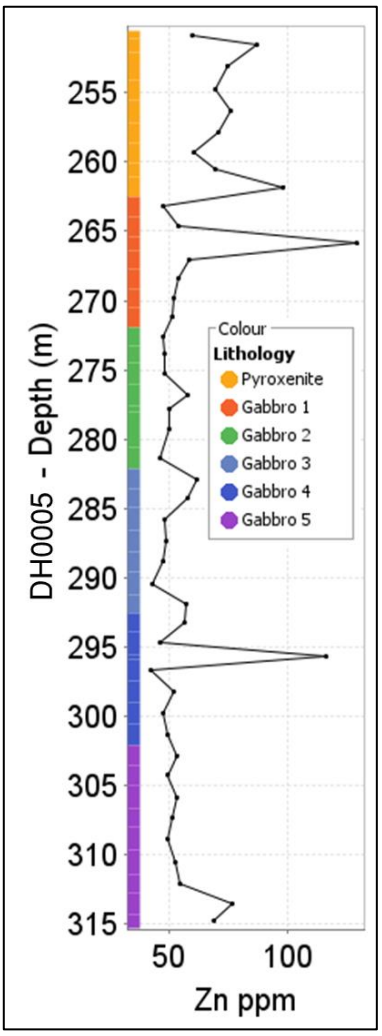

Figure 25 – Downhole Zn concentration plot with 10-meter-intervals for enrichment assessment.

4.2.1.4 Selenium

Another common penalty element is Se. The correlation between this element and all three selected sulfides is clear, especially for pentlandite, on which the coefficient of determination is 0.66 for the regression line. This indicates a good fit for the trend of the samples. Talc and chlorite, on the other hand, show negative correlation with this penalty element (Figure 26). The average concentration of the element is 4.8 ppm, and the range is 1.8-13.3 ppm. The zones Gabbro 1 and 5 are the two having average concentrations above 5 ppm (Figure 27). In the same fashion as for Bi and Zn, if the worst-case enrichment scenario is considered, Se grade in the concentrate would be around 250 ppm. A common limit for the element in Cu smelters is 300 ppm, i.e., above the estimation. However, for Ni concentrates this limit can be lower (Table 2). Due to the uncertainty in charging thresholds for

Se, it was not considered as an additional variable, however, its concentration is reported in the domains.

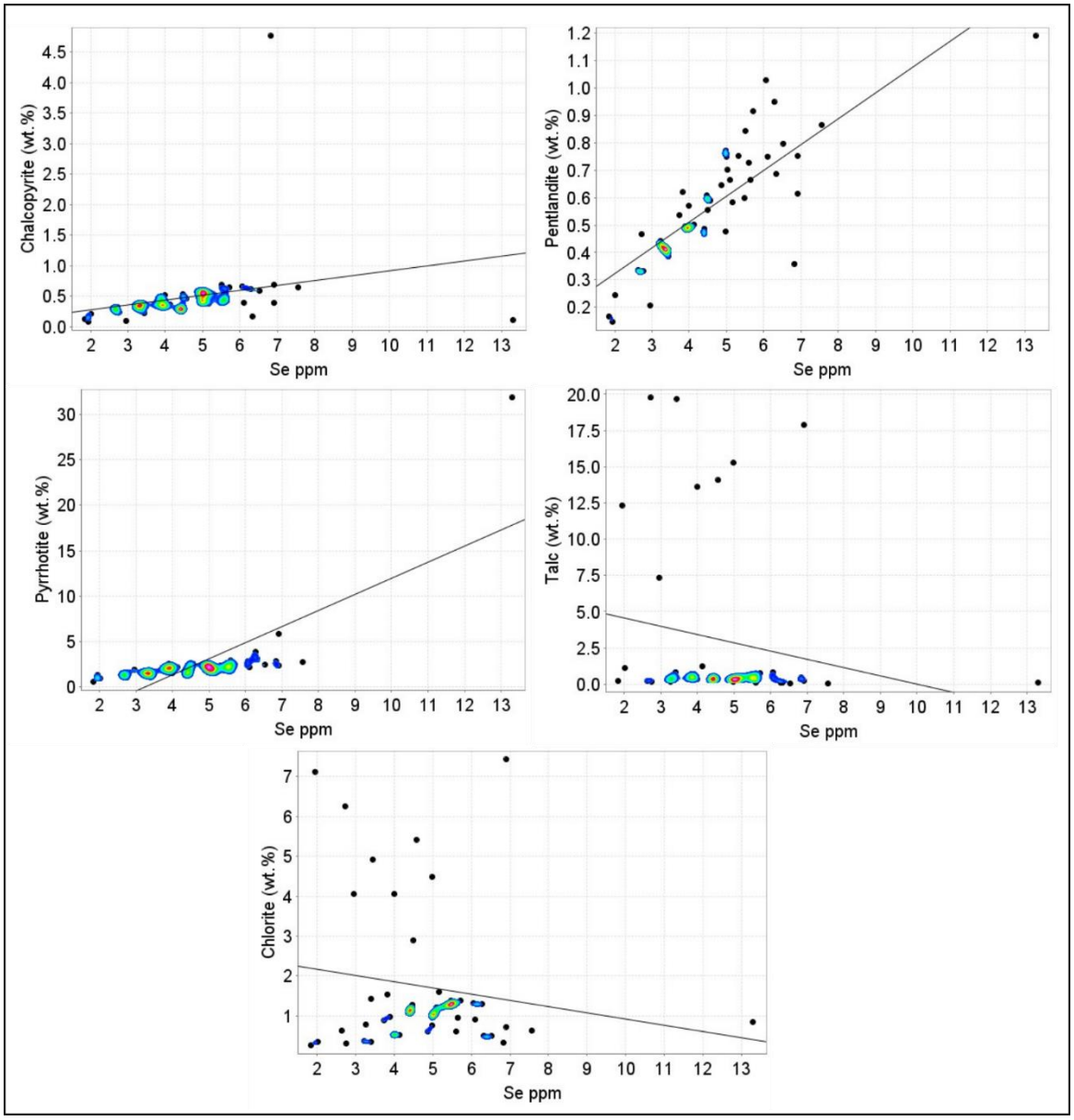

Figure 26 - Selenium vs. Ccp, Pn, Pyh, Tlc, Chl and total sulfides, displaying point density opacity.

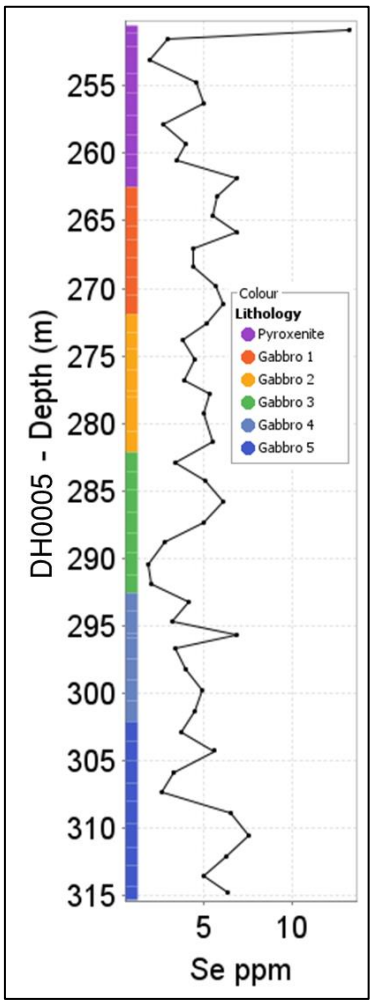

Figure 27 - Downhole Se concentration plot with 10-meter-intervals for enrichment assessment.

4.2.1.5 Magnesium

The last penalty element for which geochemical assay was available is Mg. As a major constituent of chlorite and talc, this element shows variable correlation with these minerals. Sulfides are not correlated with Mg (Figure 28).

Magnesium concentrations are consistently above 10 wt% in the pyroxenite zone and around 5 wt% for the gabbro (Figure 29). Magnesium deportment to chlorite and talc were calculated using Mg content of 13 wt% and 16 wt%, respectively (Gregory, 2021), and LIBS modal mineralogy. To estimate Mg grade in the concentrate, the following scenarios are considered: 1) worst-case enrichment scenario: considers that both talc and chlorite would report to the concentrate and Ni grade in the concentrate at 15 wt%; 2) in this case scenario, only talc would report to the concentrate (see section 1.3.1.1) and Ni grade in the concentrate at 15 wt%.

The calculated average Mg contained in chlorite and talc is around 0.5 wt% out of a total of 6.01 wt% Mg for the whole interval.

For the first and worst-case scenario, on which chlorite and talc are expected to report to the concentrate (Table 14), total Mg in the concentrate can be up to 6.9 wt% in the pyroxenite zone. In the second scenario, on which only talc would report to the concentrate, the total estimated Mg grade in the concentrate would be around 5.3 wt% in the pyroxenite zone (Table 15).

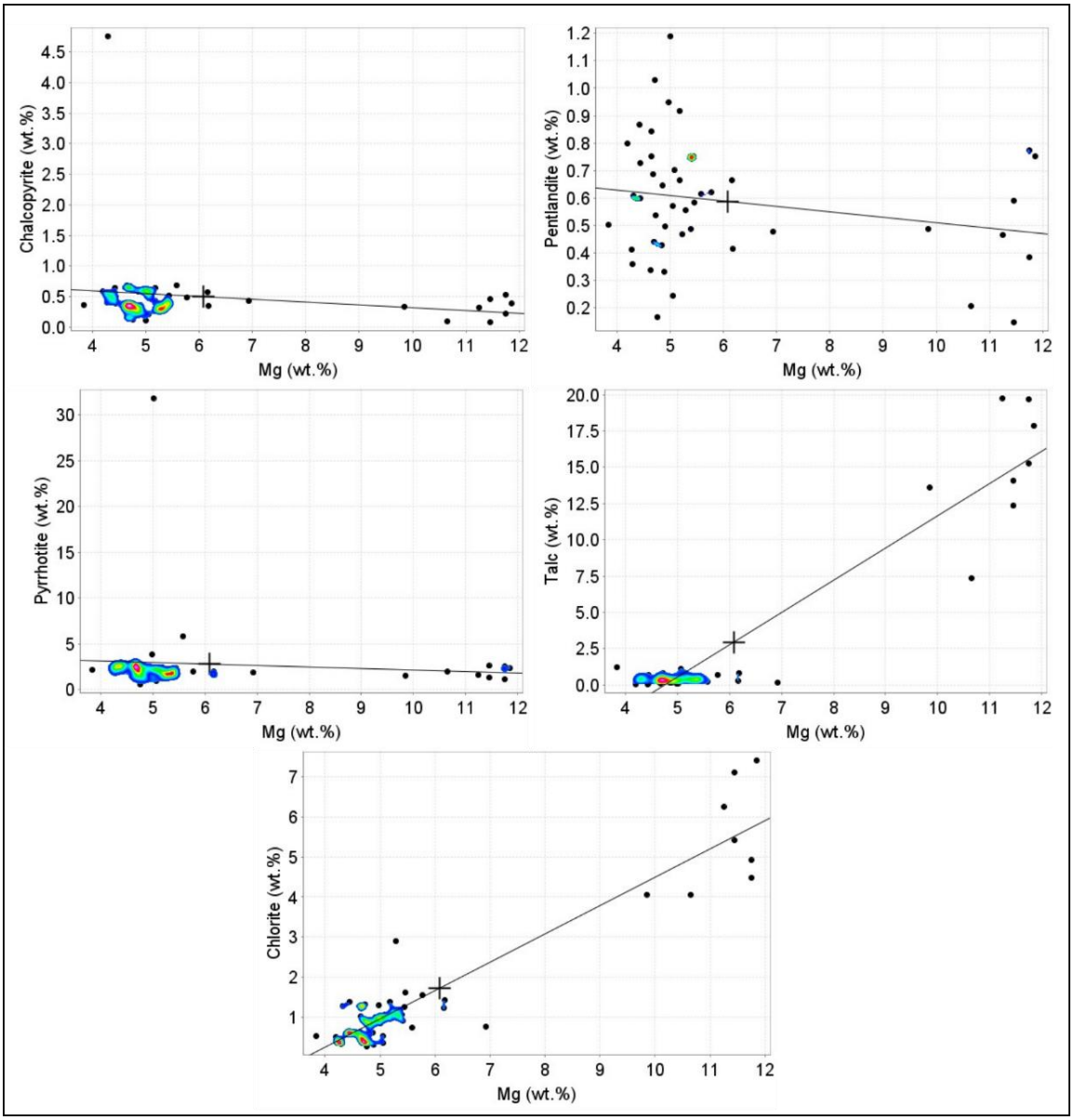

Figure 28 - Magnesium vs. Ccp, Pn, Pyh, Tlc, Chl and total sulfides, displaying point density opacity.

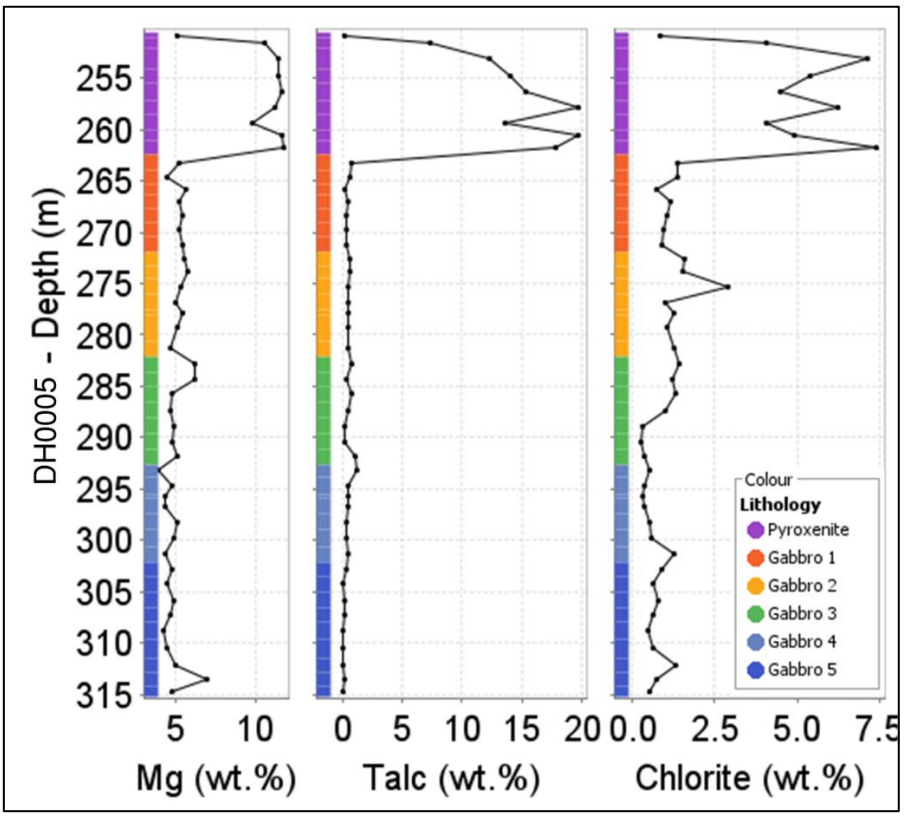

Figure 29 - Downhole Mg, Chl and Tlc concentrations plots with 10-meter-intervals for enrichment assessment.

Table 14 – Worst-case scenario, considering that both chlorite and talc would report to the concentrate. Levels close or above no charge limits are highlighted in red.

DH0005	tlc %	chl %	tlc % in conc	chl % in conc	Mg in tlc conc (%)	Mg in chl conc (%)	total Mg in conc (%)
Pyroxenite	13.3	5.0	32.9	12.2	5.3	1.6	**6.9**
Gabbro 1	0.4	1.1	5.2	12.7	0.8	1.7	**2.5**
Gabbro 2	0.5	1.5	5.9	17.2	1.0	2.3	**3.2**
Gabbro 3	0.6	0.8	8.5	12.9	1.4	1.7	**3.1**
Gabbro 4	0.5	0.6	6.6	6.9	1.1	0.9	**2.0**
Gabbro 5	0.1	0.7	2.0	10.1	0.3	1.3	**1.7**

Table 15 - Case scenario considering that only talc would report to the concentrate. Levels close or above no charge limits are highlighted in red.

DH0005	tlc %	tlc % in conc	Mg in tlc conc (%)
Pyroxenite	13.35	32.89	**5.32**
Gabbro 1	0.44	5.16	**0.84**
Gabbro 2	0.52	5.90	**0.95**
Gabbro 3	0.56	8.52	**1.38**
Gabbro 4	0.54	6.56	**1.06**
Gabbro 5	0.14	1.98	**0.32**

Considering that the smelter limits range from 5 to 7.5 wt% (Table 2), in both scenarios the concentration of Mg is within warning levels. When considering chlorite in the concentrate, textural properties, such as grain size and mineral association are of high importance (Pietrobon, et al., 1997) (see section 1.3.1.1). In Figure 30, the mineral grain size distribution for chalcopyrite, pentlandite, chlorite and talc indicate that the Mg-bearing silicates are finer than the sulfides, with P_{80} of 150 µm for talc and 700 µm for chlorite. Mineral association data indicates that 2.2 wt% of total sulfides are associated to talc and 29.8 wt% to chlorite. If considering only valuable sulfides, chalcopyrite and pentlandite, 1.3 wt% are associated to talc and 16.1 wt% to chlorite. In Figure 31 chlorite is commonly observed filling plagioclase pore space and associated to hornblende, and also occur associated to pentlandite and chalcopyrite, mostly in the border of coarse pyrrhotite grains. Talc abundance is lower and is mainly associated with chlorite and hornblende. In the pyroxenite zone, where its abundance can be as high as 20 wt%, it occurs throughout the groundmass replacing hornblende and chlorite, and is also commonly observed associated to sulfides.

Given that chlorite and talc can decrease flotation efficiency (see section 1.3.1.1) and that they have local abundances up to 7.5 wt% and 20 wt%, respectively, both minerals were previously selected as variables for the domaining. Moreover, as Mg concentration is directly correlated with them, their enrichment is expected to also cause the enrichment of Mg. Thus, Mg was not selected as an additional variable.

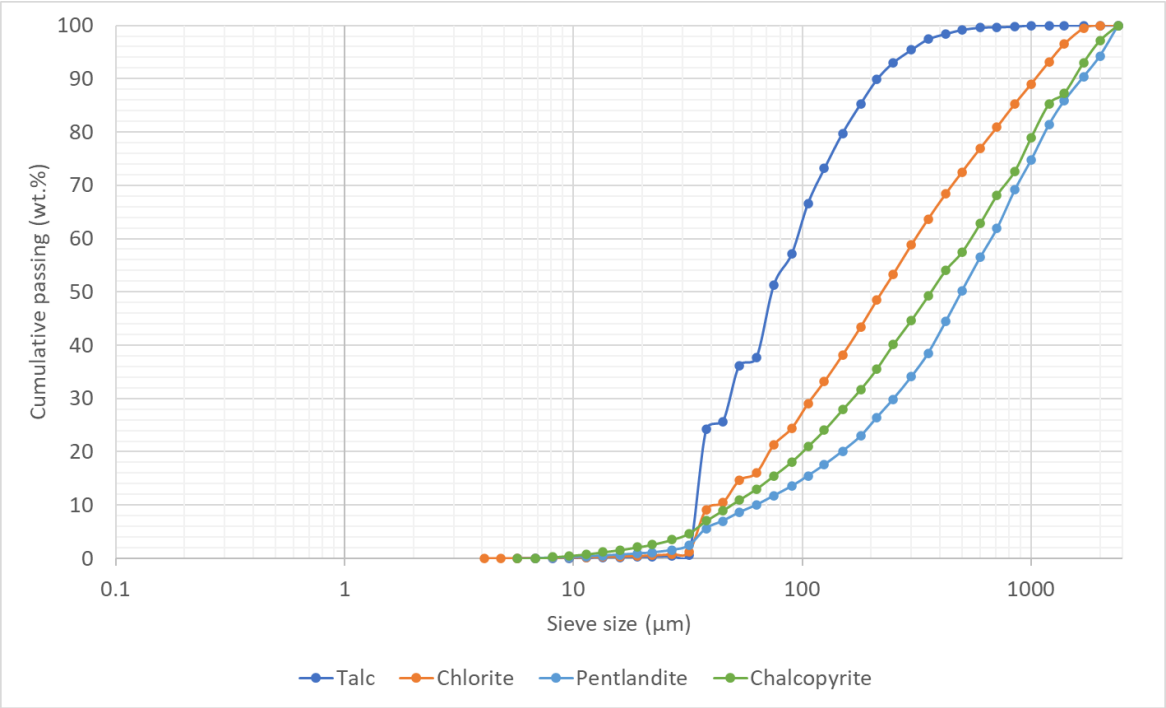

Figure 30 - Mineral grain size distribution for Ccp, Pn, Tlc and Chl. MLA data in high-grade zone from DH0005.

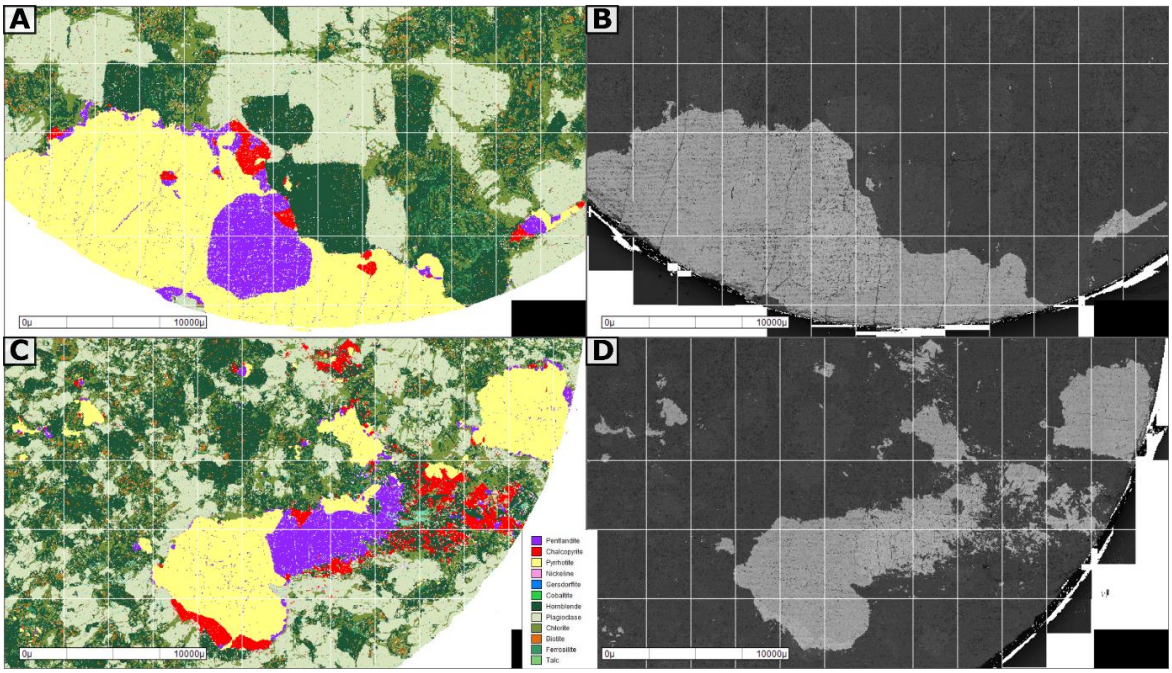

Figure 31 – Sulfide and Mg-bearing silicates texture in MLA samples in high-grade zone from KUK0005. Pentlandite and chalcopyrite rims and intergrowth on pyrrhotite are very common. Ccp has a finer grain size and is usually more disseminated in the groundmass. Chlorite occurs associated with hornblende and, since is more abundant than talc, is also more commonly associated to the valuable sulfides. A and C: interpreted mineral maps. B and D: BSE images.

Table 16 summarizes the penalty elements grades in the mineralised interval, the results for the estimations of their grades in the concentrate, and the ranges of no-charging limits considered in this study. Arsenic and magnesium are above the threshold, whereas selenium is within an uncertainty zone.

Table 16 – Summary of penalty elements analysis for high-grade zone in DH0005.

DH0005			
Penalty element	**Average grade**	**Estimated grade in conc. in worst-case scenario**	**No-charging limit range**
As	56.6 ppm	5796 ppm	300-2000 ppm
Bi	1.1 ppm	50.6 ppm	200-500 ppm
Zn	59.8 ppm	3400 ppm	30000 ppm
Se	4.8 ppm	250 ppm	10-300 ppm
Mg	6.1 wt%	6.9 wt%	5.0-6.5 wt%

4.2.2 DH0005 – Clustering results

The input variables were pentlandite, chalcopyrite, pyrrhotite, talc, chlorite and arsenic. K-means (Jin, X. & Han, J., 2011), a centroid-based algorithm for grouping data with similarities, was used for clustering analysis (Figure 32). Attempts using DBSCAN were also carried out, using several parameters, however, it was not effective for segregating the dataset in more than one cluster. It may either indicate low heterogeneity within the samples or not enough density to form multiple clusters (Kriegel et al., 1996; Schubert et al., 2017). A third attempt applying U-MAP, based on the likelihood of two data points being connected at high and low dimensions, for dimensionality reduction (nearest neighbours = 10; minimum distance = 0.1) (McInnes et al., 2020), from 6 to 2 dimensions, and then DBSCAN (Ester et al., 1996), a density-based algorithm, for clustering, resulted in domains very similar to the results observed using K-means (Figure 33; Figure 34).

K-means was used for k = 2 and k = 3 (5000 tries) and the results are displayed in Figure 32, Figure 33 and Figure 34. For k = 3, it is observed that samples within clusters 1 and 2 present more similarities than to samples in cluster 3. In fact, the first two clusters are merged when k = 2. For k = 3, cluster 1 presents high As and the highest sulfides concentrations, even though their variability is low throughout the whole interval. Cluster 2 also presents high As, which is low in cluster 3, that in turn presents high chlorite and talc abundances. For k = 2, cluster 1 is As-

rich, whereas cluster 2 has high chlorite and talc concentrations. DBSCAN optimal configuration (minimum points in cluster = 4; epsilon = 2) resulted in 3 clusters. In the same fashion as in k = 3, K-means, clusters 1 and 2 are more similar to each other than to cluster 3. The main difference between the formers is the As concentration: cluster 1 is As-moderate, whereas cluster 2 is As-rich. Cluster 3, in turn, has low arsenic and high chlorite and talc contents. Clusters 1 and 2 in k=3, 1 in k=2 and 1 and 2 in DBSCAN may present high Se levels.

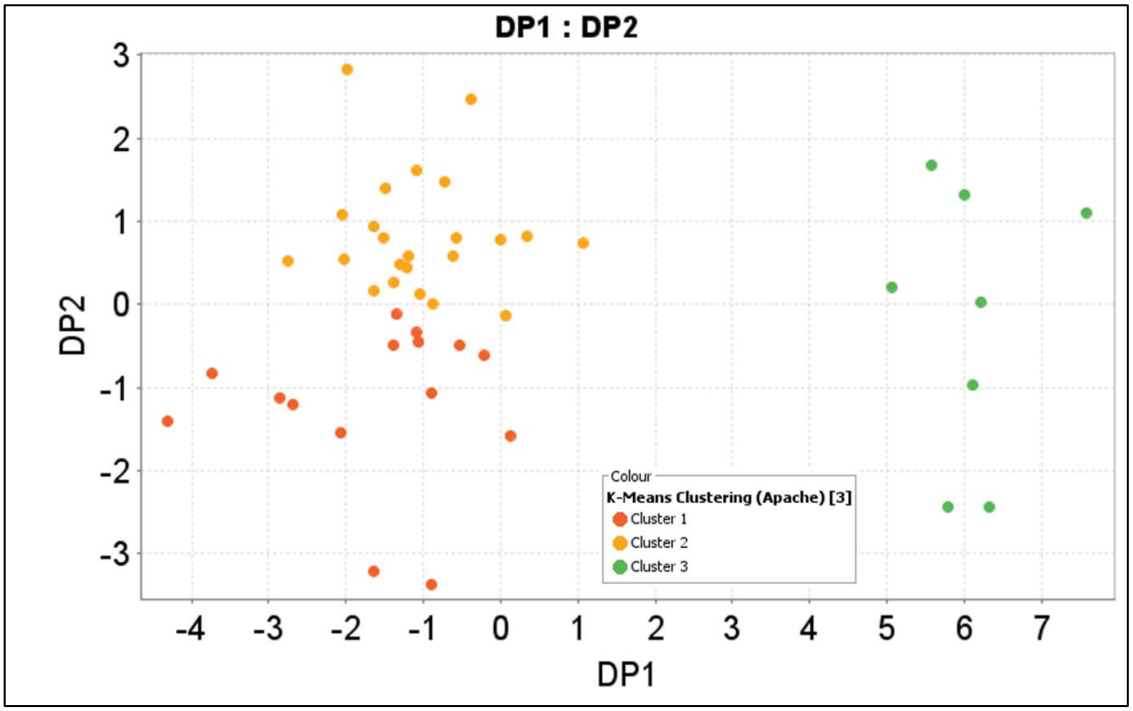

Figure 32 – K-means clustering result for k = 3 represented in two dimensions, DP1 against DP2.

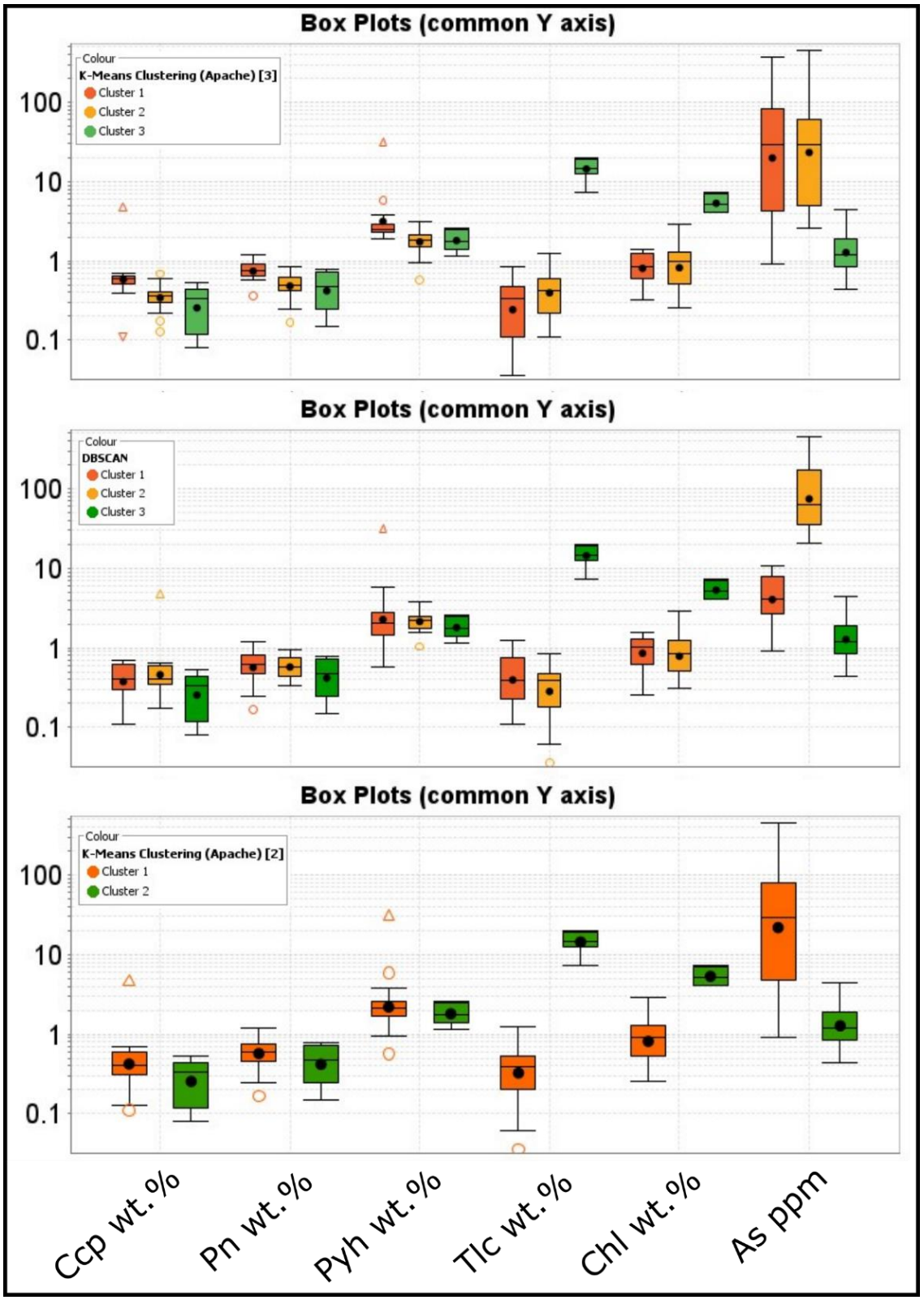

Figure 33 – Box plots displaying K-means and DBSCAN clustering results in logarithmic scale for abundances of the variables considered in the analysis. In the top plot, k = 3 and in the bottom plot, k = 2, both for K-means. The central plot displays the results for DBSCAN.

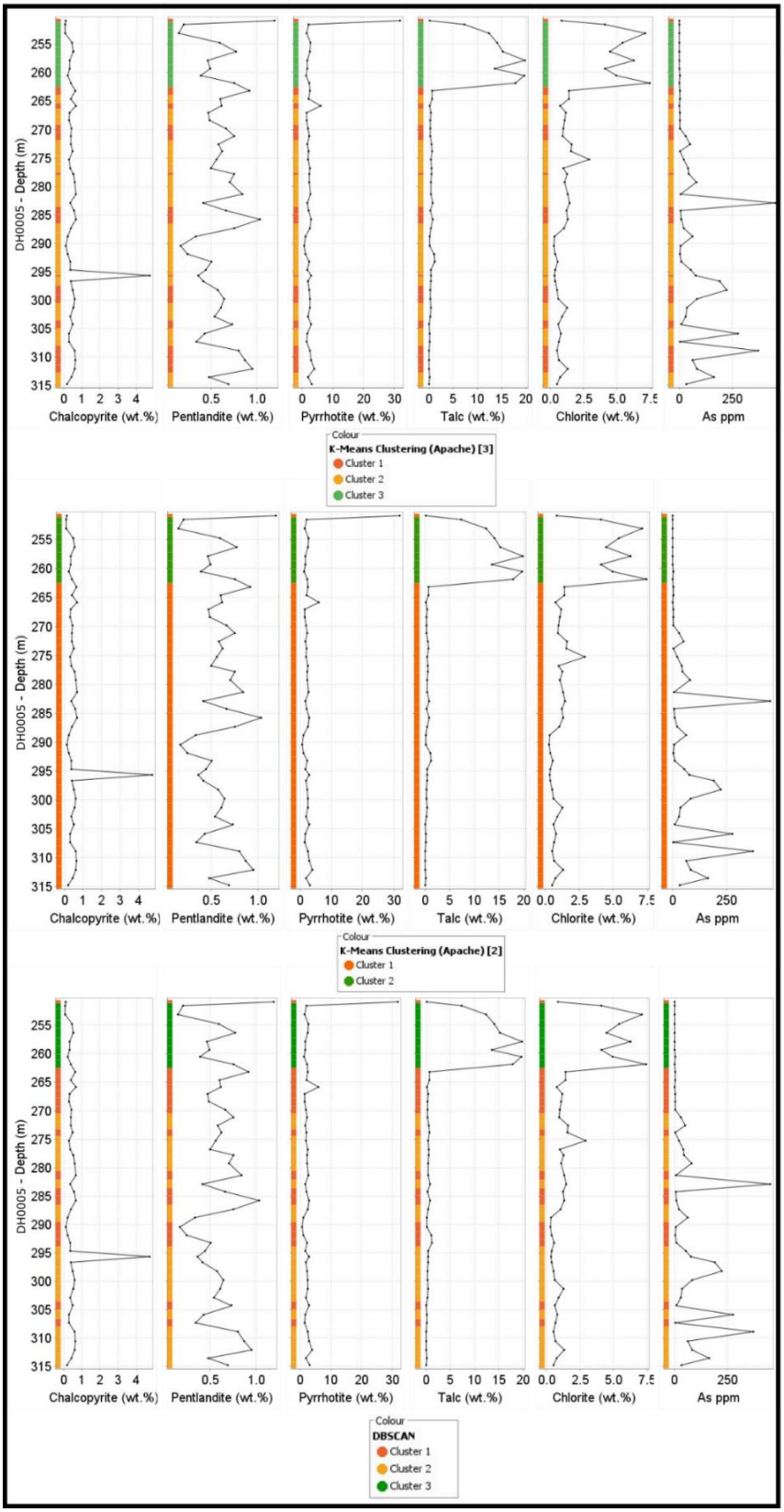

Figure 34 – Downhole plots displaying K-means and DBSCAN clustering results for abundances of the variables considered in the analysis. In the top plot, k = 3 and in the bottom plot, k = 2, both for K-means. The central plot displays the results for DBSCAN.

Downhole P_{80} for sulfide grain sizes from MLA mineralogy were compared to the sulfide modal mineralogy from LIBS and DBSCAN clustering results (Figure 35). It is observed that the three sulfides, i.e., chalcopyrite, pentlandite and pyrrhotite, present overall similar grain size variations along the interval, reaching a maximum P_{80} of around 2000 µm at 270-280 meters-deep. At the end of the interval, around 310 m, the grain size becomes coarser again. The intervals from 255 to 270 m and 280 to 295 m tend to have fine-grained sulfides, with P_{80} around 270 µm. The comparison of sulfide grain size variations with mineralogical and assay domaining using DBSCAN show a trend of coarser sulfide grain sizes in cluster 2, which is the As-rich domain. The mineralogical composition of cluster 2 also indicates that it is slightly enriched in plagioclase (53.6 wt%) and hornblende (22.4 wt%) and depleted in biotite (4.7 wt%) and ferrosilite (10.0 wt%) compared to cluster 1, with 46.3 wt% plagioclase, 19.6 wt% hornblende, 5.5 wt% biotite, and 12.7 wt% ferrosilite. The differences increase when comparing to cluster 3: plagioclase, 0.5 wt%, hornblende, 16.3 wt%, biotite, 3.3 wt%, and ferrosilite, 50.4 wt%.

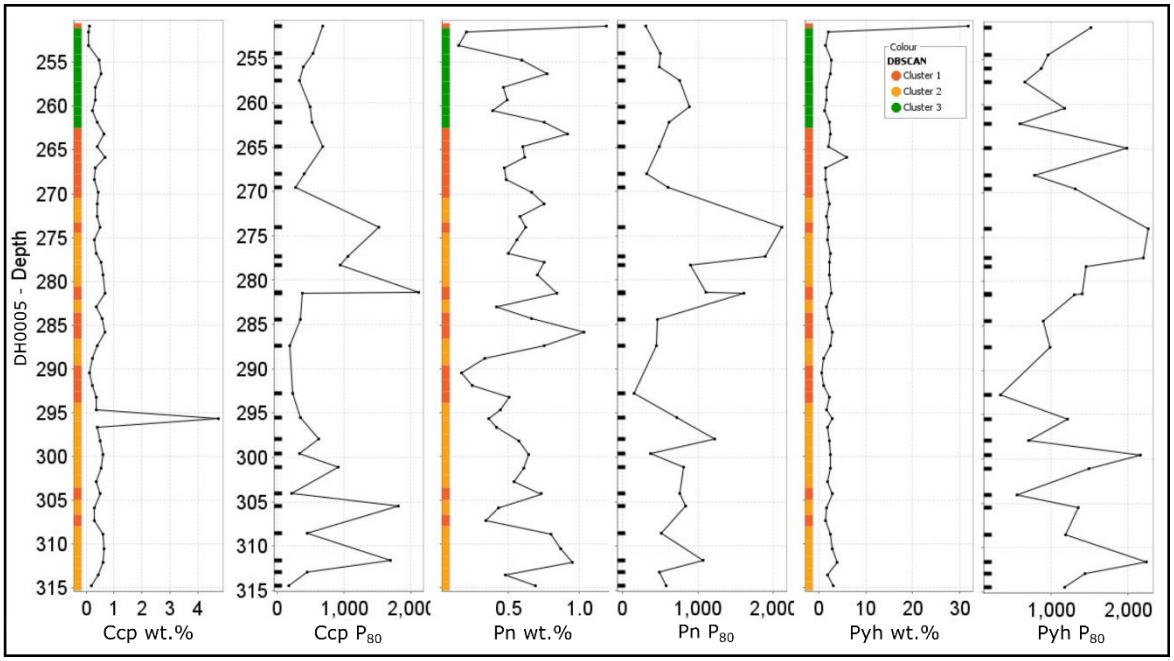

Figure 35 – Downhole plots for sulfides abundances and P_{80} (µm) for grain sizes in DH0005. DBSCAN clustering classification is also displayed.

4.2.3 DH0016 – Analyses of penalty elements

The high-grade zone scanned for LIBS data acquisition (Table 10) is at moderate resolution and was thus selected for domaining analysis. The whole interval, 262 m to 293.7 m, was previously logged as gabbro. Mineral Liberation Analyser (MLA) data is not available for this drill hole.

Chalcopyrite, pentlandite, pyrrhotite, talc and chlorite were considered as proxies to assess mineralisation variability and penalty element deportment (see section 4.1.2). The following results assess the correlation between penalty elements described in section 1.3.1 and the initially selected mineralogy.

4.2.3.1 Arsenic

Arsenic presents overall poor correlation with all selected minerals, except talc (Figure 36). The correlation is particularly stronger with sulfides. The 10-m interval 272-282 m has an average As grade of 19 ppm, whereas the average for the remaining intervals is lower than 1 ppm. The average for the whole interval is 6 ppm (Figure 37).

Two scenarios were considered to predict As enrichment in the concentrate: 1) worst-case enrichment scenario: considers an EF=46 and all As-bearing phases reporting to the concentrate (Nc, Gdf and Cbt) (see section 4.1.2); 2) only sulfides reporting to the concentrate (Gdf and Cbt), with EF=26 and 46. For the worst-case scenario, As levels in the concentrate would be around 875 ppm in the high-As interval (Table 17). For the second scenario, the concentrations are lower: 163 ppm and 288 ppm for EF=26 and 46 in the high As-interval, respectively, and 7 ppm and 13 ppm, respectively, for the low-As intervals. None of the estimates are above common charging limits, which starts from 2000 ppm (Table 2).

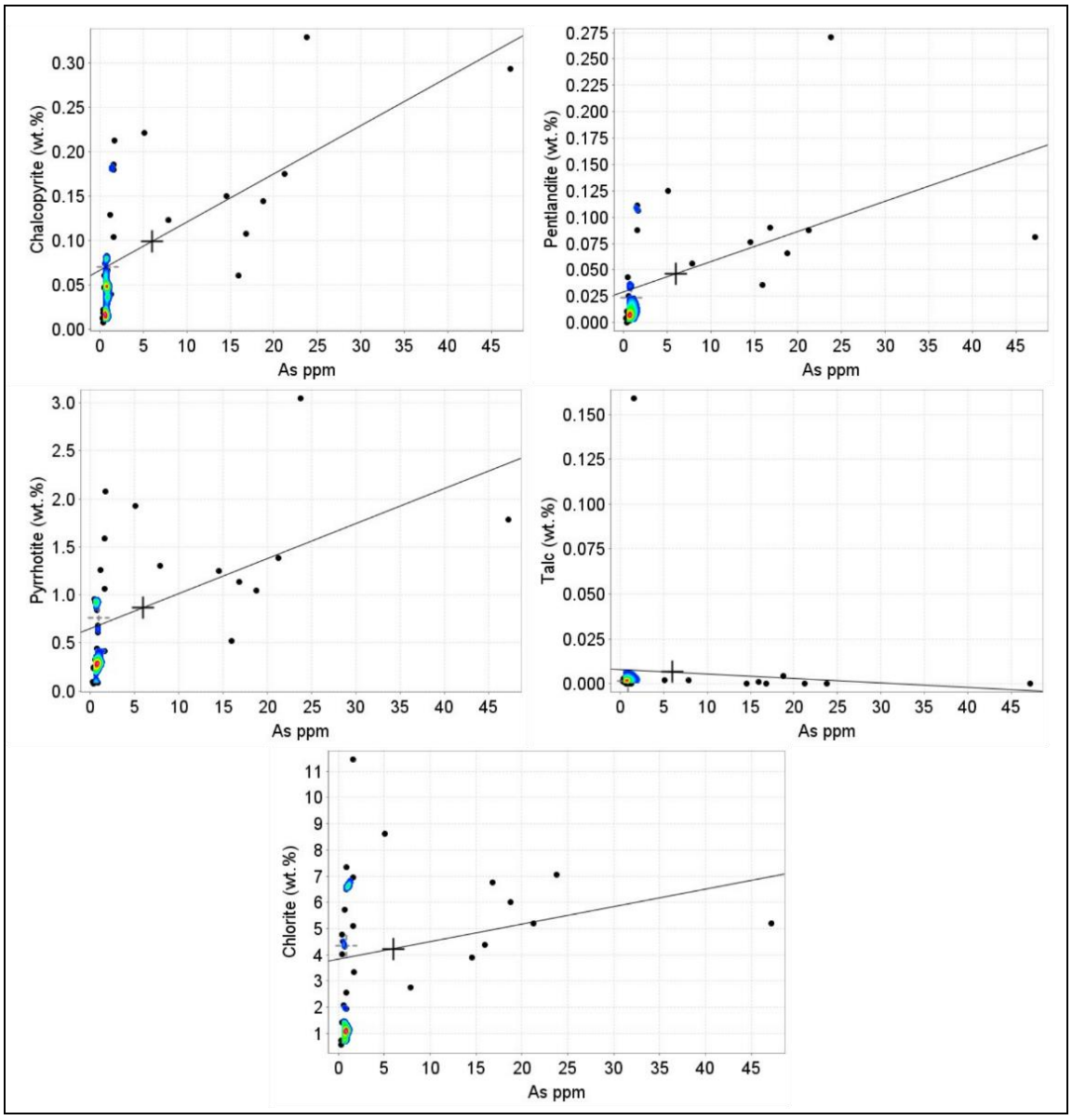

Figure 36 - Arsenic vs. Ccp, Pn, Pyh, Tlc, Chl and total sulfides, displaying point density opacity.

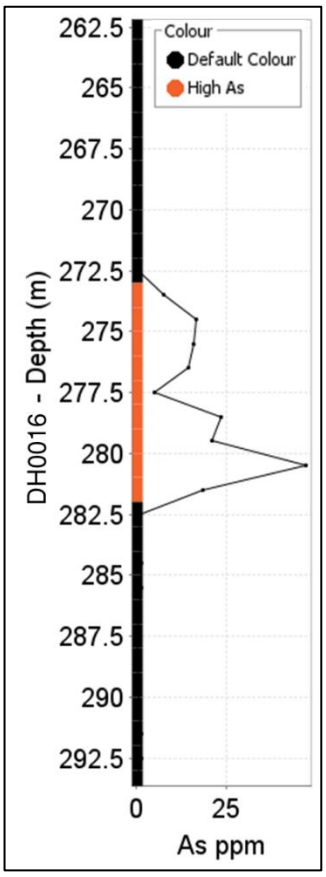

Figure 37 - Downhole As concentration plot with 10-meter-intervals for enrichment assessment.

Table 17 - Estimations of arsenic enrichment in the concentrate. 1) considering all As-bearing minerals, i.e., gersdorffite, nickeline and cobaltite; Enrichment factor 46. 2) considering As-bearing sulfides, i.e., gersdorffite and cobaltite; Enrichment factor 26 and 46.

DH0016 - interval	Total As (ppm)	1) EF 46 (ppm)	As from Cbt+Gdf (ppm)	2) EF 26 (ppm)	2) EF 46 (ppm)
High As	19.03	875.33	6.27	162.90	288.21
Low As	0.85	39.20	0.28	7.30	12.91

4.2.3.2 Bismuth

Bismuth shows moderate to poor correlation with all selected mineralogy, except talc (Figure 38). It has an average concentration of 0.35 ppm for the whole interval. Intervals 1, 2 and 3 in Figure 39 present average Bi grades of, respectively, 0.13, 0.71 and 0.23 ppm. Even in a worst-case enrichment scenario, on which all Bi would report to the concentrate and considering EF=46, the maximum bismuth grade in the concentrate would be around 33 ppm for interval 2, less than common charging limits, which start at 200 ppm (Table 2).

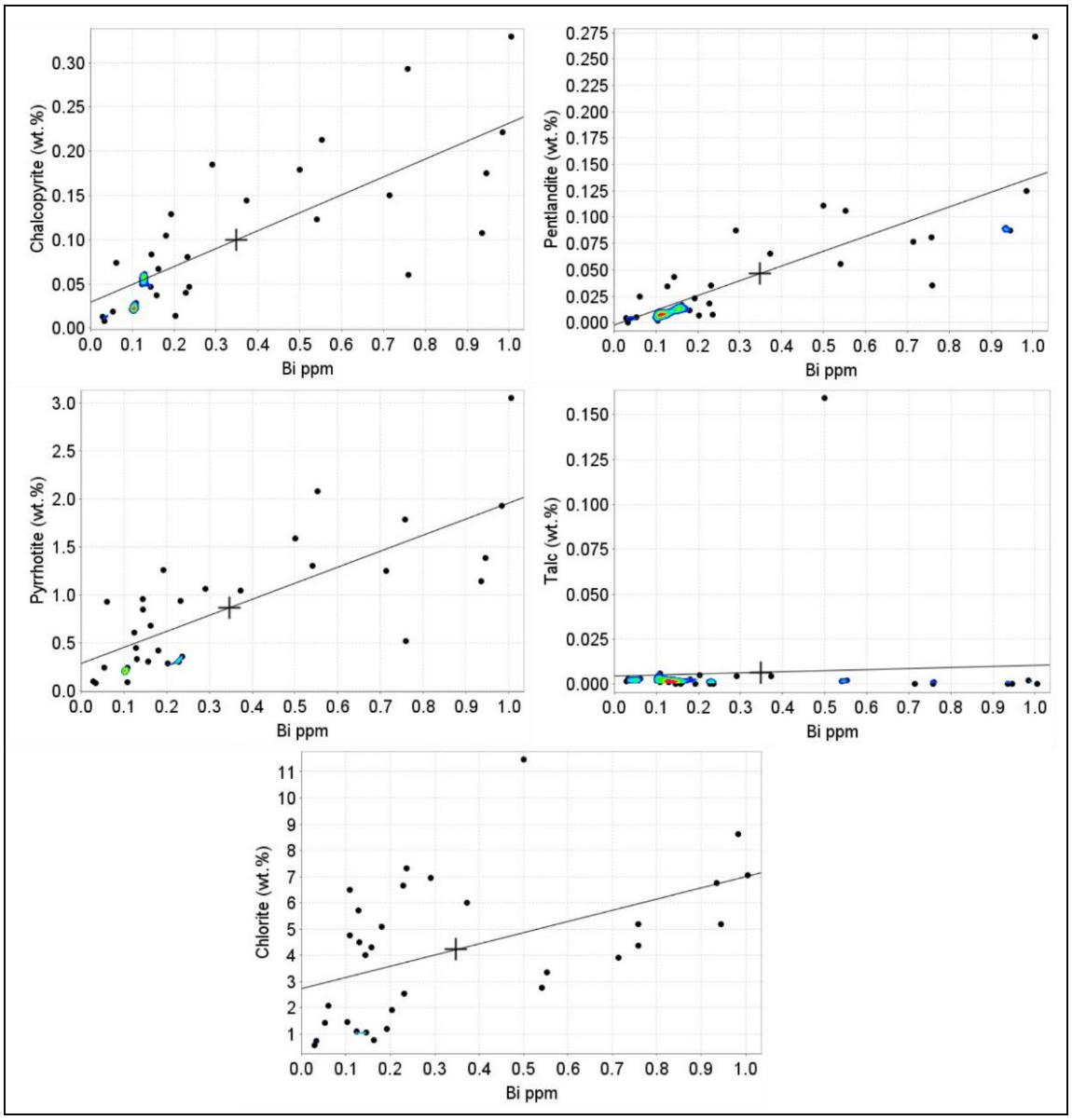

Figure 38 – Bismuth vs. Ccp, Pn, Pyh, Tlc, Chl and total sulfides, displaying point density opacity.

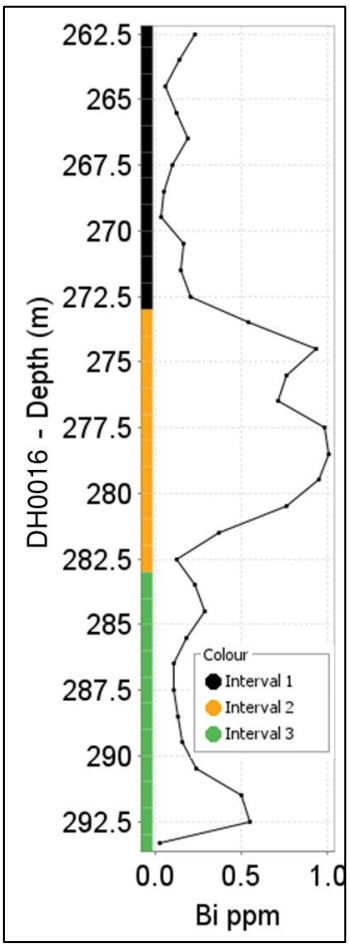

Figure 39 – Downhole Bi concentration plot with 10-meter-intervals for enrichment assessment.

4.2.3.3 Zinc

Even though correlated with selected mineralogy for the whole dataset, Zn does not present correlation with these same minerals in this interval (Figure 40). Moreover, charging limits for Zn (Table 2) are more than 300 times above the average for the interval, which is 92 ppm.

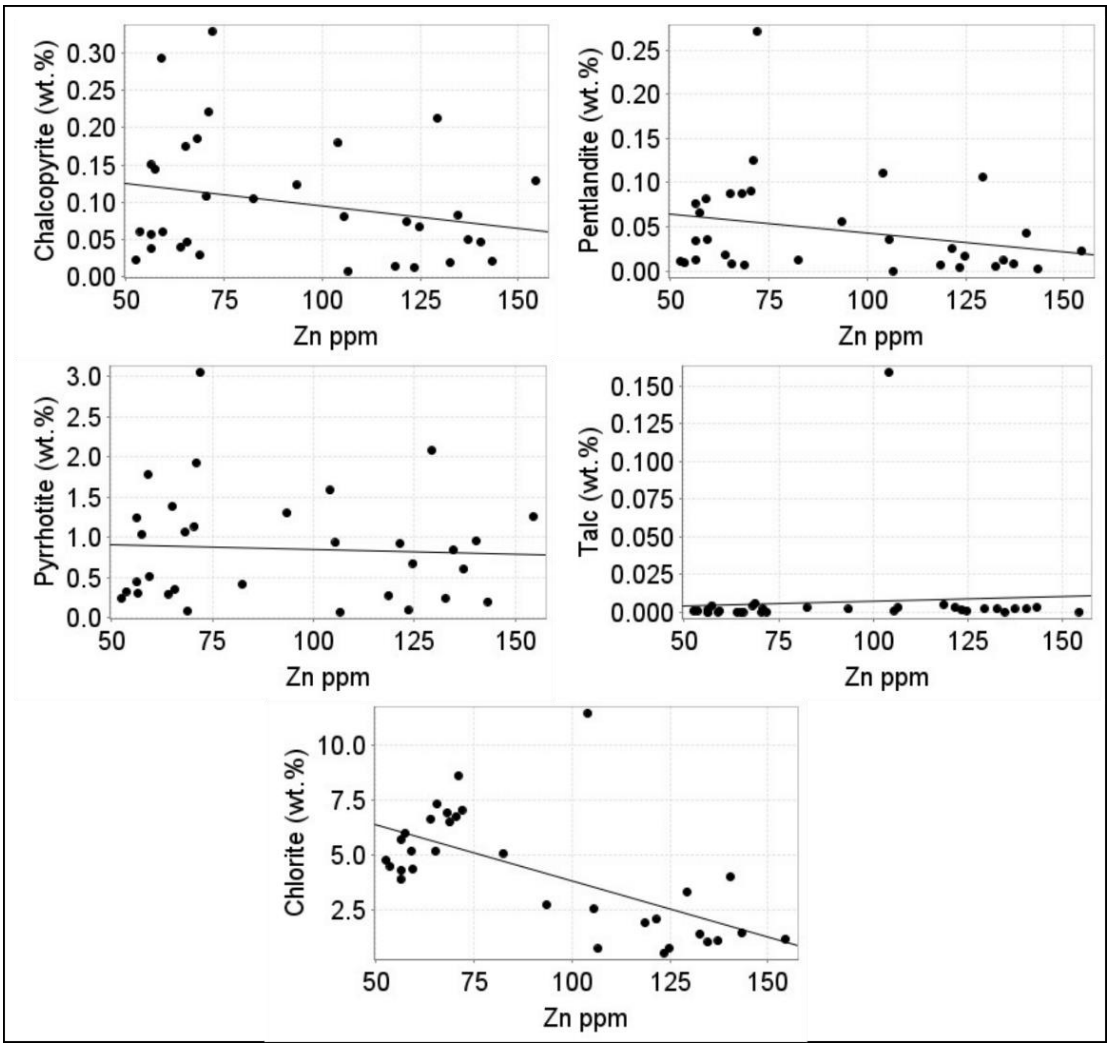

Figure 40 – Zinc vs. Ccp, Pn, Pyh, Tlc, Chl and total sulfides.

4.2.3.4 Selenium

Similar to Bi, Se correlates with all selected minerals, except talc (Figure 41). The average Se grade for the whole interval is 1.76 ppm, increasing to an average of 2.92 ppm in the interval 272-282 m (Figure 42). In a worst-case scenario, with EF=46, selenium levels in the concentrate would reach around 130 ppm. As discussed for DH0005 (see section 4.2.1.4), references for Se limits are quite variable (Table 2), thus this element concentration is reported in the domains.

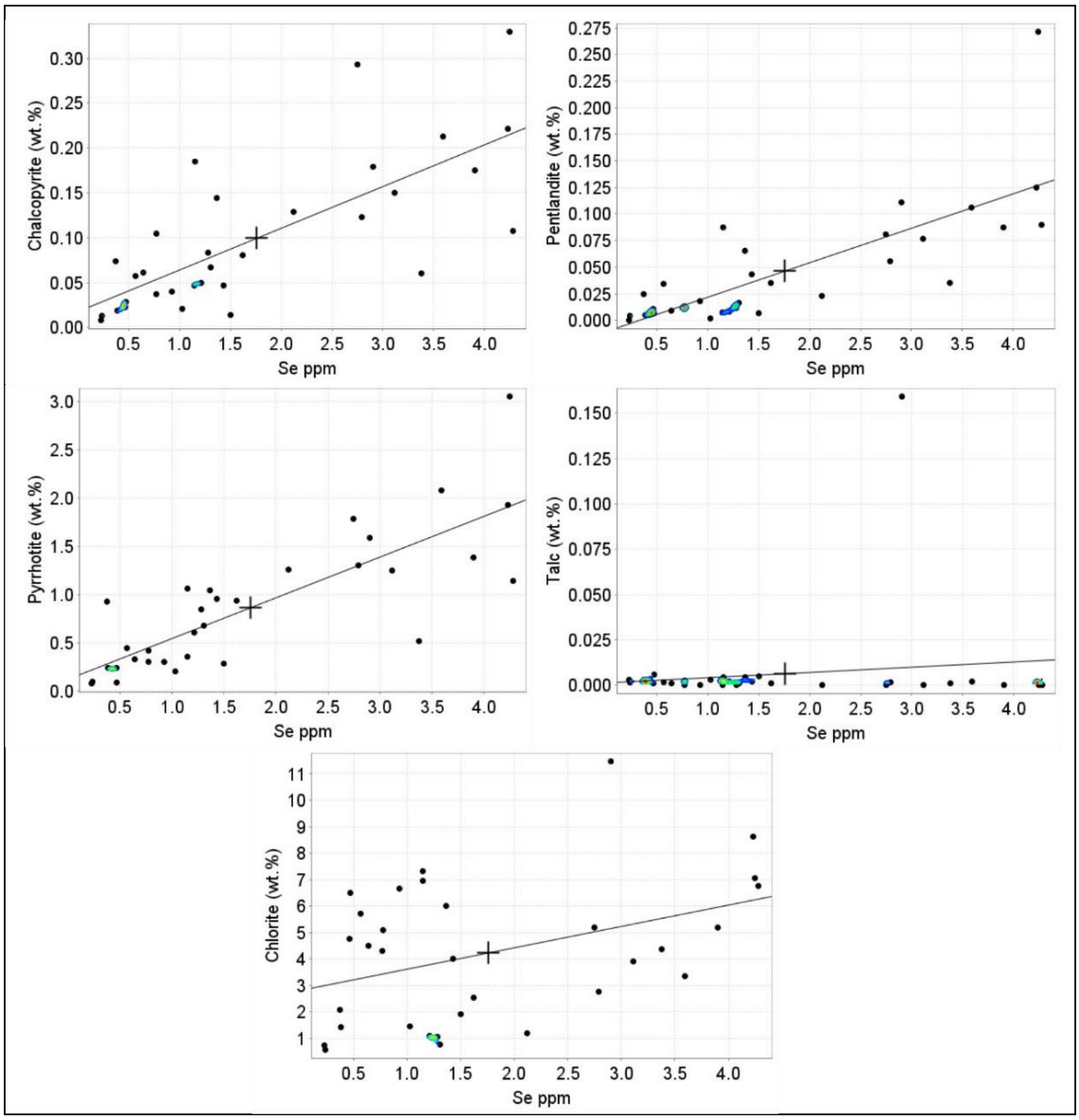

Figure 41 – Selenium vs. Ccp, Pn, Pyh, Tlc, Chl and total sulfides, displaying point density opacity.

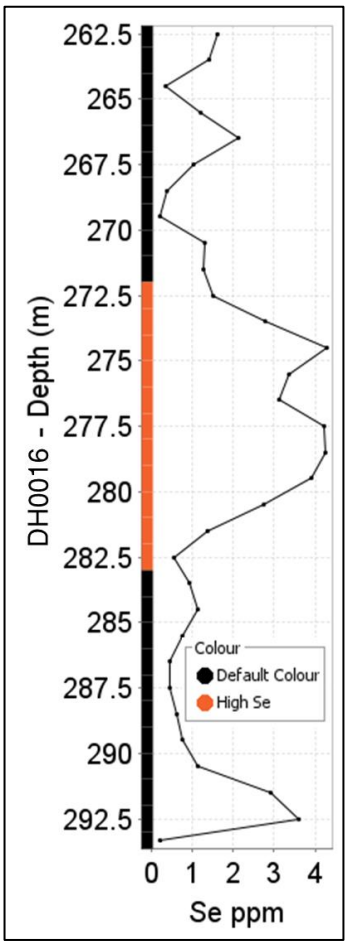

Figure 42 – Downhole Se concentration plot with 10-meter-intervals for enrichment assessment.

4.2.3.5 Magnesium

Magnesium correlation with Mg-silicates is not very clear, especially for talc, which is roughly absent in this interval (Figure 43 and Figure 44). Thus, deportment analysis is carried out to exclude Mg from other gangue mineralogy that is not expected to report to the concentrate. The average Mg grade in the 30-m interval is 5.96 wt%, which is very close or above common smelter charging limits: 5.0 to 7.5 wt% (see section 1.3.1) (Table 2).

Two scenarios are considered to estimate Mg levels in the concentrate: 1) talc and chlorite reporting to the concentrate (Table 18); 2) only talc reporting to the concentrate, given its hydrophobic character (Table 19) (see section 1.3.1.1). Results indicate that chlorite is the main responsible for high magnesium levels in the given interval. If this mineral reports into the concentrate during flotation, final Mg grade would be above 5 wt% for all 3 intervals; whereas if considering only talc in the concentrate, the grade decreases to a maximum of 0.02 wt%.

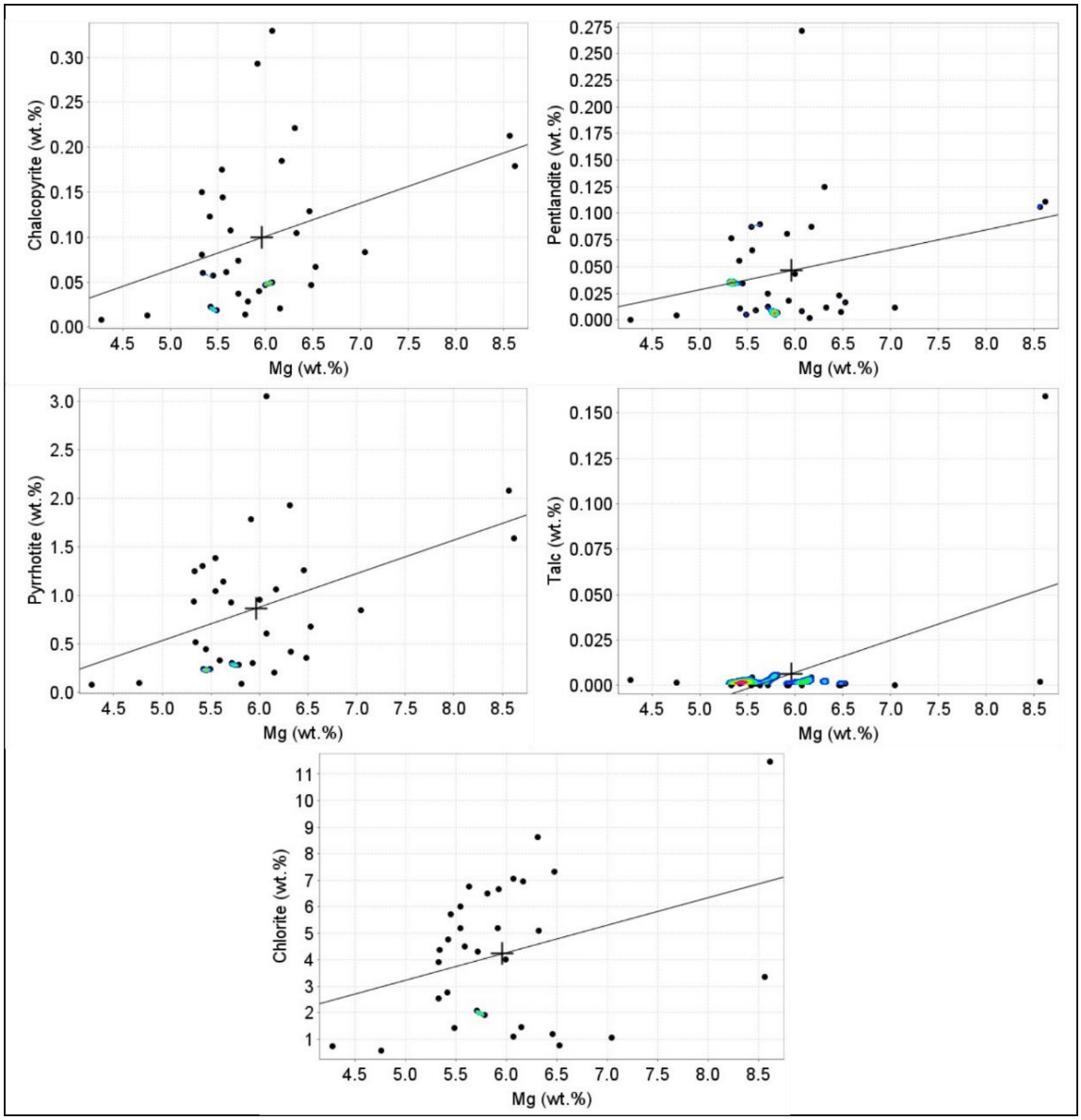

Figure 43 – Magnesium vs. Ccp, Pn, Pyh, Tlc, Chl and total sulfides, displaying point density opacity.

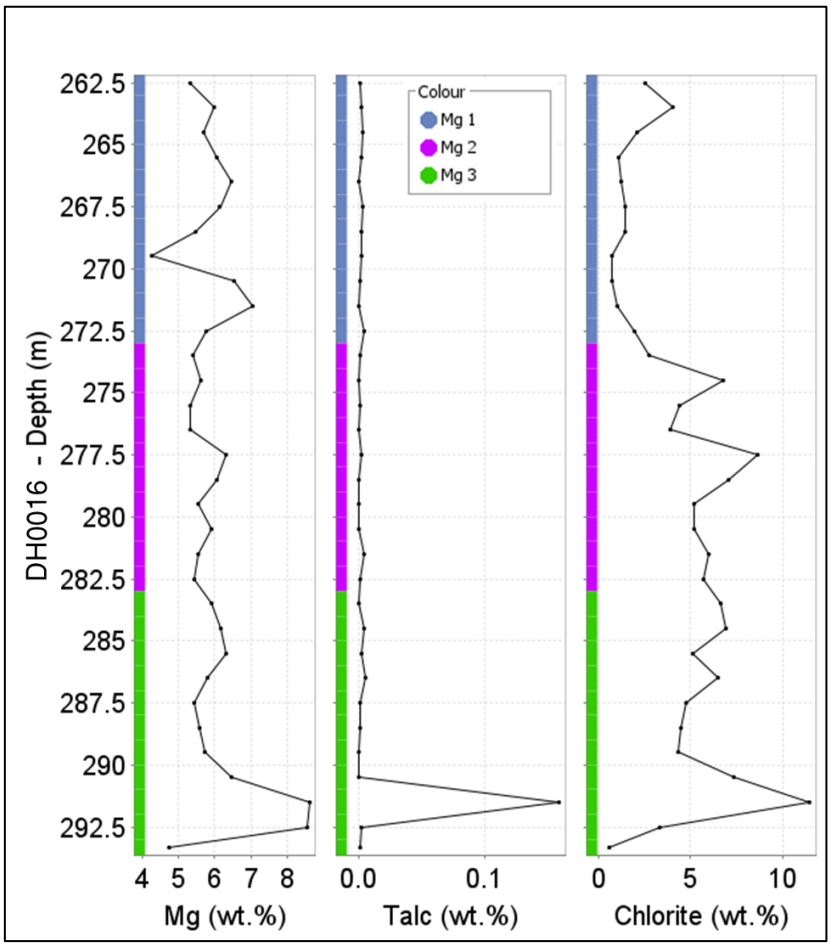

Figure 44 – Downhole Mg, chl and tlc concentrations plots with 10-meter-intervals for enrichment assessment.

Table 18 – Worst-case scenario, considering that both chlorite and talc would report to the concentrate. Levels close or above no charge limits are highlighted in red.

DH0016	tlc %	chl %	tlc % in conc	chl % in conc	Mg in tlc conc (%)	Mg in chl conc (%)	total Mg in conc (%)
Mg 1	0.00	1.67	0.05	42.10	0.01	5.57	**5.58**
Mg 2	0.00	5.56	0.01	46.31	0.00	6.13	**6.13**
Mg 3	0.02	5.59	0.15	52.83	0.02	6.99	**7.02**

Table 19 – Case scenario considering that only talc would report to the concentrate.

DH0016	tlc %	tlc % in conc	Mg in tlc conc (%)
Mg 1	0.00	0.05	**0.01**
Mg 2	0.00	0.01	**0.00**
Mg 3	0.02	0.15	**0.02**

Table 20 summarizes the penalty elements grades in the mineralised interval, the results for the estimations of their grades in the concentrate, and the ranges of no-charging limits considered in this study. Magnesium is above the threshold, whereas arsenic and selenium are within an uncertainty zone.

Table 20 – Summary of penalty elements analysis for high-grade zone in DH0016.

DH0016			
Penalty element	**Average grade**	**Estimated grade in conc. in worst-case scenario**	**No-charging limit range**
As	6 ppm	875.3 ppm	300-2000 ppm
Bi	0.35 ppm	33 ppm	200-500 ppm
Zn	92 ppm	4232 ppm	30000 ppm
Se	1.8 ppm	130 ppm	10-300 ppm
Mg	6.0 wt%	7.0 wt%	5.0-6.5 wt%

4.2.4 DH0016 – Clustering results

The input variables were pentlandite, chalcopyrite, pyrrhotite, talc, chlorite and arsenic. Even though the estimations presented in section 4.2.3.1 indicate that As levels in the concentrate would not be above charging limits for this interval, the penalty element was still selected as a variable for standardization purposes in both datasets, i.e., DH0005 and DH0016. K-means was the algorithm selected for clustering the mineralised zone of DH0016, using k = 3 (5000 tries) (Figure 45; Figure 46; Figure 47). An attempt using k = 2 did not produce good results in terms of identifying the main characteristics from the selected variables.

It is important to notice that none of the variables present major contrasts within the 30-m interval. From 274 to 282 m, cluster 3, it is observed the main dissimilarity, with high arsenic and slight enrichment in sulfides and chlorite. Cluster 2 presents the lowest values for roughly all variables and the lowest count in samples, i.e., 5. Cluster 1 has characteristics closer to the average for the whole interval, thus, could be described as a good representation of the mineralisation zone in DH0016, whereas the other two domains would be the extremes in the dataset.

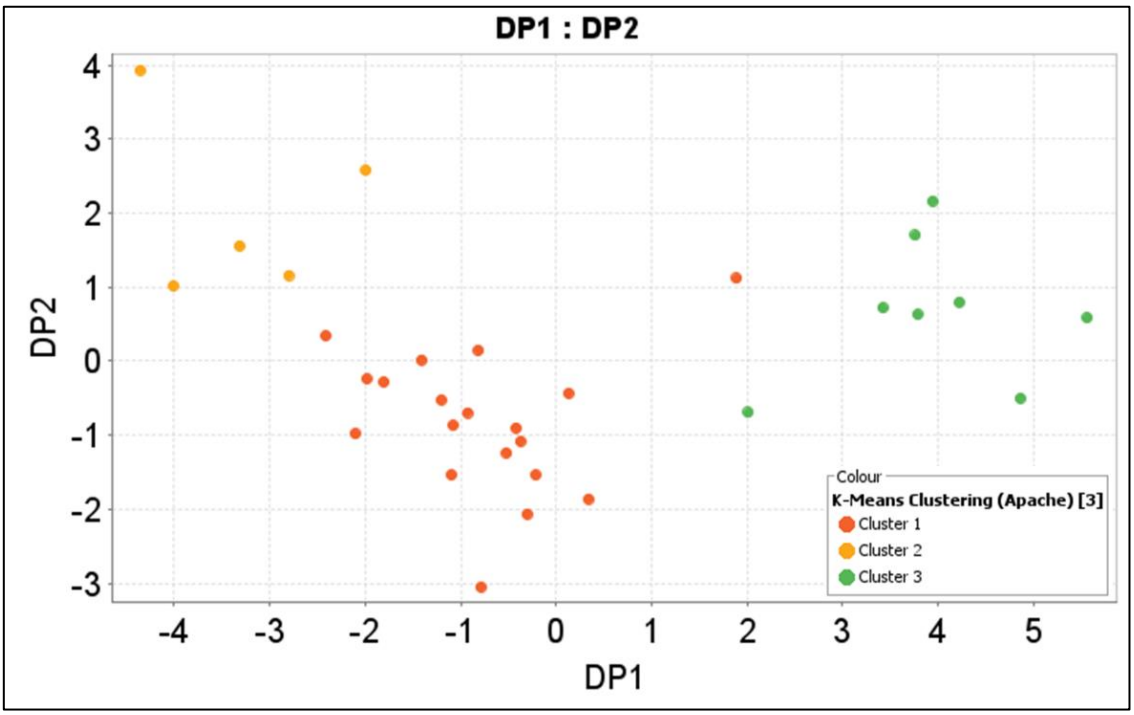

Figure 45 – K-means clustering result for k = 3 represented in two dimensions, DP1 against DP2.

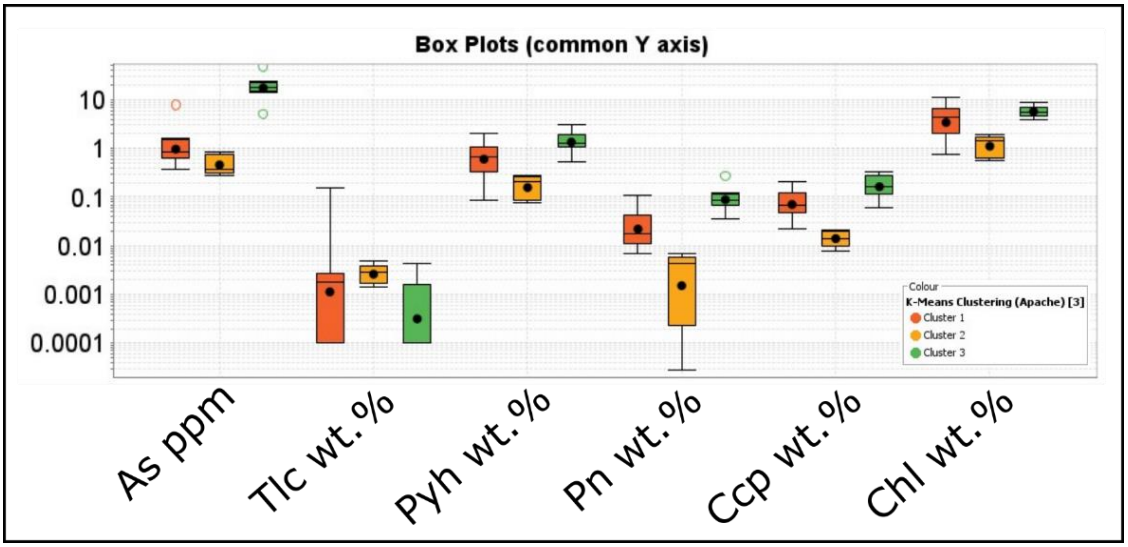

Figure 46 – Box plots displaying K-means clustering results for k = 3 in logarithmic scale for abundances of the variables considered in the analysis.

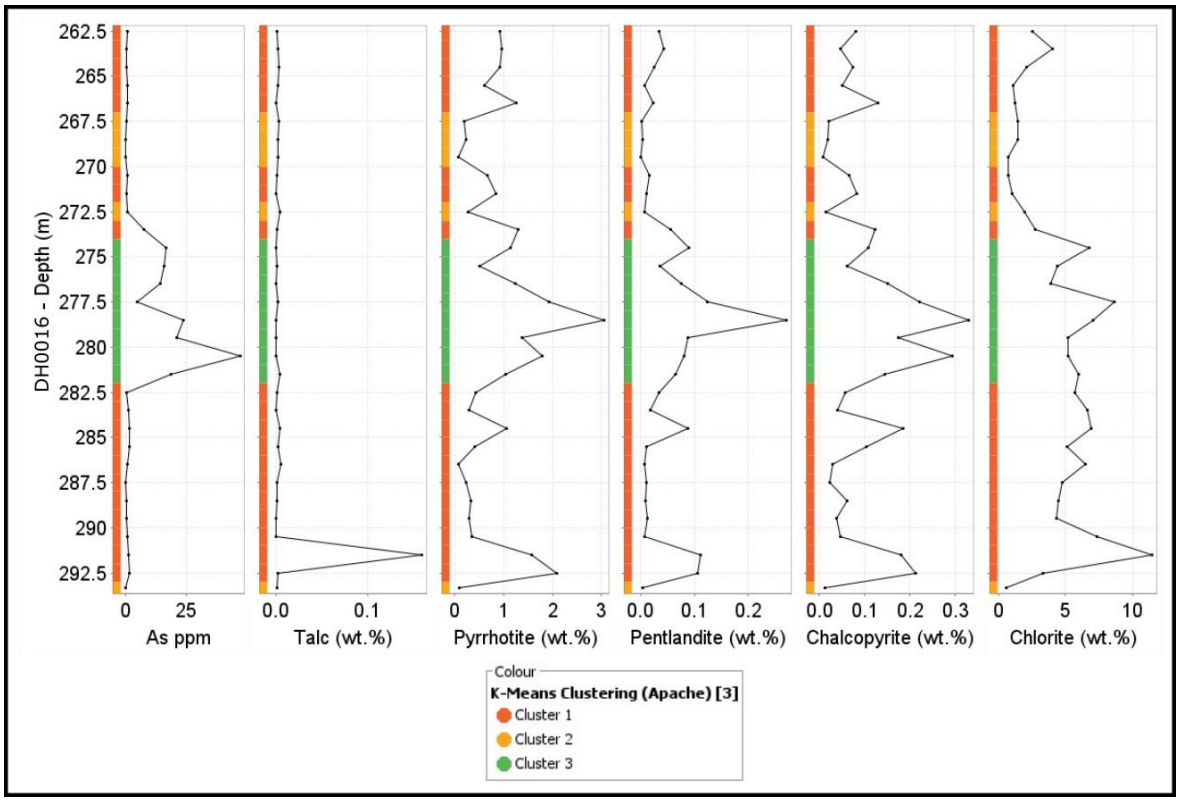

Figure 47 – Downhole plots displaying K-means clustering results for k = 3 in logarithmic scale for abundances of the variables considered in the analysis.

4.3 Discussions

EDA and clustering analysis for both DH0005 and DH0016 indicates that sulfides are uniformly distributed throughout the mineralized zone, thus the segregation of the high-grade zone based on sulfide modal mineralogy is not very efficient. Even though MLA data is not continuous, sulfide grain size data indicates consistent variations along the mineralized interval in DH0005. The variations also match well mineralogical and assay domaining, indicating that As-rich intervals in the gabbro tend to be also coarse-grained (Figure 31-A) and slightly more differentiated, with higher felsic minerals content. This might be explained by the high partition coefficient of chalcophile elements like As and Bi (Barnes, 2018). These metals might have been retained into the sulfide melt up to a late stage, when a more evolved gabbro was crystallizing and the sulfide droplets had coalesced and been able to displace the silicate mush, creating coarser sulfide grains. The last phases to precipitate would have been the secondary sulfides, such as gersdorffite and cobaltite, which are observed as rims around valuable sulfides. Bi-Te-bearing-tetradymite group minerals are observed in SEM analysis preferentially at the

coarse-grained-sulfide zones (Gregory, 2021). Due to the coarse grain size of the valuable sulfides, comminution would probably not be required in very fine fractions (Kittelty & Smith, 2021). This might also avoid the liberation of arsenic phases that are not associated to valuable sulfides.

For the grains of gersdorffite and cobaltite that are liberated, as well as for pentlandite-pyrrhotite selective flotation, the use of depressants, such as TETA (triethylenetetramine) and sodium metabisulfite may be considered (S. Kelebek & C. Tukel, 1999; Toronto (CA) Patent No. 10/960,527, 2004). The addition of cyanide to the flotation cell is also reported to produce a depressant effect on gersdorffite at specific pH conditions (Senior et al., 2009).

Clustering was more sensitive to the variations in the concentrations of chlorite, talc and arsenic. Since these are directly related to the lithologies, the results are very similar to the lithological logging available for DH0005. That is, for k = 3, cluster 3 matches the pyroxenite and clusters 1 and 2, the gabbro. These two lasts would possibly represent minor internal faciological variations within the gabbro. For k = 2, cluster 2 is related to the pyroxenite. In this case, samples from the previous clusters 1 and 2, for k = 3, were merged into one single cluster, due to the proximity of their samples. This result matches lithological logging. Since As enrichment within the gabbro is not constant, more detailed domaining may be useful for assessing zones of enrichment on this element. In this regard, DBSCAN results are more accurate and sensitive to the variations of arsenic. Selenium levels are homogeneous, with an average of 4.8 ppm. Considering that maximum levels for this element can go from 50 ppm to 300 ppm (Table 2), further consideration should be made, as an enrichment of 10 times for this element during concentration could result in charges from smelters.

Being As a chalcophile element (Haldar, 2017), it was expected to be correlated with the sulfide phases. However, this correlation is probably not observed since the element was partitioned into As-bearing sulfide phases, such as cobaltite, gersdorffite, and the Ni arsenate nickeline. The probable sub quantification of these minerals, as described in section 4.1.2, is expected to be the reason for the unclear correlation of As to the selected mineral phases. Tetradymite group inclusions, which were observed in MLA, possibly explain the indirect moderate

correlation between sulfides and Bi. Thus, it is important to highlight that the correlations that are observed between penalty elements and sulfides, talc and chlorite may be indirect, as a result of the partition of these elements into mineral phases that are associated to each other and occur within the same mineralized zones. This is probably what happens in zinc against chlorite and talc, for instance (see section 4.2.1.3).

The interval 251.05 m to 262.51 m in DH0005 is chlorite- and talc-rich. These minerals are, in general, finer than the valuable sulfides (Figure 30), and especially chlorite, can be commonly associated to the sulfides, as described in section 4.2. These are thus likely to be liberated during comminution, producing fines in excess, or still attach to sulfide grain surface. In both cases it can lead to decreased efficiency during flotation by, respectively, entrainment of fines to the froth or by prevention of valuable sulfides from floating (see section 1.3.1.1). In this case, pH control, as well as the use of soda ash or even Carboxy Methyl Cellulose (CMC) group as dispersants may be efficient. Internal report indicate that reduced pulling may be required (Kittelty & Smith, 2021). Talc, as hydrophobic mineral, can poison the concentrate and reduce its grade. In addition, it can contribute to decrease Fe:MgO ratio, which is desired to be above 5 (Correia, et al., 2020). The use of the depressant foenum-graecum (FGM) has shown good selectivity for both talc and chlorite depression by adsorbing into the surface of these minerals plus resulting in weak interaction with Cu and Ni minerals (Zhao, et al., 2015).

For further geometallurgical assessment in DH0005, two main zones are recommended to be prioritized for metallurgical testing. The first is defined as cluster 3 in K-means (k = 3) and DBSCAN domaining, and as cluster 2 in K-means (k = 2). It is mainly related to the enrichment in Mg-silicate phases, i.e., talc and chlorite. This interval is roughly 10-meter-long, starting from depth 251 m, and presents good correlation with what has been logged as pyroxenite. Magnesium- and Fe-deportment analysis is key for improving this domain's knowledge. The other priority zones are better defined by DBSCAN clustering, and are labelled as cluster 2, being related to arsenic enrichment. They occur within what has been logged as gabbro and requires further assessment on assay of minor elements, such as As itself. In general, detailed studies and tests on grinding size, liberation, flotation

concentration quality and response per mineral are necessary in order to confirm the early results and interpretations provided.

For DH0016, the whole interval was previously classified as a gabbro. For this DH, the variability in the parameters is even more subtle compared to DH0005. Chlorite concentration increases to over 5 wt% from 274 m deep and is the most significant change observed. Thus, clusters 1 and 3 should be investigated for this matter. In the same fashion as in DH0005, cluster 3 in DH00016 also presents high Se levels, up to 4 wt%. Depending on the specifications for this element in the concentrate, an enrichment of 13 times would result in the application of charges. Calculated arsenic levels are below charging limits even in a pessimistic scenario.

In summary, the relative mineralogical homogeneity in DH0016 indicate that chlorite could be the main object of concern for this high-grade zone intersect. Because of that, manual clustering based on this mineral concentration should be enough for compositional assessment within the interval. The low number of samples and addition of parameters that are roughly constant throughout the interval enhances small scale details, which are probably not relevant at a stage of exploration. Information on mineral association and grain size is recommended in order to confirm whether the high-grade zone in DH0016 is homogeneous in terms of texture.

Ideally, LIBS modal mineralogy data using the same configuration and resolutions for acquisition from both DH0005 and DH0016 would allow the comparison and integration of the domaining assessment and results for the two datasets. Cluster 3 from DH0005 correlates well to cluster 2 from DH0016 when considering Mg silicates. Both present the highest talc and chlorite averages: talc > 9 wt% and chlorite > 5 wt%. When considering As, none of the DH0016 samples reaches levels as high as the ones observed in cluster 2 of DH0005. For the first DH, cluster 2 has the highest average, 20.42 ppm, whereas in cluster 2 from DH0005, it is 114.05 ppm.

5 ASSESSMENT ON ACID ROCK DRAINAGE (ARD) POTENTIAL

In this case study, the target metals Ni and Cu are mainly hosted by pentlandite and chalcopyrite, which are in turn associated with pyrrhotite. The last

is the most abundant sulfide, with an average of 1.64 wt% within the high-grade zone and reaching up to 32 wt% in some intervals.

Even though pyrrhotite can contain up to 0.8 wt% Ni and 0.5 wt% Cu, indicated by MLA results, it is aimed to be separated from pentlandite and chalcopyrite during flotation, generating a pyrrhotite concentrate. Due to this, it is possible to consider this concentrate as a by-product and further evaluate the environmental impact that would be avoided by treating this material as a valuable product rather than as a passive or a mine waste. In addition to the ROM, the low-grade and barren zones, which are the focus of this assessment, can also be characterized, as it commonly represents the largest volume of material to be disposed from mining activities.

5.1 Workflow

The workflow described herein provides a general overview of the approach followed in order to use LIBS mineralogy and geochemical assay data to provide insights in terms of acidification potential. Estimations on the behaviour of the low-grade and barren zones material are considered. Even though it is a case specific methodology developed for the prospect, it can be adapted and used as a guide as part of an early environmental impact assessment at exploration stage in other mineral prospects (Figure 48).

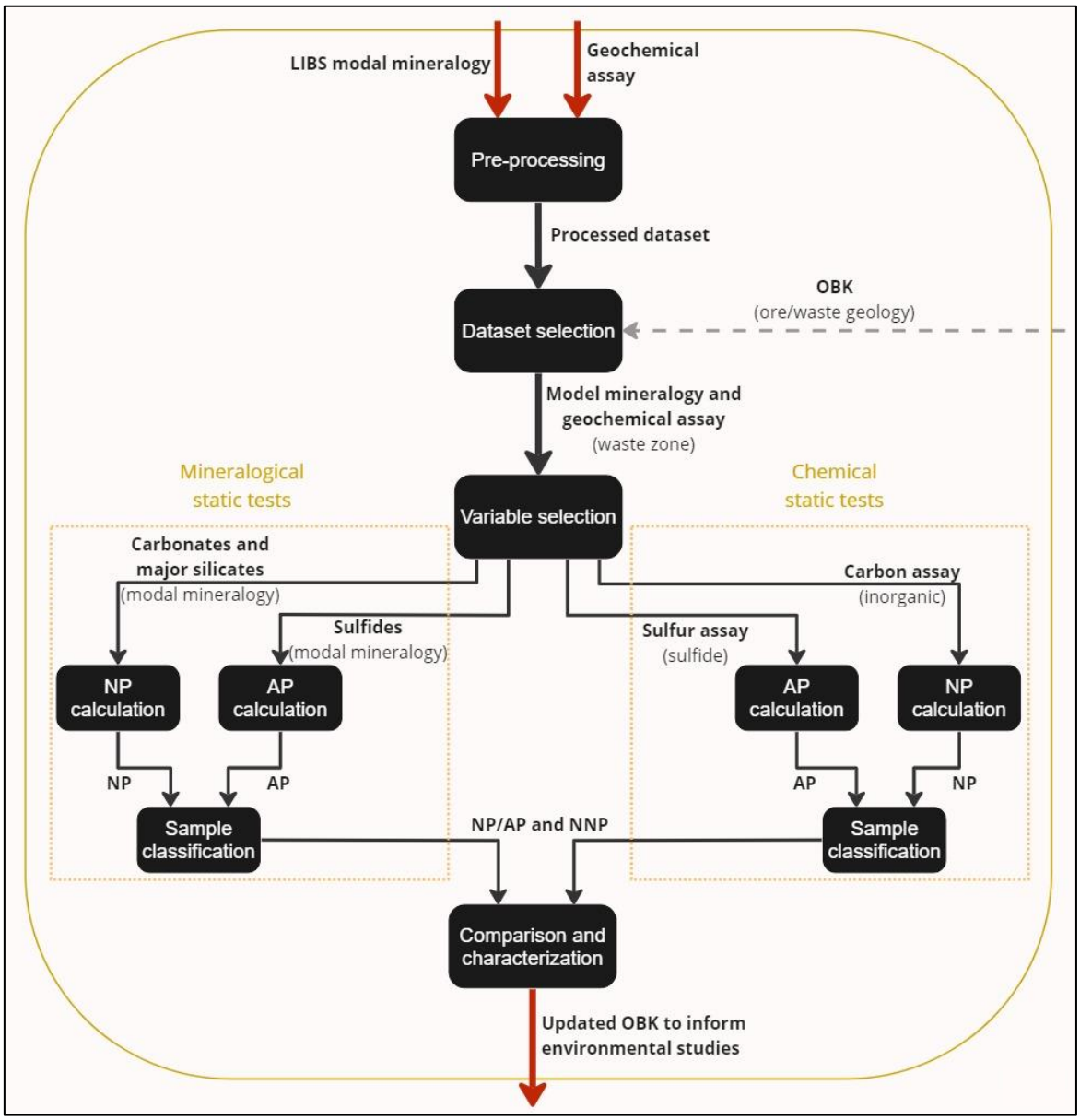

Figure 48 – Workflow for ARD assessment using mineralogical and geochemical static tests.

5.1.1 Dataset selection

The low-grade and barren zones were defined based on samples lying outside the shell for Ni > 0.2 wt% (see section 3.3). It includes samples previously logged as intrusive and country rocks that can potentially be classified as waste. The DHs DH0016 to DH0021 were considered for the assessment using modal mineralogy, given the data resolution (see section 3.1.1) and because the acquisition was made using the same configuration (MVP). For LIBS mineralogy, the dataset is composed of 1828 samples composited in 1-m long intervals. The main mineralogy is plagioclase (55.1 wt%), biotite (24.1 wt%), hornblende (11.7

wt%), quartz (4.4 wt%), chlorite (2.4 wt%) and prehnite (1.4 wt%) (Table 21). For the geochemical assay, the same interval comprises 654 samples. The low-grade and barren zones dataset for all DHs are also considered in the geochemical static tests, totalizing 1719 samples.

Table 21 – Low-grade and barren zones LIBS modal mineralogy.

Mineral	Average (wt%)
Apatite	0.105
Biotite	24.138
Calcite	0.060
Chalcopyrite	0.017
Chlorite	2.458
Chromite	0.002
Ferrosilite	0.070
Hornblende	11.737
K-feldspar	0.254
Pentlandite	0.004
Plagioclase	55.152
Prehnite	1.379
Pyrrhotite	0.198
Quartz	4.409
Talc	0.010
Titanite	0.007

Carbon assay is equivalent to total, and for this assessment it is inferred that no graphite or any other organic-carbon-bearing mineral is present. Graphite was not detected by LIBS as it was not included in the mineral library at the time of the analysis. However, drill core logging reports the presence of graphite in DH0020, interval 510-515 m. Additionally, graphite is reported in the region where the prospect is located: graphite-bearing Laukunkangas intrusion (Peltonen, 2005); graphite in Vammala type intrusions (Makkonen, 2015); graphite in the ultramafic complex of Hitura prospect (Isohanni, et al., 1985); and 5-15 wt% graphite in Outokumpu schists and Talvivaara mudstones (Eilu, 2012).

The correlation between C geochemical assay and calcite from LIBS is poor (Figure 49), which may be a combination of the presence of graphite and possible underestimation of calcite. Graphite occurrence, however, is considered limited as it was logged in a narrow interval. Carbon geochemical assay average is 0.16 wt%,

up to 1.88 wt%, whereas calcite from LIBS average is 0.06 wt%, up to a maximum of 1.1 wt%. If all the carbon was hosted in calcite, 0.16 wt% average carbon would result in an average calcite of 1.3 wt%. On the other hand, the correlation between sulphur geochemical assay and the sum of sulfides, i.e., pyrrhotite, chalcopyrite and pentlandite, is excellent. Sulphur average content is 0.23 wt% in the same dataset used for modal mineralogy assessment (Figure 49) and 0.24 wt% for the whole dataset.

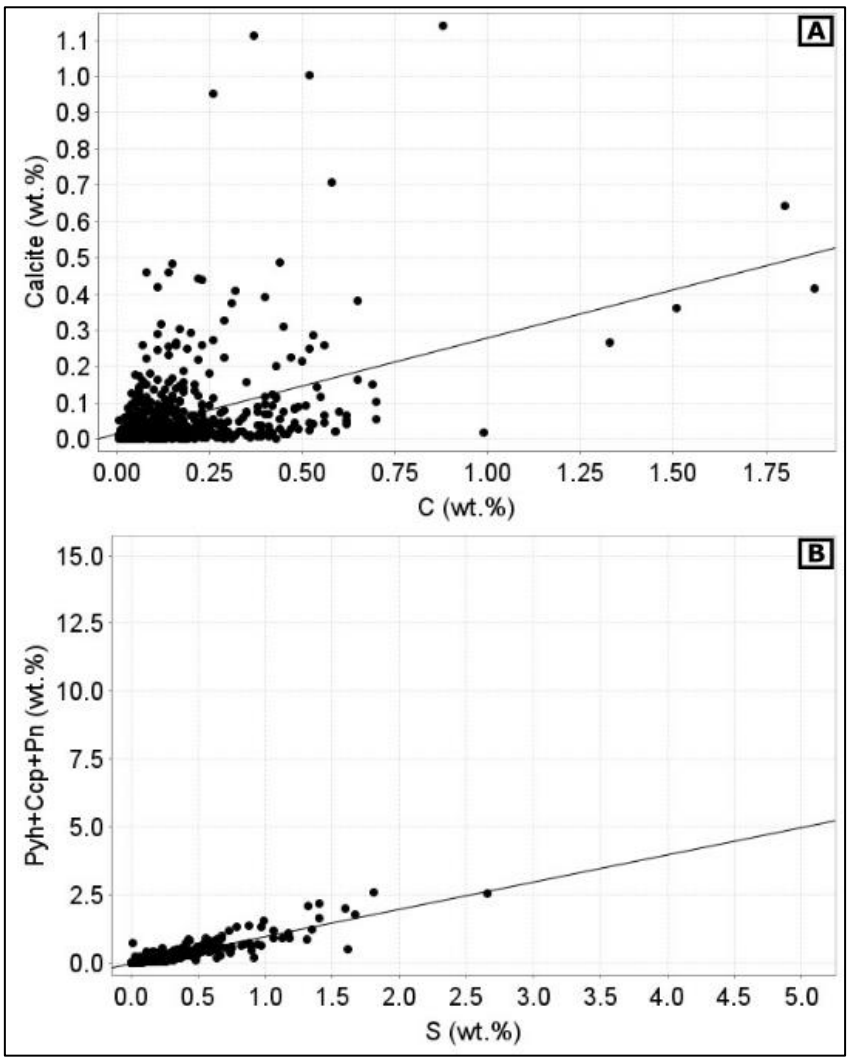

Figure 49 – LIBS modal mineralogy against geochemical assay. A) Calcite vs total carbon. B) Pyrrhotite, chalcopyrite and pentlandite against sulphur.

5.1.2 Geochemical static test

Geochemical static tests were performed for both the whole dataset and for the dataset comprising DH0016 to DH0021, which is equivalent to the DHs scanned at moderate resolution for LIBS (Table 8). The restriction to the second dataset aims

to compare results from geochemical against mineralogical tests. Equation 3 and Equation 4 were used to estimate the AP and NP, respectively. These results were then used to estimate the Net Neutralization Potential (NNP) and the NP/AP ratio (see section 1.3.2), which are classified according to Figure 2.

5.1.3 Mineralogical static test

Acid rock drainage estimations were also carried out using mineralogical assay tests, according to *Equation 5* for AP and *Equation 6* for NP. LIBS scanning modal mineralogy provides continuous information along drill cores. The application of these tests, therefore, aims to improve representativeness and robustness of estimations, as described in section 1.3.2. NP/AP ratio and NNP estimation results are classified according to Figure 2.

For both AP and NP calculations, minerals that occur in larger amounts than 1 wt% are included, as well as important minerals related to the AP and NP, sulfides and carbonates, respectively, in lesser amounts (Karlsson et al., 2018). The individual AP for chalcopyrite, gersdorffite, pentlandite, pyrite and pyrrhotite were calculated and then summed to find the total AP. For the total NP, individual mineral NP was calculated for biotite, chlorite, hornblende, plagioclase, quartz and calcite. Prehnite was not considered as its concentration in the reduced dataset is lower than 1 wt%. Calcite abundance was calculated from C geochemistry, assuming total C as inorganic. The relative reactivity considered the 30 wt% average mineral class content for simplification purposes in the estimations (Table 4).

5.2 Results

5.2.1 Geochemical static tests results

For the whole dataset using geochemical static tests, AP range is 0.16-159.36 kg $CaCO_3$/t, with an average of 7.62 kg $CaCO_3$/t. For NP, results range from 0.42 to 156.60 kg $CaCO_3$/t, at an average of 11.27 kg $CaCO_3$/t. According to NP/AP ratio diagram (Figure 50-A), 33.1% of the samples are classified as acid-generating, 18.8% are in the uncertainty zone and 48.1%, in the acid-consuming zone. The intrusive rocks have 41% of its samples falling within the acid-generating zone. This number drops to 15.3% for the host rocks. In the NNP classification diagram (Figure 50-B), the majority of the samples are classified as uncertain (87.9%), whereas acid-

generating and acid-consuming are, respectively, 8.1% and 4.0% of the samples. Samples from intrusive rocks are 5.7% acid-generating and, from host rocks, only 0.2%. The NNP varies from -148.5 to 126.3 kg $CaCO_3$/t, at an average of 3.6 kg $CaCO_3$/t.

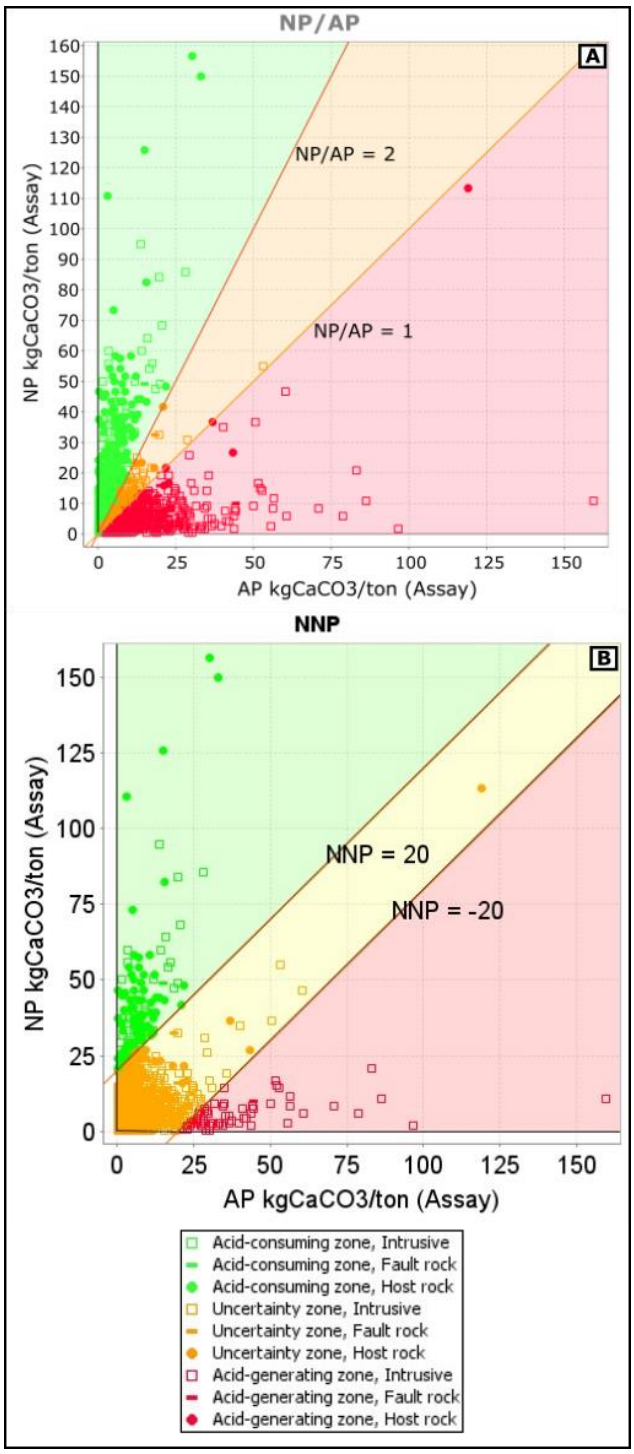

Figure 50 – NP/AP ratio (A) and NNP (B) classification diagrams using geochemical static tests for the whole dataset. In addition to colour classification for acidity potential, samples are also classified according to their major rock-type groups.

Considering only samples from DH0016 to DH0021, geochemical static tests result in AP from 0.16 to 83.1 $CaCO_3$/t and average 7.4 $CaCO_3$/t. 27.5% of the samples are classified as acid-generating, 16.9% as uncertain and 55.6% as acid-consuming. This represents an increase in 7.5% of the samples falling into the acid-buffering zone (Figure 51). The classification based on NP/AP ratio shows that the main potentially acid-generating zones are: 1) whole DH0016 extension; 2) top of DH0017, until 44 m; 3) central portion of DH0018, from 168 to 450 m; 4) and top part of DH0019, from 32 to 75 m (Figure 52).

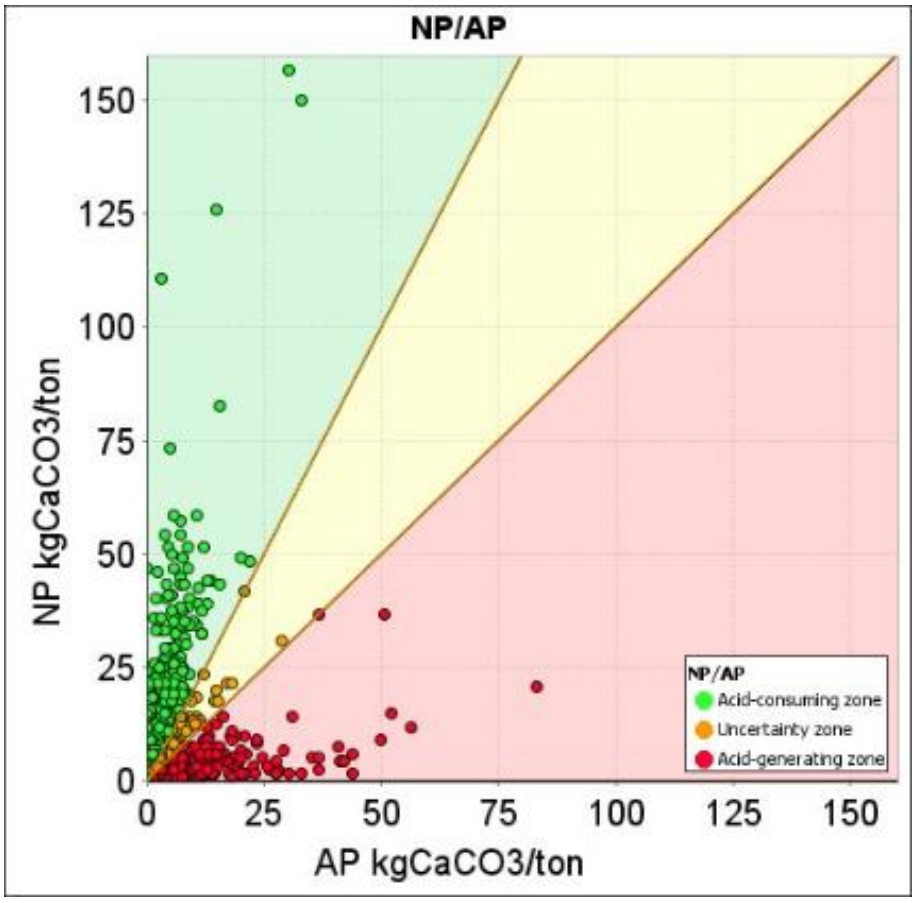

Figure 51 – NP/AP ratio classification diagram from assay geochemical tests for dataset DH0016 to DH0021.

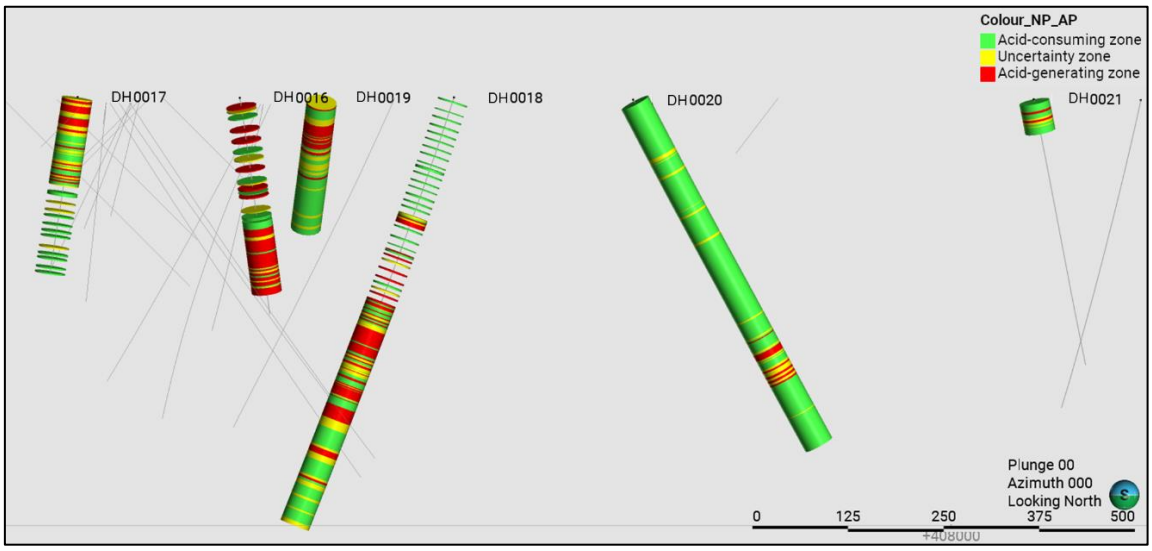

Figure 52 – Drillhole views looking north of NP/AP ratio classification using geochemical static tests in DH0016 to DH0021.

5.2.2 Mineralogical static tests results

The results for calculated NP and AP per mineral are presented in Figure 53 and Figure 54, respectively. For the first, calcite and chlorite present the strongest neutralization potentials, with maximum at 150.0 and 139.5 kg $CaCO_3$/t, respectively, and averages 14.5 and 10.4 kg $CaCO_3$/t, respectively (Figure 53). For the second, the acidification potential of pyrrhotite is much higher than all the other minerals, with a maximum of 32.6 and average of 1.8 kg $CaCO_3$/t. Chalcopyrite is the second strongest acid-potential producer, with a maximum of 4.3 and average 0.1 kg $CaCO_3$/t (Figure 54).

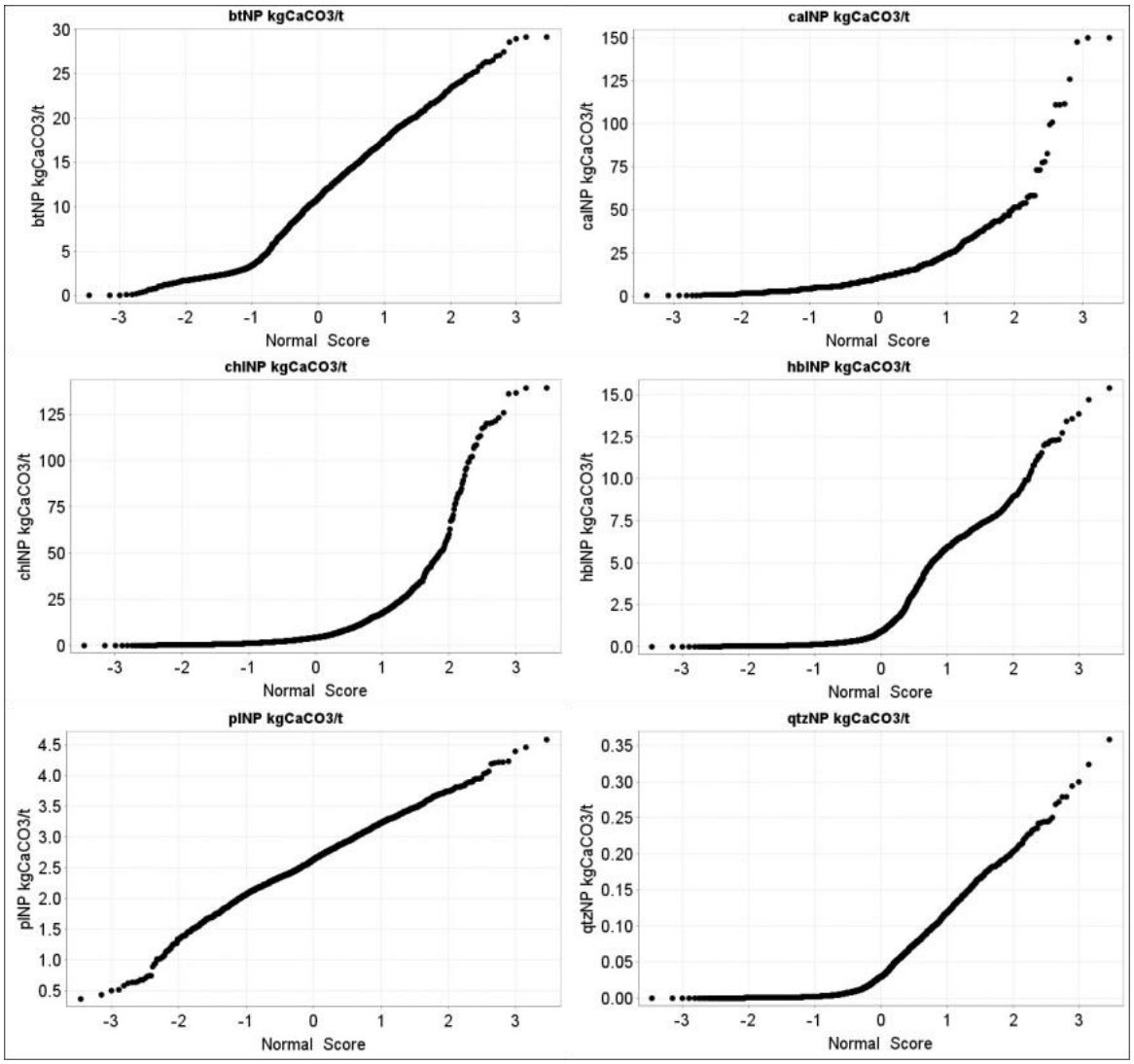

Figure 53 – Calculated NP distributions per mineral, based on mineralogical static tests.

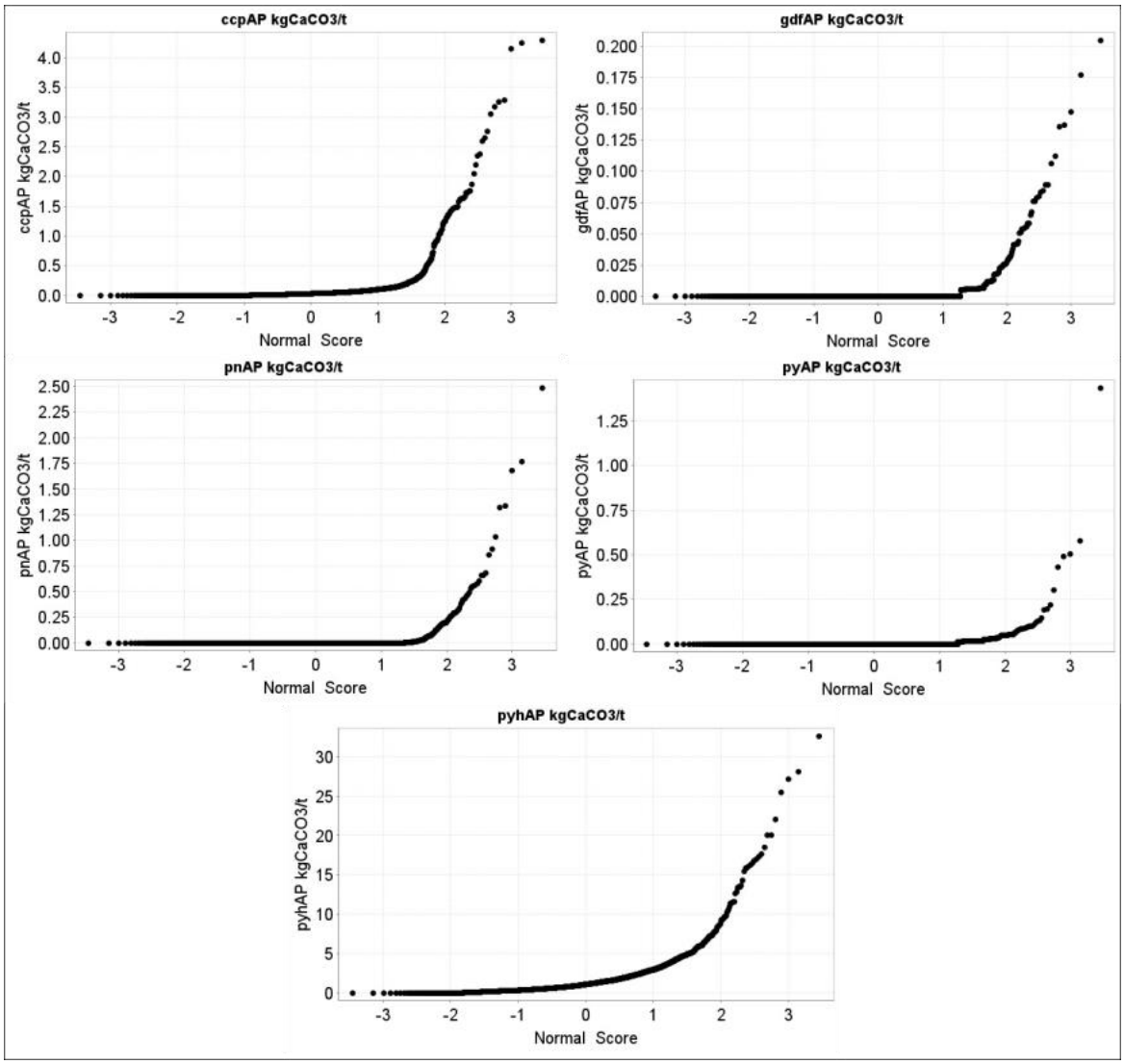

Figure 54 – Calculated AP distributions per mineral, based on mineralogical static tests.

The estimated total NP average is 42.2 kg $CaCO_3$/t, varying from 10.3 to 202.4 kg $CaCO_3$/t. The interval 180-260 m in DH0016, the first 25 m of DH0017, a short interval around 425 m in DH0018 and discontinuous intersects in DH0020, starting from 225 m to 520 m, are the zones with highest calculated NP (Figure 55-A). For AP, the calculated average is 6.5 kg $CaCO_3$/t, range 0.2-70.6 kg $CaCO_3$/t. The zones with strongest acidification potentials are 180-260 in DH0016 and 400-430 m in DH0018 (Figure 55-B). These zones match well the areas with the highest neutralization potentials. When the modal mineralogy that was used to calculate NP and AP is observed down holes, along with these estimations, in DH0016, chlorite enrichment and hornblende enrichments starting around 180 m correlates with the increase in the NP (Figure 56-A). For the same DH, AP increases around the same

zone. In this case, all sulfides present abrupt increase in their abundances, with matching the enrichments down hole (Figure 56-B).

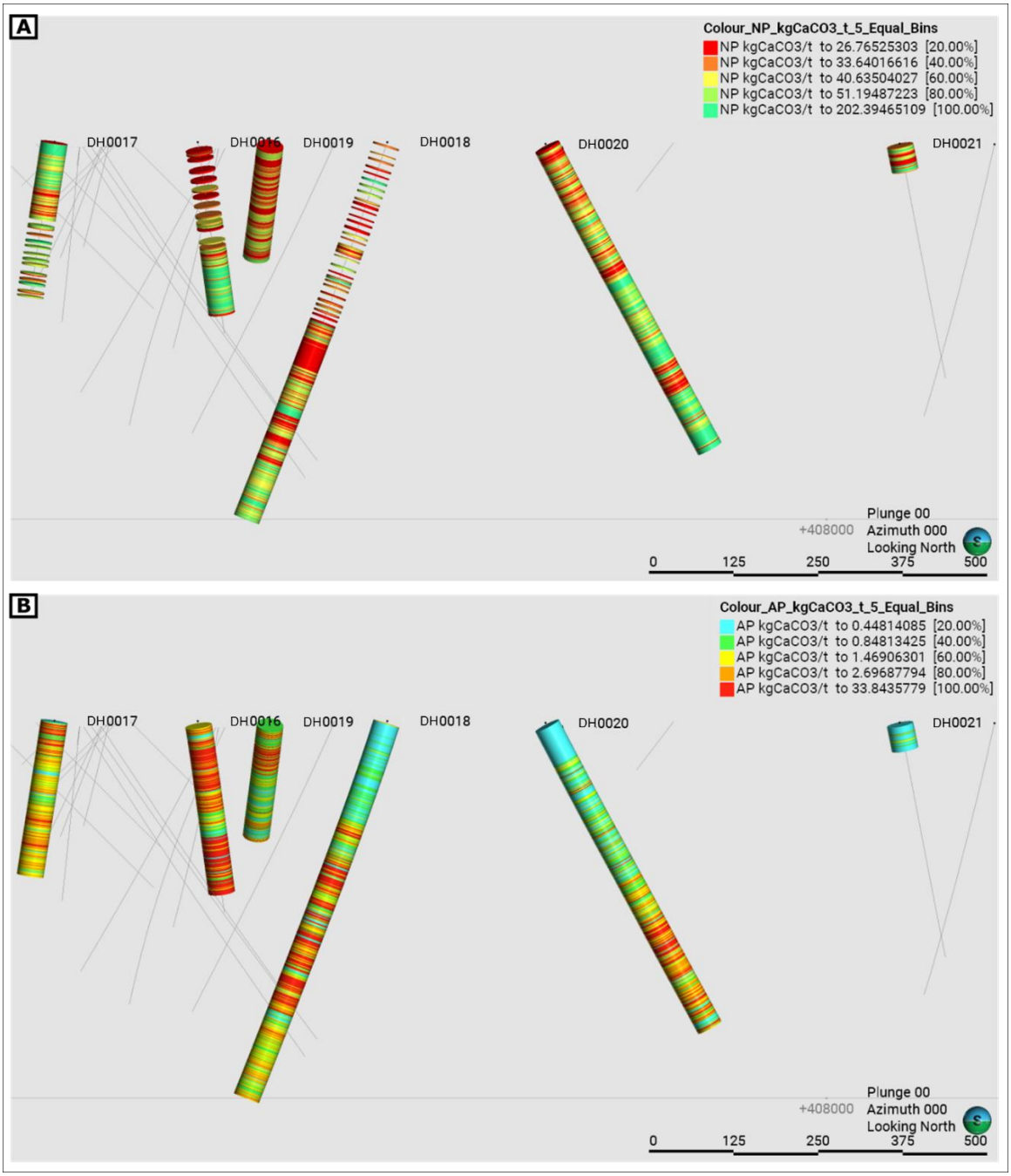

Figure 55 – Drillhole views classified according to calculated NP (A) and AP (B).

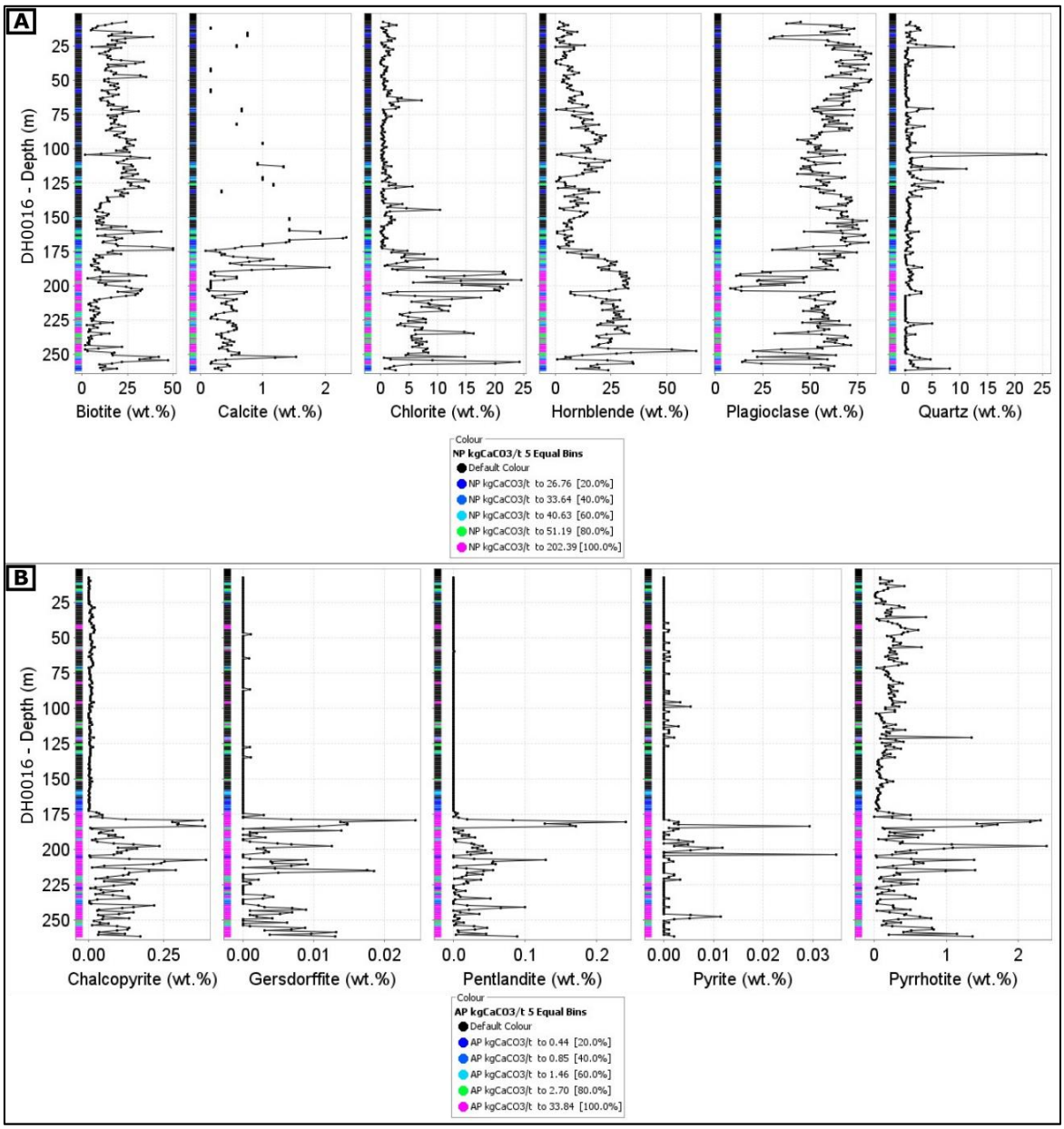

Figure 56 – Downhole NP (A) and AP (B) estimations for DH0016 with respective accounted mineralogy.

Only 0.84% of the samples fall within the uncertainty zone, none within the acid-generating zone and the remaining 99.16% are classified as non-acid generating or acid-consuming when considering NP/AP ratio (Figure 57-A). Less than 5-m long intervals restricted to drillholes DH0016 below 180 m and below 290 m in DH0018 are in the uncertainty zone (Figure 58-A). When considering NNP, still no sample is acid-generating. 8.15% are in the uncertainty area and 91.85% in the acid-consuming classification field (Figure 57-B). The majority of the uncertain samples are spread along DH0016 and DH0018 (Figure 58-B).

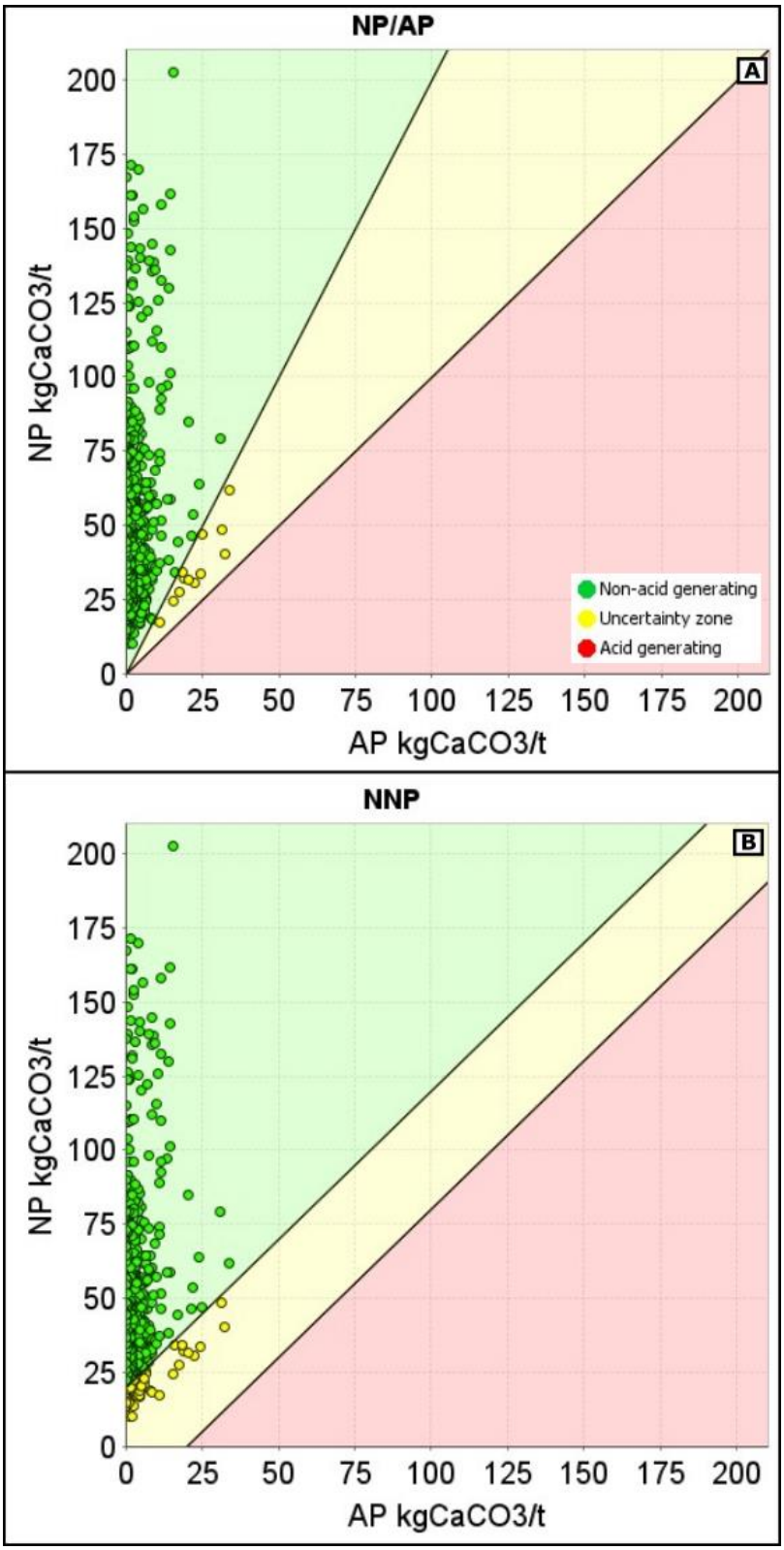

Figure 57 – NP/AP ratio (A) and NNP (B) classification diagram for mineralogical tests in DH0016 to DH0021.

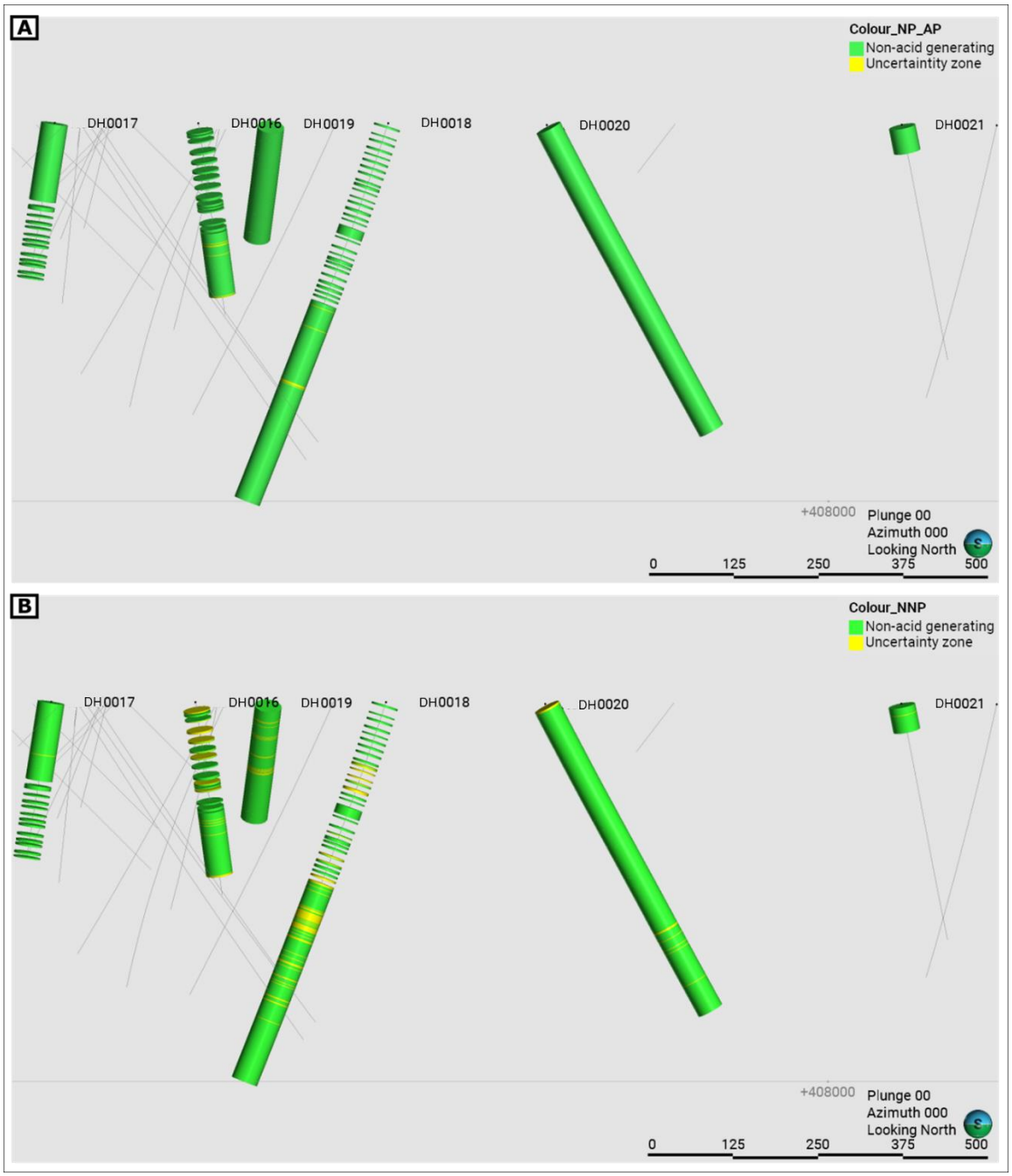

Figure 58 – Drillhole views classified according to NP/AP ratio (A) and NNP (B) using mineralogical static tests.

When results of mineralogical and geochemical static tests are compared (Figure 59), it is noticed that there is moderate correlation between the results for both NP and AP. However, calculated NP via mineralogical static tests tend to be slightly stronger. In some cases, samples that resulted in NP below 50 $CaCO_3$/t using carbon assay, for instance, have NP above 100 $CaCO_3$/t when using modal

mineralogy. Inversely, results via geochemical static tests for calculating AP tend to be higher than when using mineralogical tests.

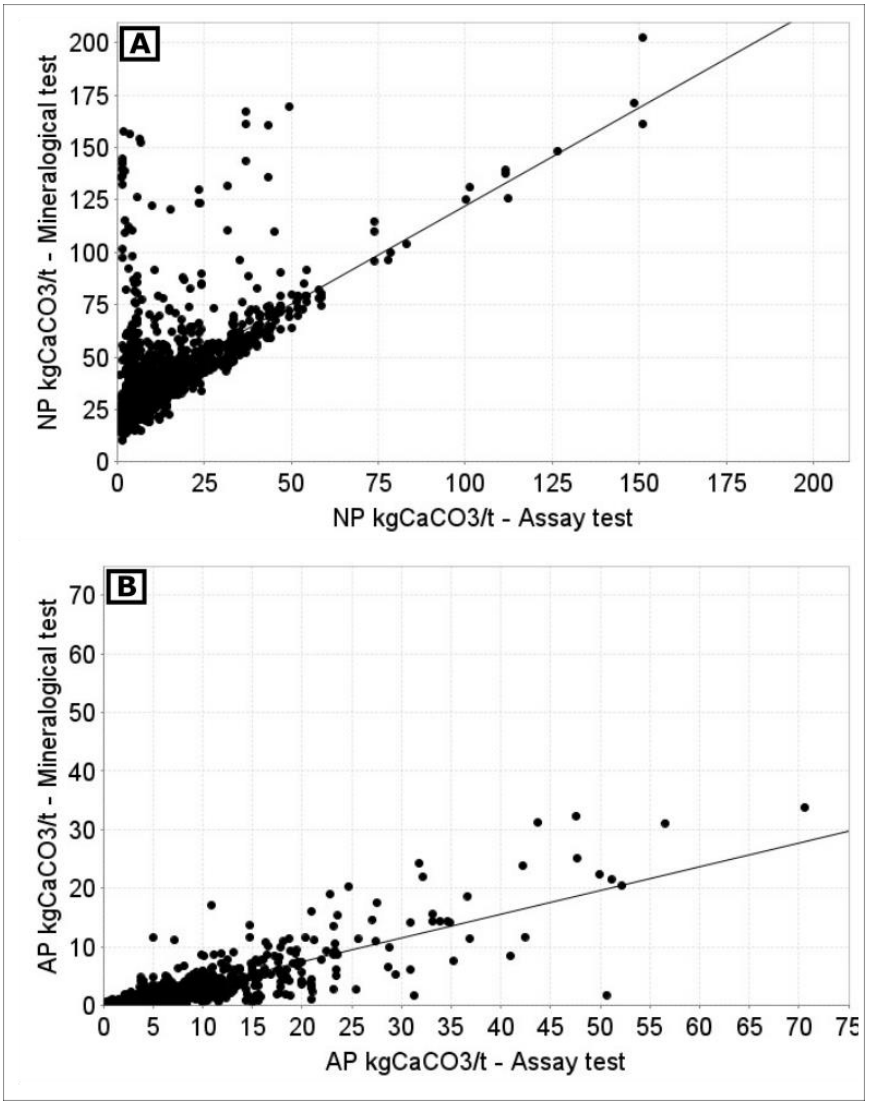

Figure 59 – Calculated NP (A) and AP (B) for mineralogical static tests against geochemical static tests for low-grade and barren zones from DH0016 to DH0021.

5.3 Discussions

One of the main limitations for the acid rock drainage estimations was the assumption of total C geochemical assay as only inorganic and completely hosted in calcite. The possible underestimation of calcite by LIBS is another limitation. There is evidence for the presence of graphite in the area of the prospect, especially in the host rocks, which are described as graphitic schists by some authors (Isohanni et al., 1985). Further investigation for confirming and quantifying the presence of this phase and/or any other inorganic compound is required for

improving ARD estimates and for assessing the potential for spontaneous combustion. The last can lead to instabilities in waste piles (Green & Borden, 2011). Sulfidic and carbon-rich wastes are subject to spontaneous combustion as exothermic oxidation generates enough heat to ignite C and organic matter (Lottermoser, 2010). Carbon assay is rarely included in exploration drilling in industry due to high costs. With project advancement and evidence of carbonates or graphite occurrence, C assay speciation is recommended.

The estimates for the whole dataset using geochemical static tests indicate that the intrusive rocks are more commonly classified as acid-generating. Even though the analysis was carried out in the low-grade and barren zones, the mafic and ultramafic intrusive rocks still have higher concentrations of sulfides than country rocks, what leads to stronger acid potential in those zones. In fact, the average AP for the dataset considering only DH0016 to DH0021 is lower than that the whole dataset. The first is comprised of only a short 30-m interval or mineralisation and a lower proportion of intrusive rocks, being dominated by gneiss. Because of that, its sulfide abundance is lower, and so is its AP, consequently.

NNP classifications are, in general, more conservative than NP/AP ratio classifications for low AP and NP values. This means that a higher proportion of samples falls within the uncertainty field for the first method due to the limits of the fields in this diagram being parallel. In the NP/AP ratio classification diagram, the uncertainty field increases for high AP and NP values.

Results of NP from mineralogical static tests versus geochemical static tests show that the NP predictions for the later are weaker. This is probably due to accounting silicates as potentially neutralizing phases in the mineralogical tests, enhancing the NP. For AP estimations, the geochemical static tests resulted in stronger AP predictions. This is probably due to the higher concentration of pyrrhotite in the prospect, instead of pyrite. The former produces less acidity, decreasing the acidification potential estimation; however, pyrrhotite is more reactive than the pyrite (Karlsson et al., 2018). The performance of kinetic tests for the estimation of the oxidation rates for the mineral phases is recommended for improving the robustness of the mineralogical tests (Chopard et al., 2017). Even though the raw estimations for NP and AP are not extremely different considering

the two tests, both classification diagrams show to be relatively sensitive to variations in its parameters. Discrete increase in the NP and decrease in the AP via the mineralogical static tests resulted in no samples being classified as acid-generating, in contrast to the more pessimistic scenario predicted by the geochemical static tests.

As an early assessment at an exploration stage, the use of modal mineralogy from LIBS scanning data for acid rock drainage predictions show to improve the sample representativeness. Additionally, accounting for the different mineral phases and their behaviours make the analysis more robust, as AP may be overestimated if a sulfide phase other than pyrite is present and as NP may be underestimated if silicates are not accounted as neutralizing phases. In fact, previous study confirmed that ARD predictions based on modal mineralogy calculations are reliable, by comparing them to waste pile drainage results (Karlsson, et al., 2018). Prospects in Finland, including Ni-Cu sulfide examples, tend to be carbonate-poor. Because of that, ARD predictions should consider silicates as neutralizing phases to avoid underestimations in the NP. The prospect has shown to have high contributions in the NP by hornblende and chlorite. Since these minerals are intermediate-weathering, considerations such as on their reactivity, grain size, association and pH conditions must be taken.

6 CONCLUSIONS

6.1 Opportunities and further developments

This study aimed to explore opportunities to increase OBK at an exploration stage, focusing on providing workflows to inform and enhance the predictability on different fields along the mineral value chain, such as metallurgy and environmental impacts. Drill core LIBS scanning data, supported by MLA and geochemical assay data, were the input for the investigations. At an exploration stage, many uncertainties arise due to limited access to robust tests and budget. Because of that, early investigations should focus on providing simplified and valuable information, which can be used by planning and operational teams to guide optimized and targeted detailed studies and decision making.

Assessments on identification and domaining of mineralisation and penalty elements in the high-grade zone have shown the possibility of using LIBS modal

mineralogy. The continuity and detail of the information provided allows the identification and mapping the length of enrichment zones. From this information, zones with higher grades or with the presence of undesirable mineralogy/elements can be flagged for next stages of the project. For this study, MLA textural information added information on grain size and mineral association, which are of utmost importance for predicting mineral processing behaviour. LIBS scanning imagery to provide quantitative information on texture is an opportunity to have continuous and detailed data in the same way as for the modal mineralogy.

LIBS data provided a contribution to OBK on environmental impact analysis. The calculated modal mineralogy allows the assessment for potential acid generation, which can be part of a preliminary assessment of AMD risk. Even though no measurements are to be proposed at this stage, likelihood for acid generation sources can be identified (Green & Borden, 2011). Reliable and representative sampling of modal mineralogy, especially for carbonates, sulfides and major silicates are recommended. It is important to consider that ARD depends on reaction rates, and that early predictions are not suitable for predicting long-term behaviour (Chopard et al., 2019). Integrating information on mineral characterization, e.g., grain size and association, that could come from LIBS, will allow accounting for mineral availability for reaction.

A series of other opportunities not covered in this study can be implemented in order to characterize an ore body when continuous and detailed information on chemistry, mineralogy and texture is available. Considering the relatively easy deployment and cost-effectiveness of LIBS scanning analysis, it can be adequate to assess additional geological information. For instance, modal mineralogy can be used to classify rock types, significantly decreasing time spent on geological logging and enhancing the standardization of the procedure. Imagery classification can help determining geological textures and assisting litho-mineralogical classification, e.g., schistosity, banding, isotropic etc.

All the OBK acquired during mineral exploration stage has the objective of informing possible flaws and opportunities for later advanced studies. The generated data and new assumptions should be investigated, refined and tested for confirmation. The integration of reliable and updated information on different

subjects, such as environmental sciences, mineral processing, geotechnics, mineralisation and grades, into a geometallurgical model will then be able to predict scenarios and guide decision making for the development of sustainable, profitable and optimized operations.

6.1.1 CO_2 mineralisation overview

Carbon mineralisation is another assessment that can greatly contribute to OBK. As discussed in Chapter 1, there is increase demand on companies to implement measures that help achieving carbon neutrality goals. Mineral industry is seen as key for energy transition due to critical materials supply, however, it still contributes with greenhouse gas emissions throughout its production chain. Scope 1 is related to direct emissions from fuels burn, scope 2 is related to indirect emissions from energy consumption and scope 3 is linked to off-site emissions in activities that support operations (Northey et al., 2013). Thus, carbon mineralisation methods can be implemented to achieve net-zero emission at operation scale or even as a new asset to be offered by the mineral industry, possibly as a secondary activity related to mineral exploitation.

Mafic and ultramafic rocks can be used for in situ permanent and solid carbon mineralisation (Kelemen et al., 2019). Carbon storage in solid form decreases the risk of leaking. The process occurs by water flow in rock pore space, promoting natural alkalinity dissolution of Mg- and Ca-bearing rocks at low pH, and consequent pH increase for carbonate precipitation, i.e., pH swing. Enough porosity and permeability in the rock allows fluid circulation and avoid clogging. The availability of alkalinity to react with carbon is a function of the dissolution rate of Mg- and Ca-bearing minerals. Brucite, wollastonite, olivine and Ca-plagioclase have the highest dissolution rates (Figure 60), respectively, and the latter is also potentialized at high temperatures. Fine grain sizes and reaction-driven cracking increase dissolution rates and reactivity, as the reaction surface becomes larger. This is especially important to avoid or decrease surface coating during reaction progress, which leads to passivation and inefficiency in dissolution (National Academies of Sciences, 2019).

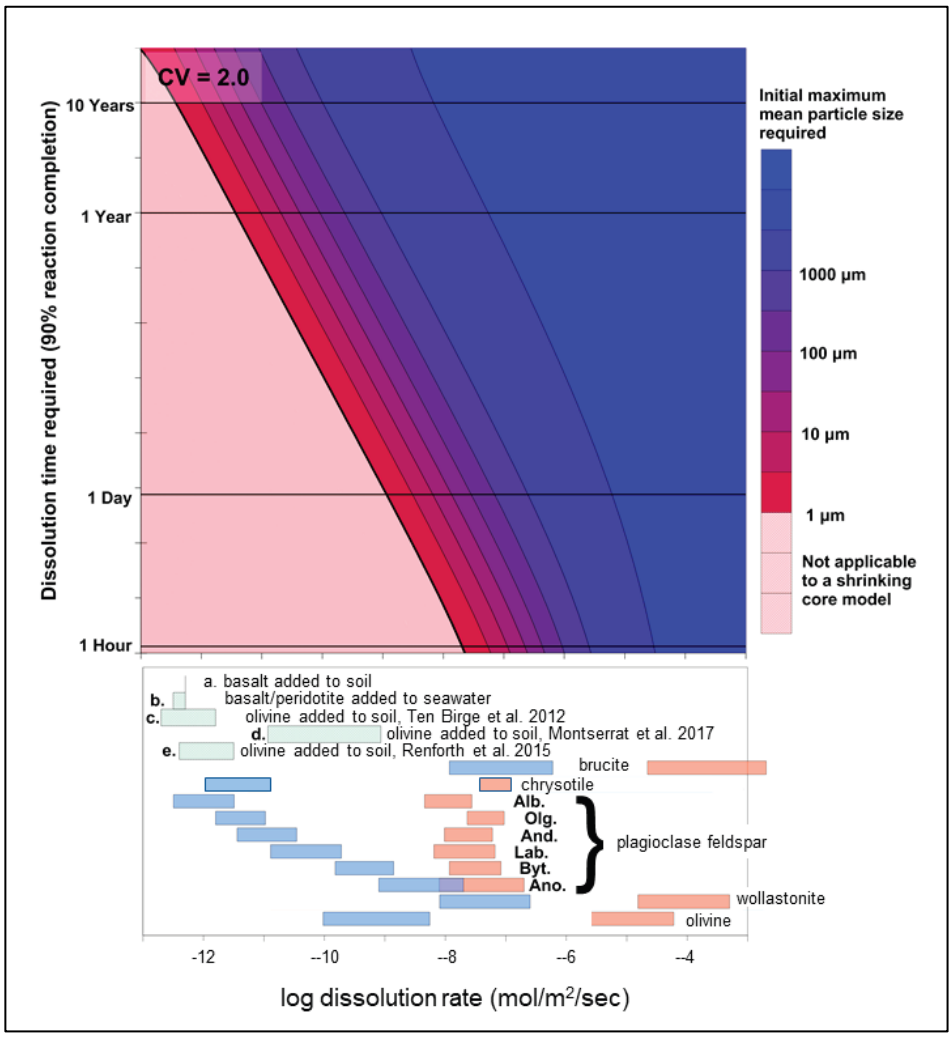

Figure 60 – Common rocks and minerals dissolution rates correlated with mean particle sizes distributions and time required to achieve 90% by volume dissolution. (National Academies of Sciences, 2019).

Mineral dissolution and subsequent carbonate precipitation, thus, is dependent on a series of conditions, such as porous rocks, high temperatures, pH swing and alkaline species. Mineralogy and texture are equally important. Considering these favourable conditions, in situ mineralisation is possible by CO_2 dissolution in water, making it likely to sink down due to increased density, facilitating injection into rocks without needing an impermeable layer, like it is done in sedimentary rocks. The source of carbon can be ambient air, CO_2-rich fluids, flue gas from power sector or high-purity CO_2. In Direct Air Capture via Enhanced Weathering (DACEW) (Kelemen et al., 2019), CO_2 is dissolved in water prior to injection, and the mineralisation can be as fast as 12 months in peridotite. This rock

type is olivine-rich, which present high reaction rates and consequent low passivation, facilitating the process. However, its porosity, fracturing and permeability is not as high as in basalts. Basaltic rocks are used in projects of carbon and H_2S storage in Finland, developed by Carbfix (https://www.carbfix.com/), also via direct capture (Ratouis et al., 2022). The company 44.01 (https://4401.earth/), in turn, develops a carbon sequestration project in Oman, with peridotite as the host rock.

Surficial carbon mineralisation is another technique that involves CO_2 reaction with alkalinity in tailings or waste piles (Paulo et al., 2023). The reactivity can be improved in these conditions, as the reaction area/volume ratio is high. Reaction rates are slower in soils, but similar to in-situ for ultramafic mine tailings (Figure 61). In surficial mineralisation, CO_2 uptake can be increased by sparging air, air + water, or CO_2-rich gas in the material. Stirring the tailings also increases reactive surface and adding microorganisms accelerates carbonate precipitation (Kelemen et al., 2019). One limitation of this technique is the low volumes of tailings, which results in low consumption opportunity; however, high uptake of C is possible, thus, creating an opportunity for net-zero emission at operation scale.

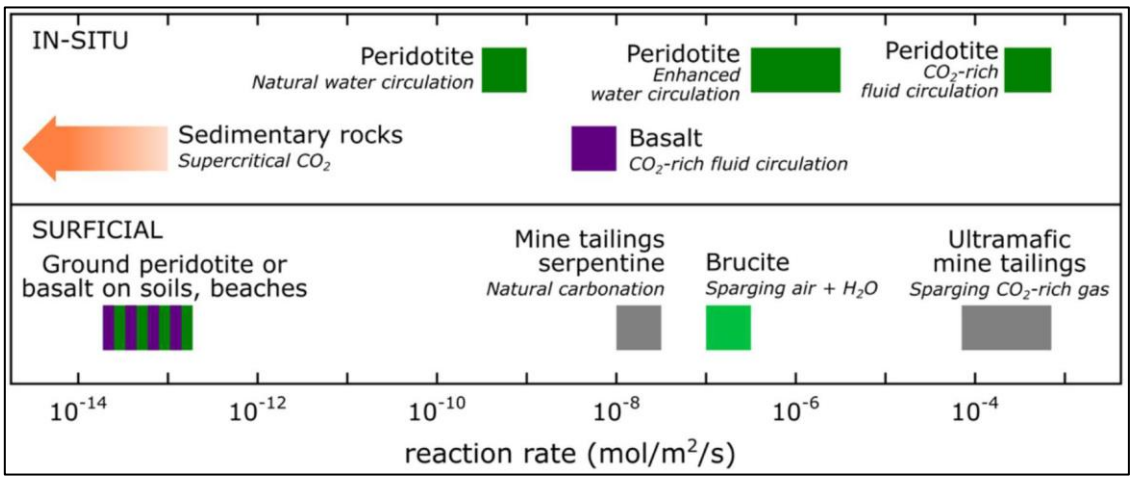

Figure 61 – Reaction rates of in-situ and surficial carbon mineralisation in mine tailings and rocks as alkalinity sources (Kelemen, et al., 2019).

The case study prospect is a mafic-ultramafic intrusion cluster formed mainly by gabbro and pyroxenite. The high abundance of Ca- and Mg-bearing mineralogy, such as plagioclase, hornblende and biotite, makes it of interest for investigating the potential for carbon mineralisation. Detailed and representative

LIBS modal mineralogy allow assessing spatial mineral variability in the prospect, what can be an opportunity for defining areas that are more likely to have alkalinity availability. Textural information from mineral maps can also provide insights on grain size for mineral reactivity, and mineral chemistry provided by LIBS scanning is recommended for anorthite composition and Mg and Ca deportment analysis. In that sense, mineral exploration teams can provide one additional preliminary assessment on opportunities for optimization and diversification of the mineral project.

6.2 Innovative aspects and study impact

The key role of exploration programmes is to increase the OBK, which will guide the development of predictive geometallurgical models that are able to forecast production performance and impacts for planning accordingly (Lishchuk & Pettersson, 2021). According to the authors, geometallurgical programmes can be classified as traditional: based on geochemical analysis; proxy: geochemical analyses and geometallurgical tests; and mineralogical: mineral quantification and texture. The use of LIBS quantified and representative mineralogy presented in this study, added to the opportunity of acquiring textural information, is a new window for early assessments at exploration stage. This is particularly important for low-grade and complex deposits, which increasingly demand high-quality and detailed information due to their sensitivity to ore variations. Moreover, this approach facilitates identifying new opportunities, that can, consequently, lead to optimized and more sustainable mineral production. In mineral processing and recovery, for instance, mineralogical and texture information are more decisive for predicting metallurgical response than chemical composition. Because of that, the ore characterization based on the last approach is more likely to result in more advanced geometallurgical programmes (Lishchuk & Pettersson, 2021).

The European Institute of Innovation and Technology (EIT) labels the Masters on Raw Materials Exploration and Sustainability, programme to which this study is presented. The EIT RawMaterials (EIT RawMaterials, 2023) is one of the nine Knowledge and Innovation Communities (KIC) for fomenting collaboration between business, research centres and universities and strengthening minerals, metals and materials sectors within Europe. It encompasses innovative solutions

throughout exploration, mining, processing, recycling, substitution and circular economy. The workflows herein proposed couple with the idea of developing technological and innovative solutions for supporting businesses and securing supply. This is done by using integrated data analysis on mineral exploration, thinking ahead the optimization of mining and processing. EIT Climate-KIC (EIT Climate-KIC, 2023) and EIT InnoEnergy (EIT InnoEnergy, 2023) are also closely related to the subjects covered by this study, as green energy transition and sustainable development are the main drivers for the ever-increasing demand for critical materials. In this scope, the diversification of opportunities that arise from improved OBK, such as assessments on acid mine drainage and combustion, carbon storage, ore concentrate quality and emissions and time-saving from efficient and integrated mineral exploration, is of utmost importance for addressing the above-mentioned primary goals.

At a local and case study scale, this project contributes to the development of Ni resources in Europe and Finland. Ni has recently been included in the list of critical and strategic raw materials by the EU, thus it is necessary to address problems related to its supply shortage predictions, price fluctuation and external dependency. In that sense, the study of the Ni-Cu sulfide prospect expands the knowledge on this type of mineral occurrence, the geology of the area and the tools for new exploration projects.

REFERENCES

Adeli, A. & Emery, X., 2017. A geostatistical approach to measure the consistency between geological logs and quantitative covariates. *Ore Geology Reviews,* Volume 82, pp. 160-169.

Alloway, B., 2013. *Heavy Metals in Soils: Trace Metals and Metalloids in Soils and Their Bioavailability.* Dordrecht: Springer Science & Business Media.

Assembly, U. G., 21 October 2015. *Transforming our world: the 2030 Agenda for Sustainable Development,* s.l.: s.n.

Australian Government, 2022. *Critical Materials Strategy,* Canberra: Department of Industry, Science, Energy and Resources.

Barnes, S., 2018. *Chalcophile Elements. In: White, W.M. (eds) Encyclopedia of Geochemistry. Encyclopedia of Earth Sciences Series..* Cham: Springer.

Barnes, S. J., Le Vaillant, M. & Lightfoot, P. C., 2017. Textural development in sulfide-matrix ore breccias in the Voisey's Bay Ni-Cu-Co deposit, Labrador, Canada. *Ore Geology Reviews,* Volume 90, pp. 414-438.

Barnes, S. J., Lesher, C. & Keays, R., 1995. Geochemistry of mineralised and barren komatiites from the Perseverance nickel deposit, Western Australia. *Lithos,* 34(1-3), pp. 209-234.

Barnes, S. J. et al., 2011. The Santa Rita Nickel Sulfide Deposit in the Fazenda Mirabela Intrusion, Bahia, Brazil: Geology, Sulfide Geochemistry, and Genesis. *Economic Geology,* Volume 106, pp. 1083-1110.

Buccianti, A. & Grunsky, E., 2014. Compositional data analysis in geochemistry: Are we sure to see what really occurs during natural processes?. *Journal of Geochemical Exploration,* Volume 141, pp. 1-5.

Burton, J., 2022. *U.S. Geological Survey Releases 2022 List of Critical Minerals.* [Online]
Available at: https://www.usgs.gov/news/national-news-release/us-geological-survey-releases-2022-list-critical-minerals

Chopard, A. et al., 2017. A contribution to improve the calculation of the acid generating potential of mining wastes. *Chemosphere,* Volume 175, pp. 97-107.

Chopard, A. et al., 2015. *Kinetic Tests to Evaluate the Relative Oxidation Rates of Various Sulfides and Sulfosalts.* Santiago, s.n.

Chopard, A. et al., 2019. Environmental Impact of Mine Exploitation: An Early Predictive Methodology Based on Ore Mineralogy and Contaminant Speciation. *Minerals,* Volume 9.

Clarotto, L., Allard, D. & Menafoglio, A., 2022. A new class of α-transformations for the spatial analysis of Compositional Data. *Spatial Statistics,* Volume 47.

Connelly, D., 2019. *Options for Removing Arsenic and Talc from a Copper concentrate.* s.l., Canadian Institute of Mining Metallurgy and Petroleum.

Contessotto, R., 2017. *Classificação de domínios mineralógicos e caracterização de minérios de níquel da mina de Santa Rita - BA, em apoio à geometalurgia.* São Paulo: Escola Politécnica, Universidade de São Paulo.

Core Resources, 2023. *Toowong Process™: Removal of Arsenic from Copper Concentrates.* [Online]
Available at: https://coreresources.com.au/process-technology/toowong-process/

Cornwall, H., 1966. *Nickel deposits of North America,* s.l.: Trading Economics – Nickel Summary.

Correia, L. et al., 2020. *NI 43-101 Technical Report Updated Preliminary Economic Assessment (PEA) of the Tamarack North Project – Tamarack, Minnesota,* s.l.: Talon Metals Corp..

Dai, Z., Wells, P. F., Garritsen, J.-A. A. & Xu, M., 2004. *Arsenide depression in flotation of multi-sulfide minerals.* Toronto (CA), Patent No. 10/960,527.

Dodge, Y., 2008. *Exploratory Data Analysis. In: The Concise Encyclopedia of Statistics.* New York: Springer.

Dold, B., 2020. Sourcing of critical elements and industrial minerals from mine waste – The final evolutionary step back to sustainability of humankind?. *Journal of Geochemical Exploration,* Volume 219.

Dominy, S. et al., 2018. Geometallurgy—A Route to More Resilient Mine Operations. *Minerals.*

Eilu, P. (., 2012. Mineral deposits and metallogeny of Fennoscandia. *Geological Survey of Finland,* Volume Special Paper 53, p. 401 pages.

EIT Climate-KIC, 2023. [Online]
Available at: https://eit.europa.eu/our-communities/eit-climate-kic

EIT InnoEnergy, 2023. [Online]
Available at: https://www.innoenergy.com/

EIT RawMaterials, 2023. [Online] Available at: https://eitrawmaterials.eu/

Elghali, A. et al., 2018. Determination of the available acid-generating potential of waste rock, part I: Mineralogical approach. *Applied Geochemistry,* Volume 99, pp. 31-41.

Elghali, A. et al., 2023. Prediction of acid mine drainage: Where we are. *Earth-Science Reviews,* Volume 241.

Eltham, J., 1973. *Approach to the Flotation of Western Australian Ni Ores.* s.l., s.n., pp. 417-430.

Emery, X. & Julián, O., 2005. Estimation of mineral resources using grade domains: Critical analysis and a suggested methodology. *The South African Institute of Mining and Metallurgy,* pp. 247-255.

Ester, M., Kriegel, H., Sander, J. & Xu, X., 1996. *A density-based algorithm for discovering clusters in large spatial databases with noise.* s.l., AAAI Press, pp. 226-231.

EU Commission, (., 2020. *Critical raw materials resilience: Charting a path towards greater Security and Sustainability,* Brussels: s.n.

European Commission, 2023. *Study on the Critical Raw Materials for the EU 2023 - Final Report,* s.l.: European Commission.

Evans, D. M., 2019. *Geological Fieldwork During 2019 in the Prospect Reservation Finland - Consulting Report for Rio Tinto Mining and Exploration Ltd.,* s.l.: AB Scandinavian Geopool Ltd..

Ferguson, K. & Morin, K., 1991. *The prediction of acid rock drainage—Lessons from the database.* Montreal, Quebec Mining Association, pp. 16-18.

Filzmoser, P. & Karel, H., 2009. Correlation Analysis for Compositional Data. *Mathematical Geosciences,* p. 41.

Fontana, F. F. et al., 2023. Laser Induced Breakdown Spectroscopy (LIBS) for whole rock geochemistry. *Journal of Geochemical Exploration,* Volume 246.

Fontana, F. et al., 2021. Integrated Laser-Induced Breakdown Spectroscopy (LIBS) and Multivariate Wavelet Tessellation: A New, Rapid Approach for Lithogeochemical Analysis and Interpretation. *Minerals,* 11(312).

Fornasiero, D. & Ralston, J., 2005. Cu(II) and Ni(II) activation in the flotation of quartz, lizardite and chlorite. *International Journal of Mineral Processing,* Volume 76, pp. 75-81.

Fouedjio, F., June Hil, E. & Laukamp, C., 2018. Geostatistical clustering as an aid for ore body domaining: case study at the Rocklea Dome channel iron ore deposit, Western Australia. *Applied Earth Science,* pp. 15-29.

Fountain, C., 2013. The whys and wherefores of penalty elements in copper concentrates. *MetPlant 2013. Australasian Institute of Mining and Metallurgy,* pp. 502-518.

Greenacre, M., 2021. Compositional Data Analysis. *Annual Review of Statistics and Its Application,* Volume 8, pp. 271-299.

Green, R. & Borden, R. K., 2011. Geochemical Risk Assessment Process for Rio Tinto's Pilbara Iron Ore Mines. In: *Integrated Waste Management - Volume I.* s.l.:InTech, pp. 365-390.

Gregory, M., 2021. *Internal Report,* Bundoora: Rio Tinto Exploration.

Haldar, S., 2017. *Chapter 1 - Introduction, Platinum-Nickel-Chromium Deposits.* s.l.:Elsevier.

Harmon, R. et al., 2019. Laser-Induced Breakdown Spectroscopy—An Emerging Analytical Tool for Mineral Exploration. *Minerals,* 9(718).

Harmon, R. S. et al., 2009. LIBS analysis of geomaterials: Geochemical fingerprinting for the rapid analysis and discrimination of minerals. *Applied Geochemistry,* 24(6), pp. 1125-1141.

IEA - International Energy Agency, 2022. *World Energy Outlook 2022,* Paris: IEA.

Isohanni, M., Ohenoja, V. & Papunen, H., 1985. Geology and nickel-copper ores of the Nivala area. *Geological Survey of Finland Bulletin,* Volume 333, pp. 211-228.

Jebb, A. T., Parrigon, S. & Woo, S. E., 2017. Exploratory data analysis as a foundation of inductive research. *Human Resource Management Review,* 27(2), pp. 265-276.

Jin, X. & Han, J., 2011. K-Means Clustering.. *Encyclopedia of Machine Learning.*

Jolliffe, I. T., 2013. *Principal Component Analysis.* New York: Springer-Verlag.

Karinen, T., 2010. The Koillismaa Intrusion, northeastern Finland – evidence for PGE reef forming processes in the layered series. *Geol. Surv. Finland,* Volume 404, p. 176.

Karlsson, T., Räisänen, M. & Lehtonen, M. e. a., 2018. Comparison of static and mineralogical ARD prediction methods in the Nordic environment. *Environ Monit Assess,* Volume 190.

Kelebek, S. & Tukel, C., 1999. The effect of sodium metabisulfite and triethylenetetramine system on pentlandite–pyrrhotite separation. *International Journal of Mineral Processing,* 57(2), pp. 135-152.

Kelemen, P. et al., 2019. Overview of the Status and Challenges of CO2 Storage in Minerals and Geological Formations. *Front. Clim.,* Volume 1, p. 9.

Kerr, A., 2003. Guidelines for the calculation and use of sulphide metal contents in research and mineral exploration. *Current Research - Newfoundland Department of Mines and Energy,* pp. 223-229.

Kittelty, D. & Smith, C., 2021. *Internal Report,* Bundoora: Rio Tinto.

Konnunaho, J., Halkoaho, T., Hanski, E. & Törmänen, T., 2015. Komatiite-hosted Ni-Cu-PGE deposits of the Finland. *Elsevier,* pp. 93-128.

Kontinen, A. & Hanski, E., 2015. The Talvivaara black shale-hosted Ni-Zn-Cu-Co deposit in eastern Finland. *In: Maier, W.D., Lahtinen, R., O'Brien, H. (Eds.), Mineral Deposits of Finland,* pp. 557-612.

Kontinen, A., Peltonen, P. & Huhma, H., 2006. *Description and genetic modelling of the Outokumpu-type rock assemblage and associated sulphide deposits,* s.l.: Final technical report for GEOMEX JV, Workspace ‘‘Geology”. Geological Survey of Finland.

Korsman, K. et al., 1997. *Suomen kallioperakartta – Berggrundskarta over Finland-Bedrock map of Finland 1: 1 000 000,* Espoo: Geological Survey of Finland.

Kriegel, H.-P., Ester, M., Sander, J. & Xu, X., 1996. *A density-based algorithm for discovering clusters in large spatial databases with noise.* s.l., AAAI Press, pp. 226-231.

Lamberg, P., 2011. *Particles - the bridge between geology and metallurgy.* s.l.:s.n.

Lane, D. J., Cook, N. J., Grano, S. R. & Ehrig, K., 2016. Selective leaching of penalty elements from copper concentrates: A review. *Minerals Engineering,* Volume 98, pp. 110-121.

Lang, A., Ellefmo, S. & Aasly, K., 2018. Geometallurgical Flowsheet as a Tool for Designing and Communicating Geometallurgical Programs. *Minerals.*

Lawrence, R. & Scheske, M., 1997. A method to calculate the neutralization potential of mining wastes. *Environmental Geology,* Volume 32, pp. 100-106.

Li, C., Maier, W. & Waal, S., 2001. Magmatic Ni versus PGE deposits: Contrasting genetic controls and exploration implications. *South African Journal of Geology,* Volume 104, pp. 309-318.

Lightfoot, P., Keays, R., Evans-Lamswood, D. & Wheeler, R., 2011. *Origin of the Nickel Sulfide Deposits at Voisey's Bay, Labrador, Canada.* Perth, s.n.

Lishchuk, V. & Pettersson, M., 2021. The mechanisms of decision-making when applying geometallurgical approach to the mining industry. *Miner Econ,* Volume 34, pp. 71-80.

Lokuwaduge, C. S. D. S. & Heenetigala, K., 2017. Integrating Environmental, Social and Governance (ESG) Disclosure for a Sustainable Development: An Australian Study. *Bus. Strat. Env.,* pp. 438-450.

Lottermoser, B., 2010. *Characterization, Treatment and Environmental Impacts.* berlin: Springer-Verlag.

Makkonen, H., 2015. Nickel Deposits of the 1.88 Ga Kotalahti and Vammala Belts. *Mineral Deposits of Finland,* pp. 253-290.

Makkonen, H. V. et al., 2017. Ni-(Cu-PGE) deposits in Finland – Geology and exploration potential. *Ore Geology Reviews,* Volume 90, pp. 667-696.

Makkonen, H. V., Mäkinen, J. & Kontoniemi, O., 2008. Geochemical discrimination between barren and mineralized intrusions in the Svecofennian (1.9 Ga) Kotalahti Nickel Belt, Finland. *Ore Geology Reviews,* Volume 33, pp. 101-114.

McInnes, L, Healy, J & Melville, J, 2020. UMAP: Uniform Manifold Approximation and Projection for Dimension Reduction. *ArXiv e-prints.*

Metso, S., 2022. *Finland - Prospect Review Report 2022,* s.l.: Rio Tinto.

Miller, S., Robertson, A. & Donahue, T., 1997. *Advances in acid drainage prediction using the net acid generating (NAG) test.* s.l., s.n., pp. 533-549.

Morin, K. & Hutt, N., 2001. *Environmental Geochemistry of Minesite Drainage: Practical Theory and Case Studies.* Vancouver: MDAG Pub..

Mutanen, T., 1997. Geology and petrology of the Akanvaara and Koitelainen mafic layered intrusions and the Keivitsa-Satovaara layered complex. *Geological Survey of Finland Bulletin,* Volume 395, pp. 1-233.

Naldrett, A., Asif, M., Krstic, S. & Li, C., 2000. The composition of mineralization at the Voisey's Bay Ni–Cu sulfide deposit, with special reference to platinum-group elements. *Economic Geology,* Volume 95, pp. 845-867.

National Academies of Sciences, 2019. Negative Emissions Technologies and Reliable Sequestration: A Research Agenda. *Engineering, and Medicine.*

Nironen, M., Korja, A., Heikkinen, P. & FIRE, W. G., 2006. A geological interpretation of the upper crust along FIRE 2 and FIRE 2A. *Geological Survey of Finland,* Volume 43, pp. 77-103.

Northey, S., Haque, N. & Mudd, G., 2013. Using sustainability reporting to assess the environmental footprint of copper mining. *Journal of Cleaner Production,* Volume 40, pp. 118-128.

Oliver, S. & Willingham, D., 2016. *Maximise Orebody Value through the Automation of Resource Model Development Using Machine Learning.* Perth, AusIMM.

Paktunc, A., 1999. Mineralogical constraints on the determination of neutralization potential and prediction of acid mine drainage. *Environmental Geology,* Volume 39, pp. 103-112.

Panoramic Resources, 2017. *Savannah Feasibility Study Optimisation - Robust economics at spot commodity prices,* s.l.: Panoramic Resources Ltd.

Patro, S. G. K. & Sahu, K. K., 2015. Normalization: A Preprocessing Stage. *arXiv,* p. 4.

Paulo, C. et al., 2023. Geochemical modeling of CO2 sequestration in ultramafic mine wastes from Australia, Canada, and South Africa: Implications for carbon accounting and monitoring. *Applied Geochemistry,* Volume 152.

Peltonen, P., 2005. Chapter 9 Svecofennian mafic-ultramafic intrusions. *Developments in Precambrian Geology, Elsevier,* Volume 14, pp. 407-441.

Pietrobon, M., Grano, S., Sobieraj, S. & Ralston, J., 1997. Recovery mechanisms for pentlandite and MgO-bearing gangue minerals in nickel ores from Western Australia. *Minerals Engineering,* Volume 10, pp. 775-786.

Plante, B., Bussière, B. & Benzaazoua, M., 2012. Static tests response on 5 Canadian hard rock mine tailings with low net acid-generating potentials. *Journal of Geochemical Exploration,* Volume 114, pp. 57-69.

Price, W., 2009. Prediction Manual for Drainage Chemistry. *Natural Resources Canada,* p. 579 p..

Rajabinasab, B. & Asghari, O., 2019. Geometallurgical Domaining by Cluster Analysis: Iron Ore Deposit Case Study. *Nat Resour Res,* Volume 28, pp. 665-684.

Rasilainen, K. et al., 2017. Assessment of undiscovered metal resources in Finland. *Ore Geology Reviews,* Volume 86, pp. 896-923.

Ratouis, T. M. et al., 2022. Carbfix 2: A transport model of long-term CO2 and H2S injection into basaltic rocks at Hellisheidi, SW-Iceland. *International Journal of Greenhouse Gas Control,* Volume 114.

Rifai, K. et al., 2022. Quantification of Lithium and Mineralogical Mapping in Crushed Ore Samples Using Laser Induced Breakdown Spectroscopy. *Minerals,* Volume 253, p. 12.

Rossi, M. E. & Deutsch, C. V., 2014. *Mineral Resource Estimation.* Dordrecht: Springer.

Santaguida, F. et al., 2015. The Kevitsa Ni-Cu-PGE deposit in the Central Lapland greenstone belt in Finland. *Elsevier,* pp. 195-210.

Santos Junior, L. & Jr, H., 2016. Modelling and Simulation of the Santa Rita Mine Milling Circuit. *Rem: Revista Escola de Minas,* Volume 69, pp. 207-211.

Schubert, E. et al., 2017. DBSCAN Revisited, Revisited: Why and How You Should (Still) Use DBSCAN. *ACM Trans. Database Syst,* p. 21 pages.

Selby, M. & White, D., 2011. Chapter 20 Commodity Marketing - Nickel. In: *Cost Estimation Handbook.* s.l.:AusIMM, pp. 502-506.

Senior, G., Smith, L., Silvester, E. & Bruckard, W., 2009. The flotation of gersdorffite in sulphide nickel systems — A single mineral study. *International Journal of Mineral Processing,* Volume 93, pp. 165-171.

Sobek, A., Schuller, W., Freeman, J. & Smith, R., 1978. Field and laboratory methods applicable to overburdens and minesoils. *US Govt Printing Office.*

Thébaud, N., Barnes, S. & Fiorentini, M., 2012. Komatiites of the Wildara-Leonora Belt, Yilgarn Craton, WA: The missing link in the Kalgoorlie Terrane?. *Precambrian Research,* Volume 196-197, pp. 234-246.

Trading Economics, 2023. *Trading Economics – Nickel Summary.* [Online] Available at: https://tradingeconomics.com/commodity/nickel

Tukey, J., 1977. *Exploratory Data Analysis..* Reading, MA: Addison-Wesley.

U.S. Geological Survey, 2022. *2022 Final List of Critical Minerals,* s.l.: U.S. Geological Survey, Department of the Interior..

Warner, A. et al., 2007. JOM World Nonferrous Smelter Survey Part IV: Nickel: Sulfide. *Journal of the Minerals, Metals and Materials Society,* pp. 58-72.

Wood Mackenzie, 2022. *Global copper concentrates long-term outlook Q3 2022 Penalty Elements,* s.l.: Commodity Market Report - Wood Mackenzie.

Zhao, K. et al., 2015. Influence of depressant foenum-graecum on the flotation of a sulfide ore which contains hydrophobic gangue. *International Journal of Mineral Processing,* Volume 141, pp. 68-76.